People's Democratic Republic of Algeria
Ministry of Higher Education and Scientific Research
University of 8 Mai 1945Guelma

Faculty of Mathematics and Computer and Material Sciences
Department of Material Sciences
Laboratory of Physical Chemistry

Thesis

Submitted in Candidacy for the Degree of
Doctorate in Third Cycle

Field: Material Sciences Stream: Chemistry
Speciality: Physical Chemistry

Presented by:
BENMABROUK Marwa

Title

Synthesis, Characterization, and In-Silico Exploration of N-Salicylideneaniline Schiff Base Derivatives: DFT, Antioxidant activity and Molecular Docking Studies

Defended on : June 25th, 2024 Before the jury composed of:

Full name	Rank	University	
Mr SERIDI Achour	Professor	Univ. of 8 Mai 1945 - Guelma -	President
Mrs SERIDI Saida	MCA	Univ. of 8 Mai 1945 - Guelma -	Supervisor
Mrs ALMI Sana	MCA	Univ. of Mohamed Khider -Biskra-	Co- supervisor
Mrs MENASRA Hayet	Professor	Univ. of Mohamed Khider -Biskra-	Examiner
Mrs ADJEL Fatima	Professor	Univ. of Mohamed Khider -Biskra-	Examiner
Mrs SELAIMIA Radia	MCA	Univ. of 8 Mai 1945 - Guelma -	Examiner

Academic year: 2023/2024

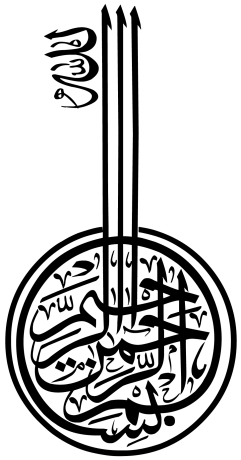

Acknowledgments

I am grateful to Almighty Allah for giving me the strength and ability to fulfill this goal. This thesis would not have been possible without the patient instruction and constant support of my supervisor *Dr. SERIDI Saida* and my co-supervisor *Dr. ALMI Sana*, who are not only two excellent academic advisors but also a thoughtful professional mentors. Their wit, insight, and feedback have immensely enriched this last stretch of my educational experience.

I would also like to thank the jury's members for accepting to review and judge this thesis: **Mr. SERIDI Achour**, Full Professor at University of 8 Mai 1945 - Guelma - for the honor he has given me by accepting to chair the defense jury of this thesis. **Mrs. MENASRA Hayet**, **Mrs. ADJEL Fatima**, Full Professors at University of Mohamed Khider -Biskra- and **Mrs. SELAIMIA Radia** Associate Professor at University of 8 Mai 1945 - Guelma - for having accepted to examine my work and to be part of the jury. I also thank them for accepting to attend the presentation of this work.

This thesis is based on research work conducted within the **Physical Chemistry Laboratory** at the University of 8 Mai 1945 - Guelma.

Dedication

To my beloved family,

This thesis wouldn't have been possible without your constant love and support. Your belief in me, even during late nights and moments of doubt, has been a constant source of strength.

Adil, my incredible husband,

Your support has been beyond measure throughout this journey. You have been not only my rock but a true partner. Your patience during countless research sessions and your invaluable assistance in the writing process have been indispensable. I cannot adequately express my gratitude for celebrating every milestone, big or small, by my side. Your unwavering presence through thick and thin fills my heart with profound gratitude.

And to my dear friends, Zeyneb and Sonya, thank you for your encouragement, listening ears, and moments of laughter that kept me going.

ملخص

تُقدم هذه الدراسة تقريرا عن توليف ثلاث مشتقات قاعدة شيف من نوع إن - ساليسيليدينانيلين. وهي : إن - (2- هيدروكسي بنزليدين) - إم - كلوروأنيلين (HBMC) ، وإن - (2- هيدروكسي بنزليدين) - إم - نيتروأنيلين (HBMN) ، وإن - (2- هيدروكسي بنزليدين) - إم - ميثوكسي أنيلين (HBMM) . لقد تم تحقيق التوصيف من خلال مزيج من تقنيات التحليل الطيفي (الأشعة تحت الحمراء، والرنين النووي المغناطيسي ذو الأشعة تحت الحمراء (1H) ، الأشعة المرئية وفوق البنفسجية) إلى جانب حسابات نظرية الكثافة الوظيفية (DFT-B3LYP) . وقد أكد التوافق الممتاز بين المعطيات التجريبية والنظرية على نجاح التوصيف البنيوي.

تم استخدام طرق حسابية لدراسة آليات مضادات الأكسدة المحتملة. كشفت حسابات طاقات تفكك الروابط (BDEs) ، وإمكانات التأين (IPs) ، وطاقات تفكك البروتون (PDEs) ، وانجذاب البروتون (PAs) ، وطاقات نقل الإلكترون (ETEs) في مذيبات مختلفة عن تحول يعتمد على المذيب. وتبدو آلية نقل الإلكترون أحادي البروتون الفاقد (SPLET) مهيمنة في البيئات القطبية، في حين أن آلية نقل ذرة الهيدروجين (HAT) مفضلة في المرحلة الغازية. وأظهر مركب HBMC أكثر الملامح الواعدة في مسح الجذور من بين المركبات التي تم فحصها.

وكشف تحليل السيليكو (ADME-Tox) عن خصائص حركية دوائية مواتية وامتثالها لمعايير التشابه الدوائي لجميع المشتقات الثلاثة، مما يشير إلى إمكانية التوافر البيولوجي الفموي الجيد. كما أبرزت دراسات الإرساء الجزيئي إمكاناتها كمثبطات لبروتين UQCRB

الكلمات المفتاحية: قواعد شيف، نشاط إزالة الجذور الحرة DFT ، بروتين الميتوكوندري UQCRB ، الالتحام الجزيئي ، ADMET

Abstract

This study reports the synthesis of three N-salicylideneaniline Schiff base derivatives: $N-(2hydroxybenzylidene)-m-chloroaniline(HBMC)$, $N-(2-hydroxybenzylidene)-m-nitroaniline(HBMN)$, and $N-(2-hydroxybenzylidene)-m-methoxyaniline(HBMM)$. Characterization was achieved through a combination of spectroscopic techniques (FT-IR, 1H NMR, UV-Vis) and density functional theory (DFT-B3LYP) calculations, demonstrating strong agreement between experimental and theoretical data.

Computational methods were employed to investigate potential antioxidant mechanisms. Calculations of bond dissociation energies (BDEs), ionization potentials (IPs), proton dissociation energies (PDEs), proton affinities (PAs), and electron transfer energies (ETEs) in various solvents revealed a solvent-dependent shift. The Single Proton Loss Electron Transfer (SPLET) mechanism appears dominant in polar environments, while the Hydrogen Atom Transfer (HAT) mechanism is favored in the gas phase. HBMC exhibited the most promising profile for radical scavenging among the investigated compounds.

In silico ADME-Tox analysis revealed favorable pharmacokinetic properties and compliance with drug-likeness criteria for all three derivatives, indicating potential for good oral bioavailability. Molecular docking studies further highlighted their potential as inhibitors of the UQCRB protein, with HBMM demonstrating the strongest binding affinity (-7.68 kcal/mol).

Keywords: Schiff bases, Radical scavenging activity, DFT, Mitochondrial UQCRB protein, ADMET, Molecular Docking

Résumé

Cette étude rapporte la synthèse de trois dérivés Schiff de $N-salicylidneaniline$: la $N-(2-hydroxybenzylidne)-m-chloroaniline(HBMC)$, la $N-(2-hydroxybenzylidne)-m-nitroaniline(HBMN)$ et la $N-(2-hydroxybenzylidne)-m-mthoxyaniline(HBMM)$. La caractérisation structurale de ces composés a été réalisée en combinant différentes techniques spectroscopiques $(FT-IR, RMN^1H, UV-Vis)$). Des calculs de Chimie Quantique basés sur la Théorie de la Fonctionnelle de la Densité (DFT-B3LYP) ont été effectués et ont montré une bonne concordance entre les données expérimentales et les prédictions théoriques.

Des méthodes computationnelles ont ensuite été employées pour étudier leurs mécanismes antioxydants potentiels. Le calcul des énergies de dissociation de liaison (BDE), des potentiels d'ionisation (IP), des enthalpies de dissociation de proton (PDE), des affinités protoniques (PA) et des enthalpies de transfert d'électron (ETE) dans différents milieux solvants a révélé une dépendance vis-à-vis de la polarité du solvant. Le mécanisme de perte d'un proton unique avec transfert d'électron (SPLET) semble dominant dans les milieux polaires, tandis que le mécanisme de transfert d'atome d'hydrogène (HAT) est favorisé en phase gazeuse. Parmi les composés étudiés, le HBMC a présenté le profil le plus prometteur pour le piégeage des radicaux libres.

Une analyse ADME-Tox in silico a ensuite été réalisée pour évaluer les propriétés pharmacocinétiques et la ressemblance à des médicaments des trois dérivés. Cette analyse a révélé des propriétés pharmaceutiques favorables et une conformité aux critères de similarité avec des médicaments, suggérant un bon potentiel de biodisponibilité par voie orale. Des études de docking moléculaire ont de plus mis en évidence leur potentiel en tant qu'inhibiteurs de la protéine UQCRB, le HBMM présentant la plus forte affinité de liaison $(-7,68kcal/mol)$.

Mots clés : Bases de Schiff , Activité antiradicalaire , DFT , Protéine mitochondriale UQCRB ,ADMET , Docking moléculaire

Table of Contents

List of Figures

List of Tables

Acronyms

ABTS 2,2'-azinobis (3ethylbenzothiazoline-6-sulfonic acid)

ADMET Absorption, Distribution, Metabolism, Excretion, and Toxicity

ADT AutoDock Tools

ALA Alanine

ASN Asparagine

ASP Aspartic Acid

ATP Adenosine Triphosphate

B3LYP Becke-3 parameter-Lee, Yang, Parr

BBB Blood-Brain Barrie

BDE Bond Dissociation Enthalpy

BHA Butylated Hydroxyanisole

BHT Butylated Hydroxytoluene

BLYP Becke, Lee, and Parr

CNS central nervous system

CUPRAC CUPric Reducing Antioxidant Capacity

DFT Density Functional Theory

DNA Deoxyribonucleic Acid

DPPH 2,2-diphenyl-1-picrylhydrazyl

EA Electron Affinity

EDTA Ethylenediaminetetraacetic

ETE Electron Transfer Enthalpy

FMO Frontier Molecular Orbital

FOX Ferrous Oxidation Xylenol Orange

FRAP Ferric Reducing Antioxidant Power

FTC Ferric Thiocyanate

FT-IR Fourier Transform Infrared Spectroscopy

GC-MS Gas Chromatography-Mass Spectrometry

GGA Generalized Gradient Approximation

GTO Gaussian-Type Orbital

HAT Hydrogen Atom Transfer

HBMC N-(2-hydroxybenzylidene)-m-chloroaniline

HBMM N-(2-hydroxybenzylidene)-m-methoxyaniline

HBMN N-(2-hydroxybenzylidene)-m-nitroaniline

HF Hartree-Fock

HIS Histidine

HOMO Highest Occupied Molecular Orbital

IC50 Half Maximal Inhibitory Concentration

IEF-PCM Integral Equation Formalism Polarizable Continuum Model

IP Ionization Potential

IZD Inhibition Zone Diameter

LC-MS Liquid Chromatography-Mass Spectrometry

LDA Local Density Approximation

LEU Leucine

LUMO Lowest Unoccupied Molecular Orbital

LYS Lysine

MIC Minimum Inhibitory Concentration

MNA Multilevel Neighborhoods of Atoms

MTT 3-(4,5-dimethylthiazol-2-yl)-2,5-diphenyltetrazolium bromide

NMR Nuclear Magnetic Resonance

ORAC Oxygen Radical Absorbance Capacity

PASS Prediction of Activity Spectra for Substances

PDE Proton Dissociation Enthalpy

PED Potential Energy Distribution

PHE Phenylalanine

QSAR Quantitative Structure-Activity Relationships

RMSD Root Mean Square Deviation

RNS Reactive Nitrogen Species

ROS Reactive Oxygen Species3

SB Schiff Base

SBDD Structure-Based Drug Discovery

SEM Scanning Electron Microscopy

SER Serine

SET Single-Electron Transfer

SET-PT Single Electron Transfer-Proton Transfer

SPLET Sequential Proton Loss Electron Transfer

TBARS Thiobarbituric Acid Reactive Substances4

TD-DFT Time-Dependent Density Functional Theory

TEM Transmission Electron Microscopy

TLC Thin Layer Chromatography

TYR Tyrosine

UQCRB Ubiquinol-cytochrome c reductase binding protein

UV-Vis Ultraviolet-Visible Spectroscopy

XRD X-Ray Diffraction

General Introduction

Oxidative stress, a pervasive imbalance driven by an overabundance of reactive oxygen species (ROS), lies at the heart of a wide array of diseases, including cancer, neurodegenerative conditions, and cardiovascular disorder [1, 2]. To mitigate the destructive effects of oxidative stress, researchers are actively seeking novel antioxidant compounds capable of protecting cells and tissues from damage. Schiff bases, with their readily modifiable chemical structures and potential for diverse biological activities, represent a promising avenue for the development of new therapeutics [3, 4, 5].

While Schiff bases have attracted significant research attention, a comprehensive understanding of derivatives formed specifically from meta-substituted anilines and 2-hydroxybenzaldehyde remains elusive. These compounds may possess unique antioxidant properties with potential therapeutic value. Additionally, exploring their interactions with the UQCRB protein, a pivotal component of mitochondrial function and a player in cancer-promoting angiogenesis, could reveal new strategies for combating cancer [6, 7].

This study investigates three novel salicylideneaniline Schiff bases: N-(2-hydroxybenzylidene)-m-chloroaniline, N-(2-hydroxybenzylidene)-m-nitroaniline, and N-(2-hydroxybenzylidene)-m-methoxyaniline. To achieve our objectives, we adopt a multifaceted approach that leverages both experimental and computational techniques.

DFT calculations provide a powerful means to explore potential antioxidant mechanisms (HAT, SPLET, SET-PT) crucial for the rational design of even more effective antioxidants. Furthermore, molecular docking will enable us to simulate binding interactions with UQCRB and gain insights that could lead to novel anti-cancer therapies. Finally, we'll use in silico ADME prediction tools to assess the bioavailability and drug-likeness of these compounds, an essential step in drug development.

This research aims to expand the frontiers of knowledge in Schiff base chemistry by providing a comprehensive analysis of specific salicylideneaniline derivatives. Our findings will illuminate antioxidant mechanisms and potentially identify novel therapeutic leads for combating diseases linked to oxidative stress. Importantly, the integration of computational methods will accelerate the discovery process and guide the targeted design of new Schiff base derivatives with enhanced therapeutic potential.

After a general introduction outlining the objectives and purpose of the work undertaken, this thesis is divided into five chapters described below:

The first chapter introduces Schiff bases, detailing their discovery, formation mechanism, and synthesis methods. It explores their chelating properties, biological activities, and various synthesis techniques, including microwave irradiation and ultrasonic methods.

In the second chapter, focus shifts to antioxidants, discussing their role against oxidative stress, types, and mechanisms of action. It elaborates on methods to evaluate antioxidant activity, and discusses the applications and safety considerations of synthetic antioxidants.

The third chapter delves into computational approaches to study antioxidants, covering Density Functional Theory (DFT), Time-Dependent DFT, and molecular docking. It also discusses the Prediction of Activity Spectra for Substances (PASS) and ADMET properties, crucial for drug development.

The fourth chapter outlines the practical aspects of the research, describing the materials, instrumentation, and methods used in synthesizing Schiff base derivatives. The chapter also details computational protocols and in silico ADMET assessment, providing the experimental foundation for the study.

The final chapter presents the analysis of NMR and vibrational spectra, confirming the structure of synthesized compounds. It discusses the predicted antioxidant activity, ADMET properties, and concludes with the therapeutic potential of Schiff bases. We conclude this work with a general conclusion that summarizes the main results obtained as well as the perspectives.

Chapter 1

Schiff Bases: Versatile Molecules with Diverse Biological Activity

Introduction

Since their discovery by German chemist Hugo Schiff in 1864 [8], Schiff bases have steadily expanded their influence across diverse scientific fields. Named after their discoverer, these compounds possess a deceptively simple core – the azomethine group ($> C = N -$). This signature functional group grants Schiff bases remarkable versatility. Their ease of synthesis from readily available aldehydes and amines, coupled with their ability to be tailored with various substituents, has unlocked a vast range of applications.

1.1 Schiff Base Formation

1.1.1 Mechanism

Schiff bases form through the condensation of primary amines with carbonyl compounds, which include both ketones and aldehydes [See Figure 1.1]. The reaction is typically catalyzed by acid or base, and in some cases, proceeds under heat [9].

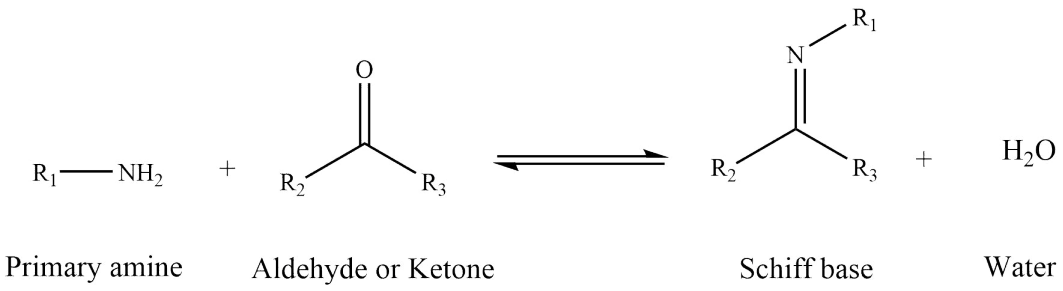

Figure 1.1: The synthesis of schiff bases

The mechanism of Schiff base formation begins with a nucleophilic attack of the amine's lone pair of electrons on the electrophilic carbonyl carbon of the aldehyde or ketone, lead-

ing to the formation of a tetrahedral, unstable carbinolamine intermediate. Next, a crucial 1,3-proton shift occurs, which primes the intermediate for the subsequent elimination of water. This step is often accelerated by the presence of acid or base catalysts [10].

The carbinolamine undergoes dehydration, driven by the removal of a water molecule (H_2O). Acid catalysts promote this reaction by protonating the -OH group, transforming it into a better leaving group. In contrast, base catalysts facilitate the elimination through deprotonation [11, 12]. The elimination of water results in the formation of a double bond between the carbon and nitrogen, yielding the characteristic imine $(> C = N-)$ or azomethine group. The resulting imine typically adopts a trans configuration to minimize steric hindrance [13].

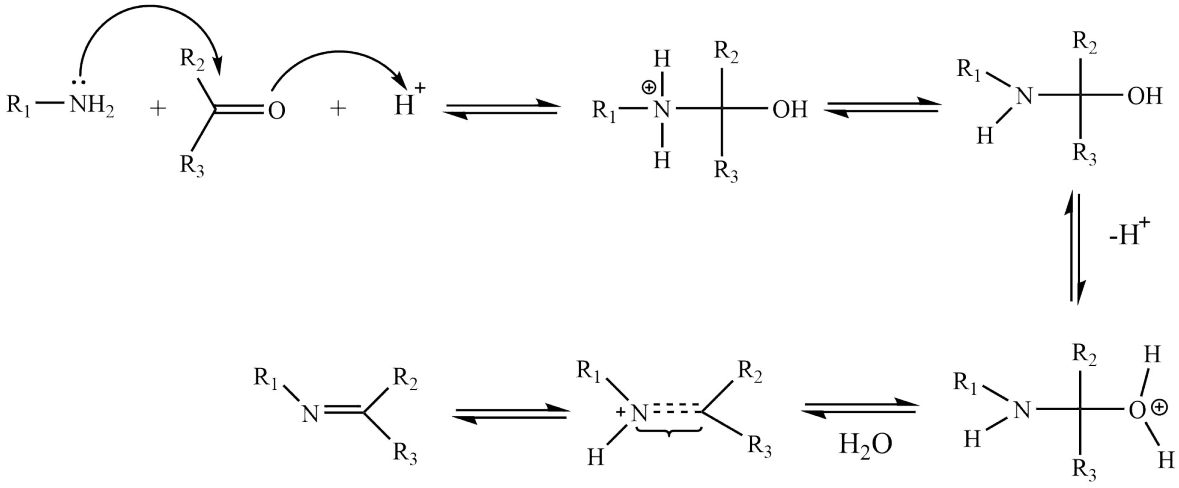

Figure 1.2: Illustration of the Schiff Base Formation Mechanism

It's important to note that Schiff bases involving aromatic amines and aromatic aldehydes benefit from greater stability due to conjugation. Conversely, Schiff bases derived from aliphatic aldehydes tend to be less stable and prone to polymerization [14, 15]. Furthermore, the Schiff base formation reaction is often reversible. Controlling reaction conditions like pH or the use of dehydrating agents can influence the equilibrium, favoring product formation.

1.2 Methods

Schiff base ligands can be prepared using an array of methods, including traditional techniques, microwave-assisted synthesis for speed, sonication, solid-supported methods for ease of separation, and natural acid catalysis for sustainability. Each method offers distinct advantages, allowing researchers to select the best approach for their goals [16].

1.2.1 Conventional method

Traditionally, Schiff bases are synthesized by refluxing equal molar quantities of a primary amine and an aldehyde in non-aqueous solvent. Acid catalysis is often used, and techniques like azeotroping aid in water removal to maximize yield. Final purification involves recrystallization or chromatography [17, 18].

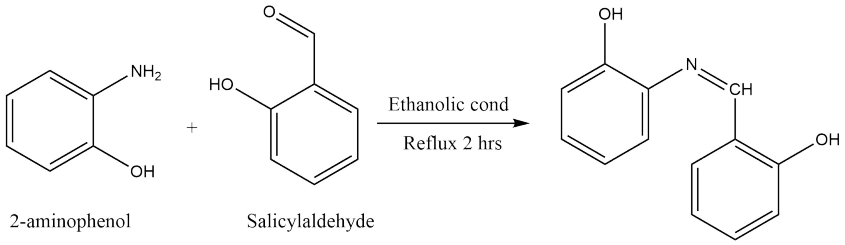

Figure 1.3: SB synthesis using conventional method

[19]

1.2.2 Using microwave irradiation

Microwave irradiation has emerged as a significant advancement in the synthesis of Schiff bases, offering a rapid and efficient alternative to traditional methods. This approach is characterized by its ability to accelerate the process, enhance yields, consume less energy, and reduce setup time. Microwave heating enables the use of eco-friendly solvents or even solvent-free conditions, enhancing catalytic reactions through rapid heating and efficient energy transfer to the reaction medium [20, 21].

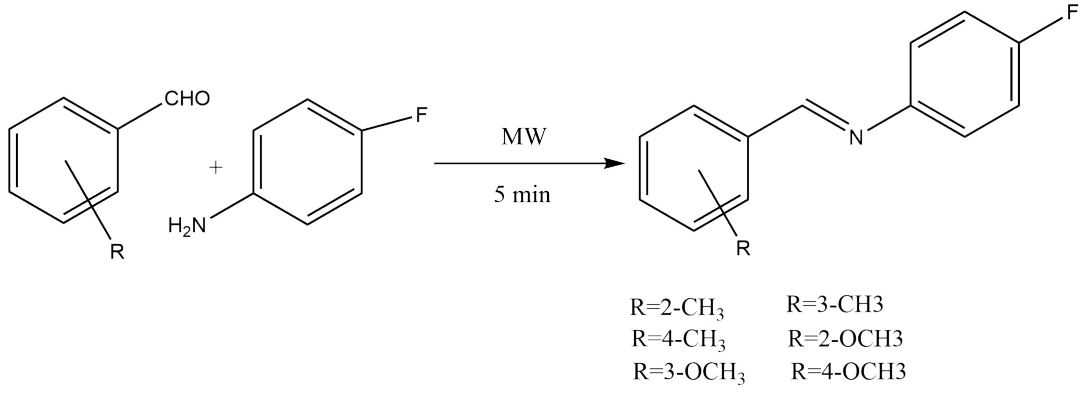

Figure 1.4: SB synthesis using microwave irradiation

[22]

1.2.3 Natural acid-catalyzed methods

The use of natural acids, like fruit juices, as catalysts has gained attention due to their benign environmental impact and low cost. These natural acids provide the necessary acidic environment for the reaction to proceed efficiently at room temperature [23, 18] .

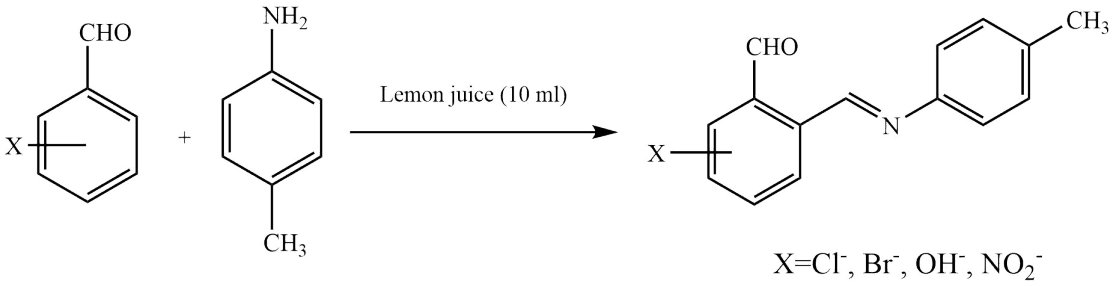

Figure 1.5: SB sunthesis using natural acid

[24]

1.2.4 Ultrasonic methods

Ultrasonication is used to excite particles, facilitating chemical reactions. This method has been shown to reduce reaction times and improve yields compared to traditional methods, benefiting from the high temperatures and pressures generated by ultrasonic waves. In laboratory settings, it is commonly used by utilizing an ultrasonic bath or probe, which is referred to as a sonicator [17, 20].

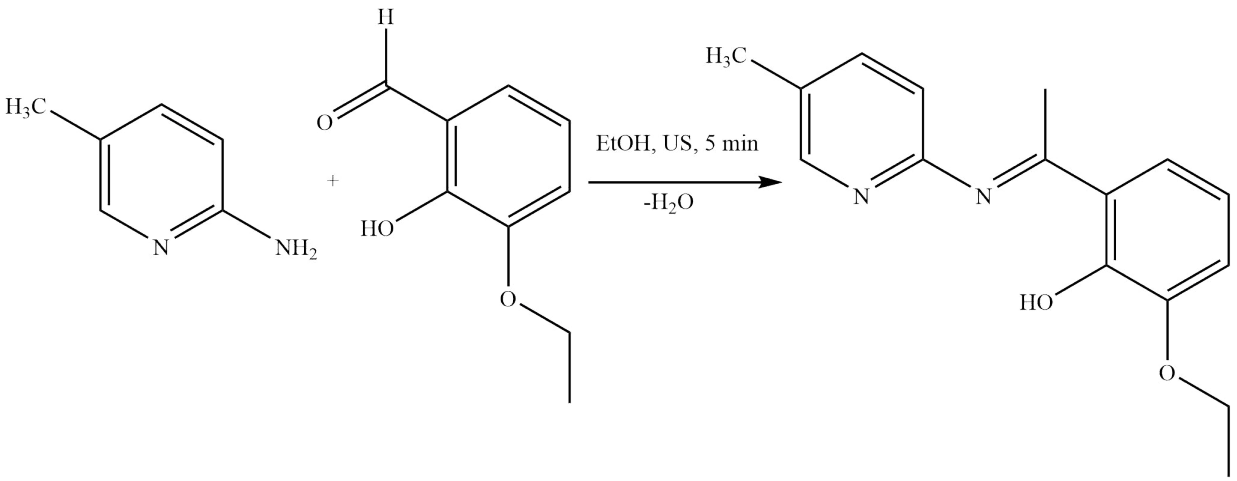

Figure 1.6: SB synthesis using ultrasonication

[25]

1.2.5 Grinding method

Solvent-free grinding, utilizing increased surface area and frictional heat, offers a green and potentially high-yielding approach to Schiff base synthesis. Catalysts like SnCl2 and CH3COOH further enhance reaction efficiency at room temperature. This method warrants exploration for sustainable synthesis of diverse Schiff bases [23].

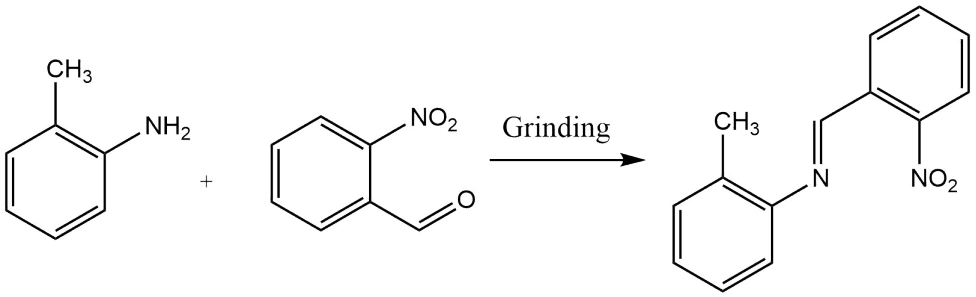

Figure 1.7: SB synthesis using grinding method

[26]

1.2.6 Magnetic nanoparticles

Magnetic nanoparticles, like Fe3O4, have garnered considerable attention as efficient and eco-friendly catalysts for the synthesis of Schiff bases in both solvent and solvent-free environments. This method boasts several advantages, including streamlined reaction procedures, significantly faster reaction times compared to conventional methods, and the ability to achieve high product yields. Additionally, the magnetic nature of the catalyst allows for its facile and loss-free recovery through simple magnetic separation, making it a highly reusable option [23, 17].

1.3 Chelating Properties of Schiff Bases

Schiff bases are excellent ligands in coordination chemistry due to their ability to act as Lewis bases. The azomethine nitrogen atom ($> C = N-$), with its lone pair of electrons, is the primary binding site for metal ions. The double-bonded azomethine system can also participate in π-backbonding with suitable d-orbitals on metal ions, further stabilizing the resulting complexes [11].

The formation of stable chelates with metal ions is enhanced when Schiff bases possess additional functional groups that facilitate the formation of five- or six-membered rings. Common chelating functionalities include hydroxyl (-OH), amine (-NH2), or sulfhydryl

(-SH) groups located near the azomethine group [20, 3].

Schiff base metal complexes often adopt tetrahedral or square planar geometries, depending on the specific ligand and metal ion involved. The properties of the complex are influenced by factors such as the metal ion's size, charge, and ionization potential [27]. Additionally, substituents on the Schiff base ligand can significantly modulate the basicity of the azomethine nitrogen, affecting how strongly it binds to the metal. This allows for fine-tuning of complex properties based on the choice of substituents [14].

Research has shown that the stability constants of Schiff base-metal complexes can vary depending on the nature of the ligand structure. Factors like the type of chelating groups, steric effects, and electronic effects associated with substituents can all play a role in determining complex stability .

1.4 Biological activity

The azomethine group has a lone pair of electrons on its nitrogen atom, which makes it chemically and biologically significant. sp2 hybridized nitrogens disrupt normal cell functions by forming a hydrogen bond with the active sites of cell components thereby inhibiting targeted diseases, enzymes or DNA replication [28, 5]. Schiff bases have shown versatil beneficial biological effects such as anti-inflammatory, pain-relieving, antimicrobial, anticonvulsant, antitubercular, anticancer, antioxidant, anthelmintic, antiglycation, and antidepressant activities. Figure 1.8 displays a pie chart that compares the different biomedical applications of Schiff bases [29].

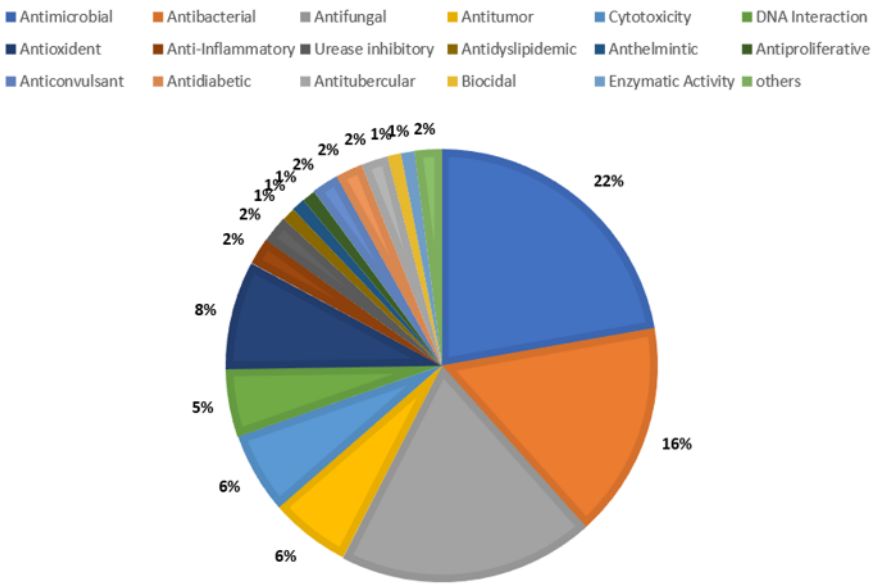

Figure 1.8: Comparison of publications on different biological activities

1.4.1 Antimicrobial activity

The global threat posed by multidrug-resistant pathogens demands the continuous exploration of novel antimicrobial agents [30]. Among the promising candidates, Schiff bases have emerged as intriguing contenders due to their diverse structural possibilities and demonstrated efficacy against various microbes [31, 32].

Schiff bases have been extensively studied for their ability to mimic the action of antibacterial drugs. They can disrupt bacterial cell walls by binding to key targets, compromising cell membrane integrity. Additionally, Schiff bases can interfere with bacterial DNA through intercalation, ultimately leading to cell death [33].

Souza et al. [34] investigated the effectiveness of 2-Salicylideneaminophenol (depicted in Figure 1.9) against Mycobacterium tuberculosis bacteria. This Schiff base compound demonstrated impressive potency, with a minimum inhibitory concentration (MIC) of just 8 micrograms per milliliter. Importantly, it also exhibited remarkable selectivity toward human macrophages. Even at high concentrations of 1000 micrograms per milliliter, over 80% of the macrophages remained viable, indicating minimal cytotoxicity.

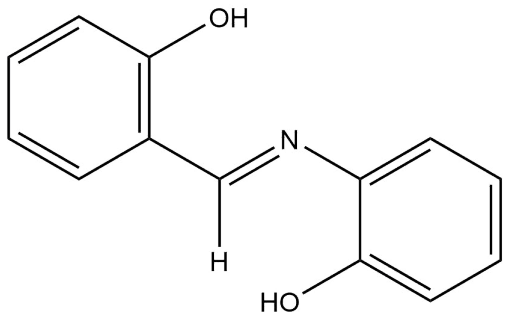

SB (1)

Figure 1.9: 2-Salicylideneaminophenol SB (1)

Turning to antifungal activity, Ejelonu et al. [35] (2018) compared the antifungal activity of N-Salicylideneaniline and N-Salicylidenesulphadiazine against 10 different fungal species (including Candida albicans, Aspergillus niger, and Fusarium oxysporium) to their corresponding metal complexes. Using the agar disk diffusion method with Mycotine as a positive control, the study found that both ligands exhibited antifungal activity against all 10 tested species. Notably, these ligands displayed larger inhibition zones than their metal complexes, suggesting superior antifungal effectiveness in this instance.

More recently, Yusuf et al. [26] (2020) synthesized and evaluated the antimicrobial activity of three SBs (2-4) against bacterial strains like E. coli, Salmonella typhimurium, and Pseudomonas aeruginosa. Notably, SB (3) displayed superior antibacterial activity, particularly against Gram-negative bacteria. Its minimum inhibitory concentration (MIC) against S. typhimurium and P. aeruginosa ($15.625\mu g/mL$ and $7.81\mu g/mL$, respectively) even surpassed that of the reference drug, chloramphenicol ($31.25\mu g/mL$ and $62.50\mu g/mL$, respectively). This suggests that compound 12 holds promise as a potential antibacterial agent, warranting further investigation.

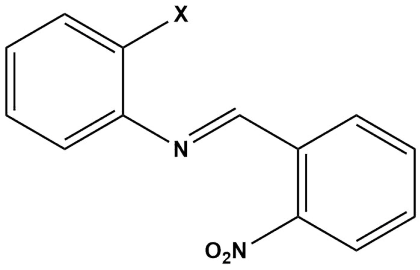

SB (2) : **X = CH3**
SB (3) : **X = CH $(CH3)_2$**
SB (4) : **X = OH**

Figure 1.10: Structure of compounds SB(2), SB(3) and SB(4)

In a 2020 study, Bayeh et al. [19] examined the antimicrobial activity of three newly synthesized Schiff bases (SBs) and compared them to established antibiotics like ciprofloxacin and chloramphenicol. Notably, one of the SBs (5) showed remarkable efficacy against both Gram-positive and Gram-negative bacteria, surpassing the reference drugs against Staphylococcus epidermidis and Pseudomonas aeruginosa. Specifically, its inhibition zone diameter (IZD) reached 32 mm compared to 24-26.7 mm for the references against S. epidermidis and 21.3-27.3 mm against P. aeruginosa. Additionally, another SB (6) exhibited superior activity against Staphylococcus aureus, with an IZD of 32.5 mm compared to 24-26.3 mm for ciprofloxacin and chloramphenicol.

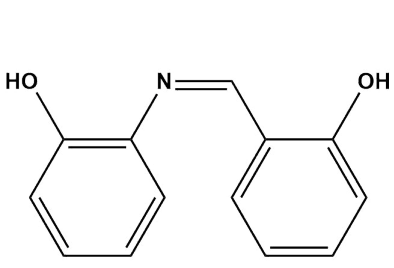

SB (5)

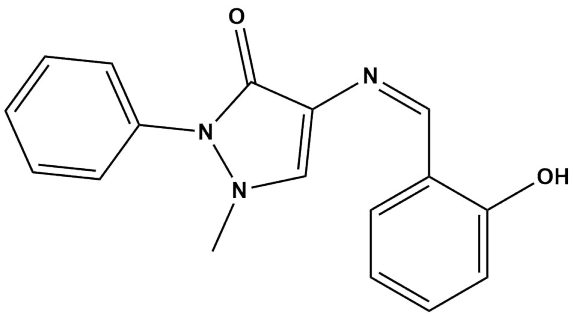

SB (6)

Figure 1.11: Structure of compounds SB(5) and SB(6)

In a 2021 study, Salihović et al. [36] synthesized two SBs (7 and 8) derived from L-cysteine and evaluated their antimicrobial activity against various bacteria and yeasts. Both compounds displayed effectiveness against both Gram-positive and) Gram-negative bacteria, but SB (7) was significantly more potent than SB (8), with a minimum inhibitory concentration (MIC) of 1.284 mM compared to 2.612 mM for SB (8). While both compounds displayed antifungal activity against Aspergillus brasiliensis, it was weaker compared to the reference drug amphotericin B. Overall, these results suggest that compound 22, with its broader and stronger antibacterial activity, has greater potential for further development as an antimicrobial agent.

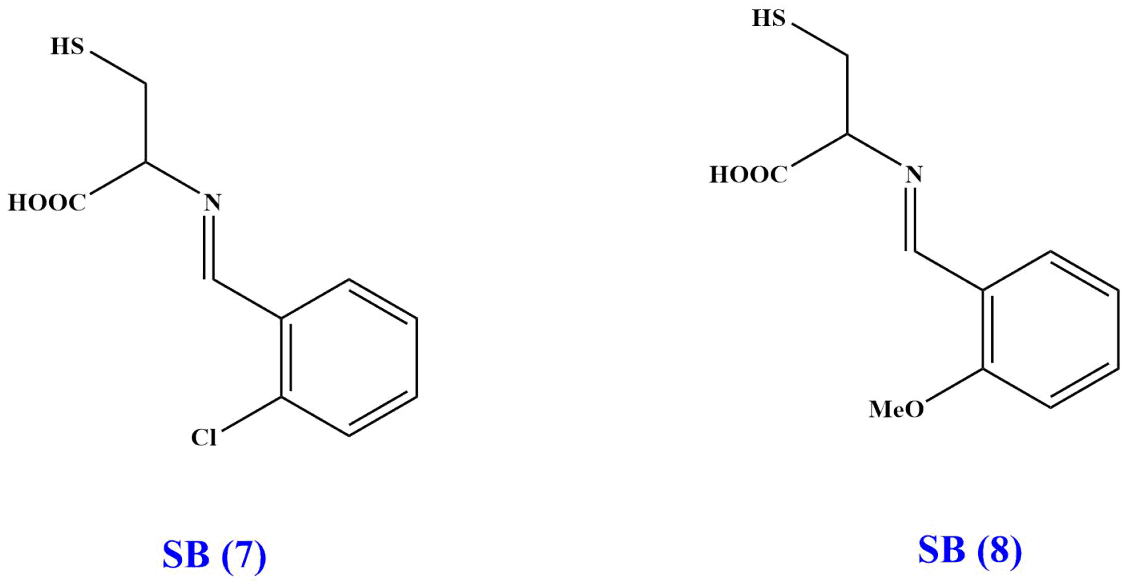

SB (7) **SB (8)**

Figure 1.12: Structure of compounds SB(7) and SB(8)

A study by Shi et al. [37] explored the potential of Schiff bases as antibacterial agents. The researchers created several Schiff bases by combining 5-chloro-salicylaldehyde with different primary amines and tested their effectiveness against various bacterial strains. Excitingly, most of these newly created compounds showed activity against at least one bacteria. SB (9) showed the most favorable antimicrobial activity

Among the tested bacteria, Pseudomonas fluorescence was particularly susceptible to these Schiff bases. SBs (10-15) and (16-18) were especially effective, even outperforming the established antibiotic kanamycin. Their minimum inhibitory concentrations (MICs), which signify the amount needed to inhibit bacterial growth, ranged from 2.5 to $5.2\mu g/mL$, compared to kanamycin's $3.9\mu g/mL$. Similarly, against Escherichia coli, SBs 10, 11, 13-15, 17, and 18 displayed promising activity with MICs between 1.6 and $5.7\mu g/mL$, again exceeding kanamycin's performance. Even against Staphylococcus aureus, although less

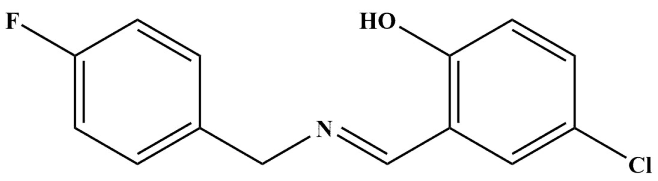

SB (9)

Figure 1.13: Structure of compound SB(12)

potent, some Schiff bases like compounds 6 and 7 showcased moderate activity. Only SB (17) showed activity against Bacillus subtilis.

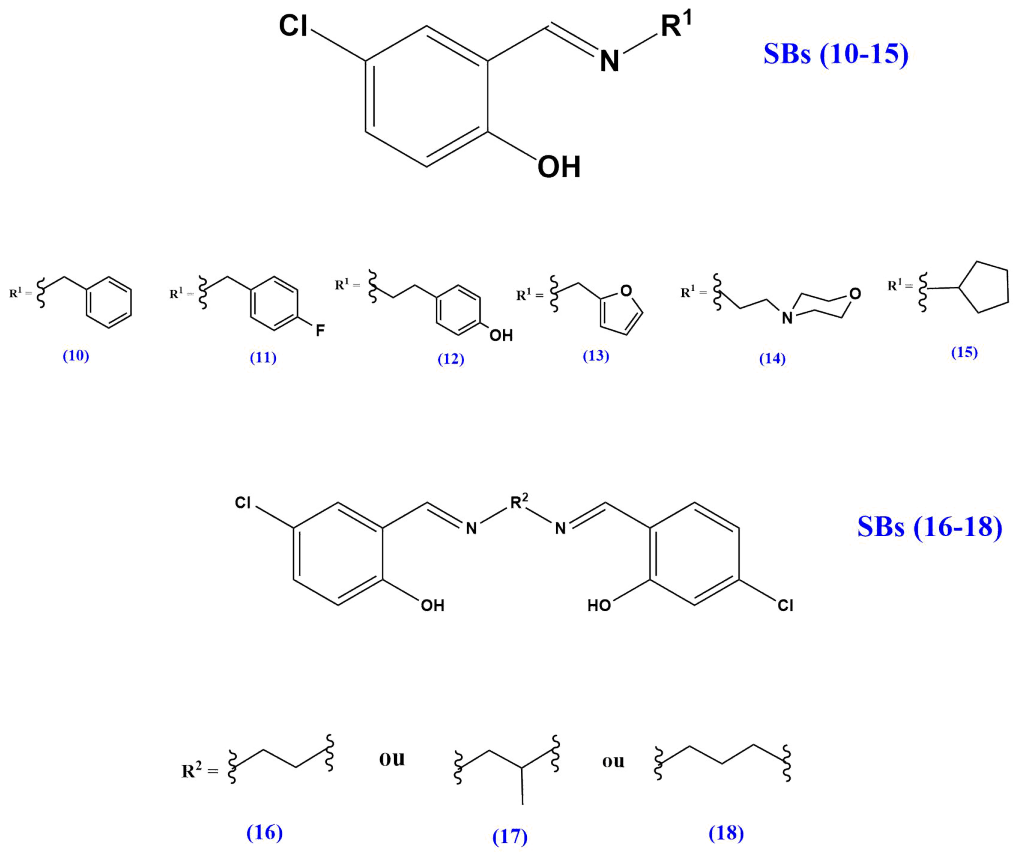

Figure 1.14: Structure of SBs (10-18)

Researchers also explored the antibacterial potential of eight newly synthesized SBs (19-26) derived from salicylaldehyde and various amines [38]. These compounds displayed promising activity against all tested bacterial strains, ranging from moderate to good effectiveness. While most demonstrated minimum inhibitory concentrations (MICs) between $100 - 200\mu g/mL$, some shone brighter, exhibiting notable activity at remarkably low concentrations of 50 µg/mL against specific bacteria. For instance, SB (19) effectively targeted P. aeruginosa (1) at $50\mu g/mL$, while SB (21) displayed impressive broad-spectrum activity against P. aurantiaca, P. aeruginosa (1), E. coli (2), S. typhi (2), and C. freundii, also at $50\mu g/mL$. Similarly, SB (22) excelled against E. coli (2), S. typhi (1), and S. maltophilia, and SB (23) specifically targeted K. pneumoniae and S. typhi (2), both with a $50\mu g/mL$ MIC. Remarkably, SB (24) inhibited P. aeruginosa (3) and C. freundii, and SB (25) tackled E. cloacae and A. lipoferum, each at $50\mu g/mL$. Finally, SB (26) targeted E. coli (2) with the same low concentration.

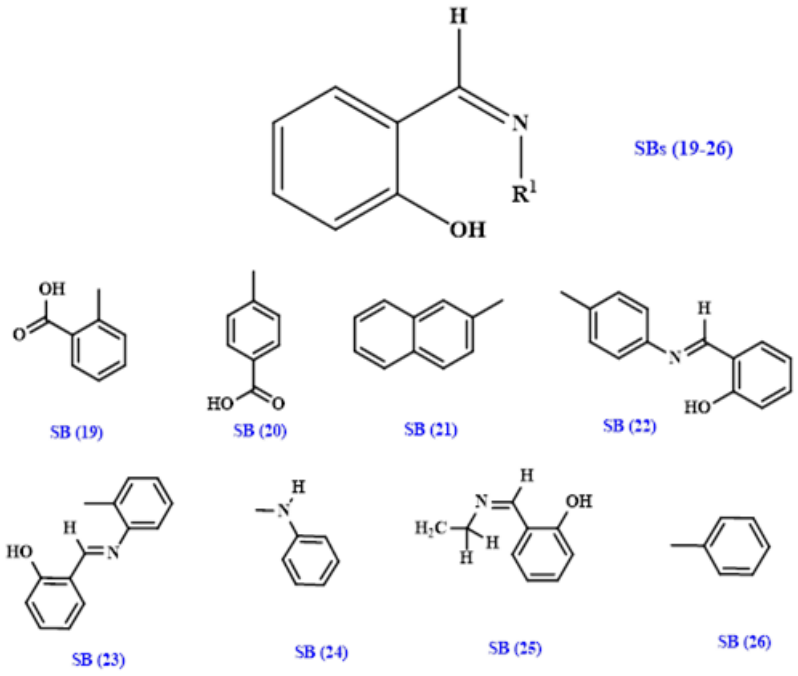

Figure 1.15: Structure of SBs (19-26)

1.4.2 Antioxidant activities

Antioxidants, molecules with high free radical scavenging capacity, play a vital role in reducing oxidative stress within living organisms. They achieve this by hindering the oxidation of susceptible substrates, ultimately protecting macromolecules and cells from free radical-induced damage [39]. Consequently, the discovery and development of novel antioxidant agents has witnessed increased research interest in recent years [15].

Schiff bases have emerged as promising candidates in this pursuit. Recent studies have demonstrated their capacity to scavenge reactive oxygen species (ROS), which encompass free radicals, highlighting their potential as antioxidants [40, 15, 41, 42].

Schiff bases are frequently cited for their ability to scavenge free radicals, with hydroxyl and amino groups playing a key role in donating hydrogen atoms to neutralize species like DPPH. When Schiff bases form metal complexes, a potential decrease in antioxidant activity is observed, likely due to the deprotonation of hydroxyl groups during coordination. However, other non-coordinating substituents on the Schiff base ligand might retain their ability to donate hydrogen atoms and act as free radical scavengers [43].

Aslam et al. [44] reported the synthesis of six Schiff bases derived from 2-aminophenol and various chloro- and nitro-benzaldehydes (27). These newly synthesized compounds

displayed remarkable antioxidant activity using the DPPH assay, with $IC50$ values range from 17.2 to $33.1\mu M$, exceeding the activity of the standard BHA. Additionally, they were assessed for antibacterial, lipoxygenase, and urease inhibitory potential.

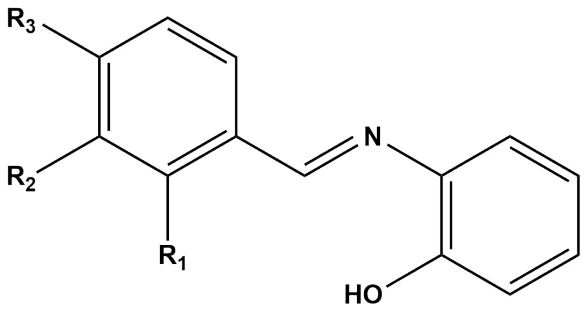

SB (27)

Figure 1.16: Structure of compound SB (27)

A study by Mermer et al. [45] investigated the antioxidant potential of novel Schiff base analogues derived from 4-methyl aniline and 3-chloro, 4-fluoro aniline [11]. They employed three different assays: DPPH, CUPRAC, and FRAP, to comprehensively evaluate antioxidant activity. Intriguingly, the Schiff bases (29, 30) exhibited superior antioxidant activity compared to those from SB 28. Among these, SBs (28-30) displayed particularly impressive results. In the DPPH assay, their IC50 values were significantly lower than the standard Trolox, indicating much stronger antioxidant capacity. Similarly, they outperformed other compounds in the FRAP and CUPRAC assays.

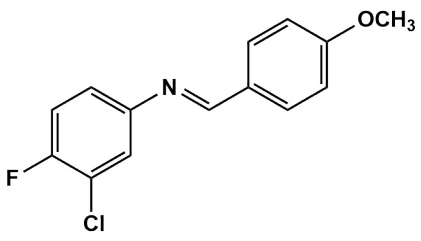

SB (28)

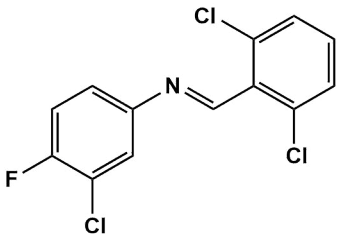

SB (29)

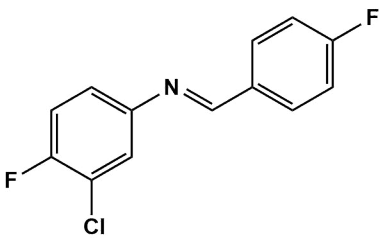

SB (30)

Figure 1.17: Structure of SBs (28-30)

A study by Alaşalvar et al. [46] explored the antioxidant properties of two newly synthesized Schiff bases (31-32). Employing diverse methods like ferric reducing antioxidant power (FRAP), hydrogen peroxide scavenging (HPSA), free radical scavenging (FRSA), and ferrous ion chelating activities (FICA), they comprehensively assessed their antioxidant potential. The findings revealed impressive results. Compared to established

antioxidant standards like BHA, BHT, and α-tocopherol, both SBs (31-32) displayed significantly higher activity across all employed methods. This suggests that these newly synthesized Schiff bases possess remarkable antioxidant potential, potentially exceeding current options.

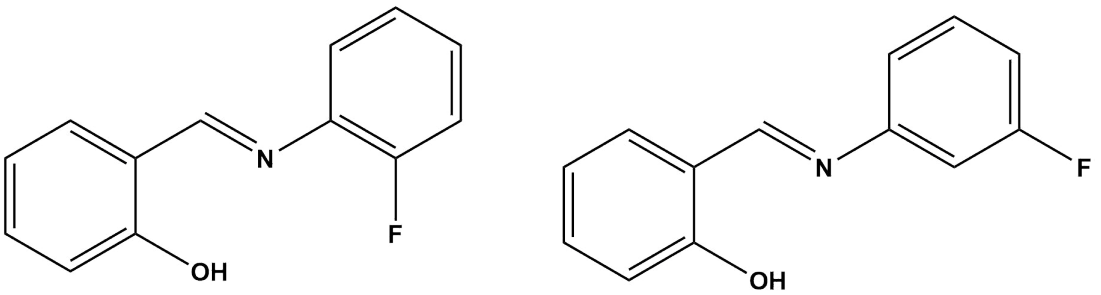

SB (31) **SB (32)**

Figure 1.18: Structure of SBs (31,32)

ŞENOCAK and AKBAŞ [47] investigated the antioxidant properties of two newly synthesized SBs (33,34) and their palladium complexes. Using the DPPH scavenging assay, they assessed the ability of these compounds to neutralize free radicals. The results showed impressive antioxidant activity for both SBs (33) and (34), with SB (34) even surpassing the standard Trolox. However, complexation with palladium had a negative impact on the antioxidant capacity of the studied compounds.

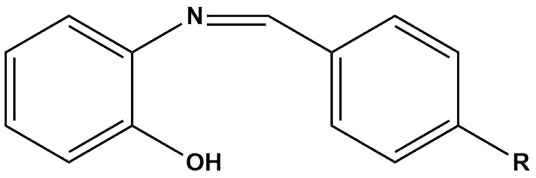

SB (33) : R = OH
SB (34) : R = OCH_3

Figure 1.19: Structure of SBs (33,34)

1.4.3 Anticancer activity

Cancer remains a significant public health challenge globally, with existing chemotherapeutic drugs often associated with severe side effects. The pursuit of more effective chemotherapeutic agents has led researchers to explore non-platinum-based complexes, with Schiff base derivatives emerging as promising candidates for their anticancer properties [48, 33].

Schiff bases have demonstrated notable anticancer activity, with various studies highlighting their potential effectiveness against different types of cancer cells:

Kratky et al. [49] developed a series of novel Schiff bases derived from sulfadiazine and salicylaldehydes. These compounds were investigated for their ability to combat liver cancer cells $(HepG2)$, as well as their antibacterial and antifungal properties.

Kaur et al. [50] developed a series of diazenyl Schiff bases and evaluated their potential for both anticancer and antimicrobial applications. The compounds were tested against HCT-116 colorectal cancer cells and screened for their ability to fight various bacterial and fungal strains.

Karthik et al. [51] reported the synthesis of Schiff bases of 4-(methylthio)benzaldehyde derivatives SB (35) , which were characterized using spectroscopic techniques. The compounds' cytotoxicity against cancer cells was evaluated, and additional investigations into their antioxidant and antibacterial activities were conducted.

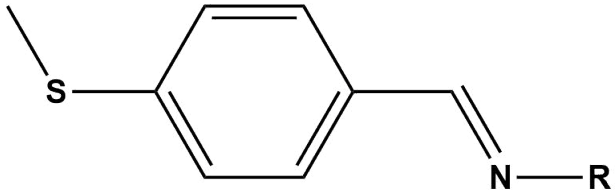

SB (35)

Figure 1.20: Structure of compound SB (35)

Luo et al. [52] successfully synthesized a series of benzaldehyde Schiff bases derived from salicylaldehyde and various diamines. These compounds were subsequently evaluated for both antitumor and antimicrobial potential. Antitumor activity was assessed using the MTT assay, revealing that the salicylaldehyde-o-phenylenediamine Schiff base exhibited selective growth inhibition against $K562$ and HEL leukemia cell lines. Further analysis yielded its $IC50$ value. In a separate assessment, the $salicylaldehyde\breve{}hydrazine$ hydrate Schiff base demonstrated notable microbicidal activity against S. aureus.

Taş et al. [53] synthesized a diverse range of Schiff bases through the condensation of amino acids and salicylaldehyde derivatives (29-37) [see Fig. 1.3]. These compounds were extensively evaluated for their anticancer potential using MTT and LDH assays against various cancer cell lines $(HT29, HeLa, MCF7, A549, C6, Hep3B)$ and normal cells $(FL, Vero)$. SB (39) demonstrated the most powerful and selective anticancer activity $(IC505.72 - 46.35\mu g/ml)$, making it a promising lead for further investigation.

Researchers synthesized a series of 18 Schiff bases through the reaction of substituted 2-amino benzothiazole and substituted benzaldehyde [54]. These compounds were evaluated for their cytotoxic potential against HeLa cells using the MTT assay. Of partic-

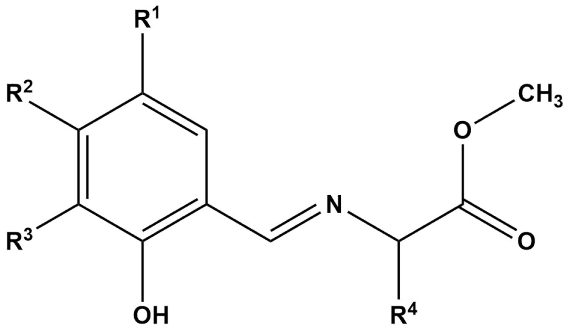

SB (36-44)

SB	R1	R2	R3	R4
(36)	Br	H	H	CH3CH2(CH3)CH
(37)	H	OH	H	CH3CH2(CH3)CH
(38)	H	H	OCH3	CH3CH2(CH3)CH
(39)	Br	H	H	PhCH2
(40)	H	OH	H	PhCH2
(41)	H	H	OCH3	PhCH2
(42)	Br	H	H	CH3SCH2CH2
(43)	H	OH	H	CH3SCH2CH2
(44)	H	H	OCH3	CH3SCH2CH2

Figure 1.21: Structure of SBs (36-44)

ular interest, Schiff base, containing a methoxy group, demonstrated impressive activity $(IC502.517\mu g/ml)$ surpassing that of the standard drug cisplatin. Additionally, SBs, incorporating hydroxyl and thiol groups, respectively, exhibited notable cytotoxicity with $IC50$ values below $25\mu g/ml$.

Chapter 2

Antioxidants and Antioxidants Methods

Introduction

Cellular damage, a relentless consequence of reactive oxygen species (ROS) attacks, lies at the core of numerous debilitating diseases. Oxidative stress, stemming from an imbalance between ROS generation and their neutralization, plays a critical role in chronic conditions like neurodegeneration, cardiovascular disease, and cancer. Thankfully, antioxidants offer a line of defense. While naturally occurring antioxidants provide valuable protection, synthetic antioxidants hold unique advantages. Specifically, their potential to be tailored with precise properties and mechanisms of action makes them a powerful tool in combating oxidative damage.

This chapter delves into the multifaceted applications of synthetic small-molecule scavengers. We will explore their chemistry, diverse mechanisms of action, and applications across various fields. Importantly, this chapter will also address the complexities of translating promising research into effective therapies, emphasizing critical safety considerations.

2.1 Free Radicals and Oxidative Stress

Free radicals, possessing an unpaired electron, are highly reactive chemical species generated through both metabolic processes (energy production in the mitochondria Immune responses, inflammation, and certain enzymes) and environmental exposures (pollutants, UV radiation, smoking, heavy metals, and certain medications) [55, 2, 56]. While playing crucial physiological roles [57, 58], excessive free radical production contributes to cellular damage and the pathogenesis of various diseases [59, 60, 61].
Reactive oxygen species (ROS) encompass a broader category, including free radicals like

superoxide anion ($O2^{\bullet -}$) and hydroxyl radical ($OH^{\bullet}$), as well as non-radical molecules like hydrogen peroxide ($H2O2$) [1].

Reactive nitrogen species (RNS), such as nitric oxide ($NO^{\bullet}$) and peroxynitrite ($ONOO^{-}$), also play significant roles in biological systems and disease. While $NO^{\bullet}$ functions as a signaling molecule, the highly reactive $ONOO-$ can cause similar types of oxidative damage as ROS [2].

2.1.1 The Essential and Detrimental Roles of ROS

ROS exhibit a dual nature within biological systems [2, 62]:

Physiological Functions:

At controlled levels, ROS are integral to [63, 64]:

- Immune Defense: Phagocytic cells employ ROS bursts to eliminate invading pathogens.
- Cellular Signaling: ROS modulate various signaling pathways involved in cell proliferation, differentiation, and adaptive stress responses.

Mechanisms of Damage:

When ROS generation exceeds antioxidant capacity, they can inflict damage on essential biomolecules [1, 65]:

- DNA: ROS induce oxidative modifications to bases (e.g., 8-oxo-7,8-dihydroguanine), as well as single- and double-strand breaks, potentially leading to mutations and genomic instability.
- Lipids: Lipid peroxidation, primarily targeting polyunsaturated fatty acids in cellular membranes, disrupts membrane fluidity, permeability, and downstream signaling events. Aldehydes generated during this process, such as malondialdehyde (MDA) and 4-hydroxynonenal (HNE), can further exacerbate oxidative damage.
- Proteins: ROS promote protein oxidation, leading to carbonylation, fragmentation, and cross-linking. These modifications compromise protein structure, function, and turnover, potentially contributing to the formation of cytotoxic aggregates.

The destructive potential of free radicals lies in their ability to set off chain reactions, as illustrated in Figure 2.1 [66]. The process begins with the initiation stage, where an external factor or internal process generates a free radical. This highly reactive molecule then attacks a nearby stable molecule in the propagation stage, stealing an electron and generating another free radical in the process. This new free radical goes on to attack another stable molecule, continuing the chain reaction. The cycle is only broken in the

termination stage, when two free radicals react with each other or when antioxidants intervene [65, 39].

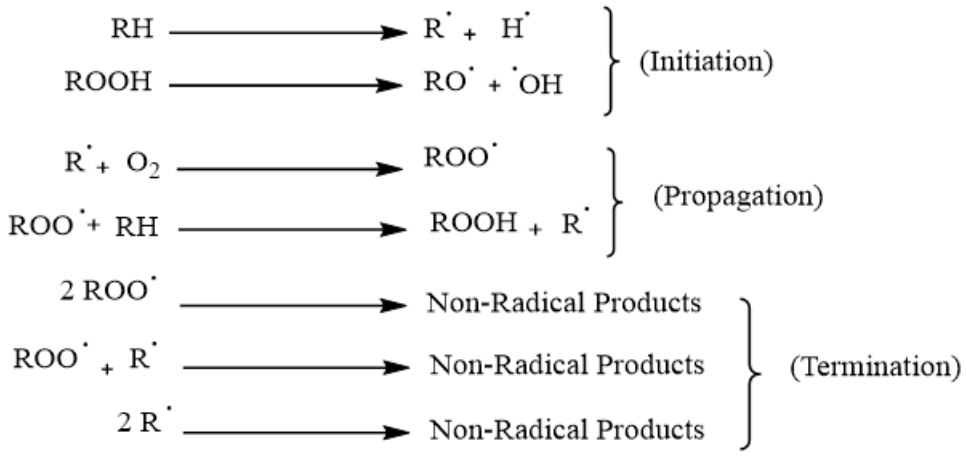

Figure 2.1: Free chain reactions

2.1.2 Oxidative Stress: A Pathogenic Imbalance

Oxidative stress arises when the dynamic equilibrium between ROS generation and endogenous antioxidant defenses is disrupted in favor of the former [58]. This imbalance is implicated in the pathogenesis of numerous chronic diseases [1], including:

- Cardiovascular diseases: Oxidative stress promotes endothelial dysfunction, inflammation, and atherogenesis [67].
- Neurodegenerative diseases: ROS-induced damage to neurons and glial cells plays a key role in Alzheimer's, Parkinson's, and other neurodegenerative disorders [68].
- Cancer: Oxidative stress can contribute to both the initiation and progression of cancer through DNA damage, altered cell signaling, and proliferation [60].
- Inflammatory and autoimmune diseases: Chronic inflammation and dysregulated immune responses are closely intertwined with excessive ROS production [69].

Understanding the sources, mechanisms, and consequences of free radicals and oxidative stress underscores the crucial importance of antioxidants. Antioxidants, including those derived from natural sources and those designed in the laboratory (synthetic antioxidants), act as scavengers to neutralize free radicals and protect our cells from their damaging effects.

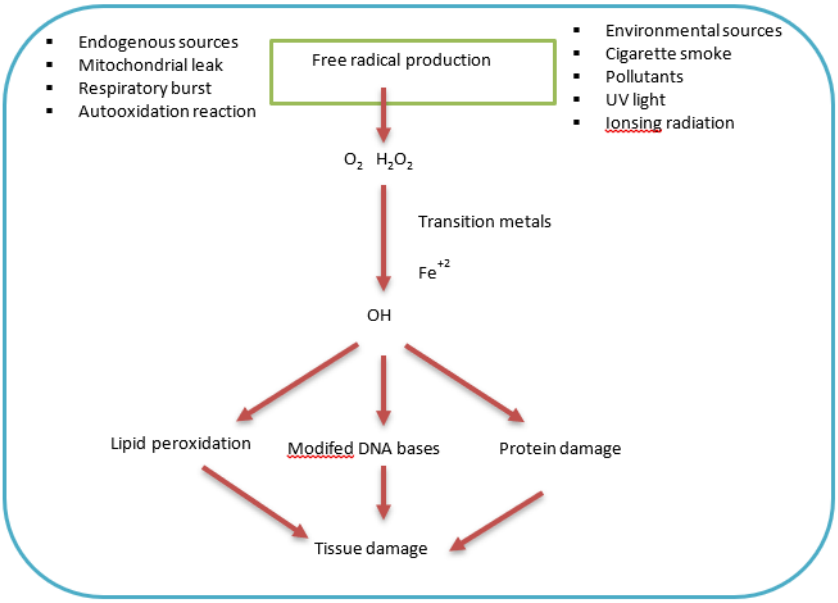

Figure 2.2: Main sources of free radicals

[66]

2.2 Antioxidants: Defense Against Oxidative Stress

2.2.1 Definition

Antioxidants are a diverse group of molecules that protect our cells and biological systems from the damaging effects of free radicals and other reactive species. While traditionally focused on reactive oxygen species (ROS), antioxidants also combat harmful reactive nitrogen species (RNS) and reactive sulfur species (RSS) [70, 71].

2.2.2 Types of Antioxidants

Antioxidants can be classified in various ways based on their source, mechanism of action, location, and other factors [See Figure 2.3] [56, 72, 62]. For this section, we'll focus on the following key categories to provide a foundation for understanding both natural and synthetic antioxidant systems:

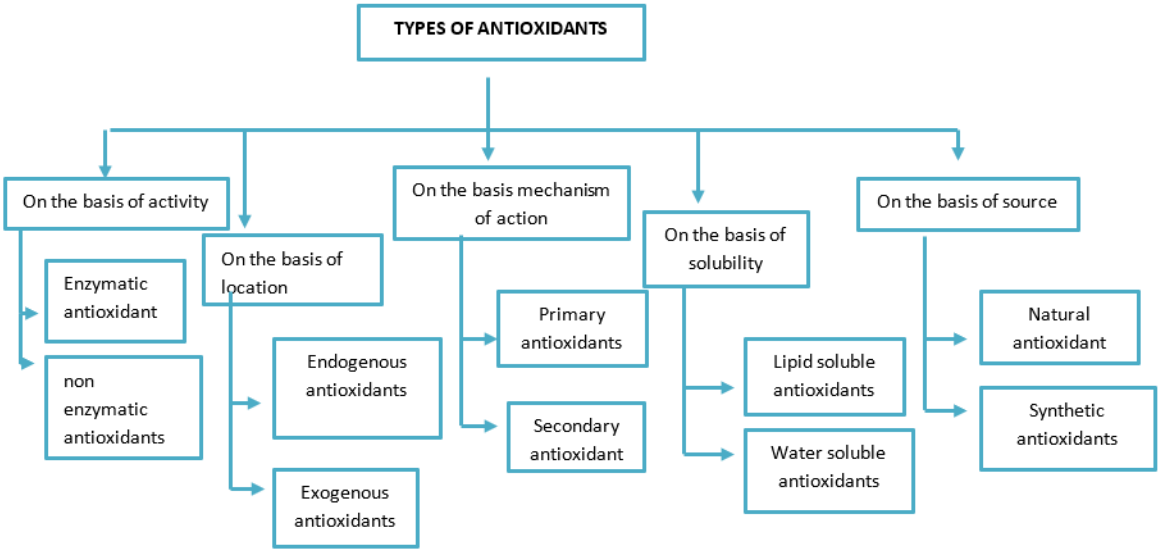

Figure 2.3: Types of Antioxidants

2.2.2.1 Endogenous Antioxidant Enzymes

These enzymes are naturally produced within our cells to neutralize free radicals and prevent oxidative damage. Key examples include:

- **Superoxide Dismutase (SOD):** This family of enzymes plays a vital role in converting the highly reactive superoxide radical $(O2^{\bullet -})$ into hydrogen peroxide $(H2O2)$ [39, 1, 2].

$$2O_2^{\bullet -} + 2H^+ \xrightarrow{SOD} H_2O_2 + O_2$$

- **Catalase (CAT):** Predominantly found within cells, this enzyme efficiently breaks down hydrogen peroxide into water and oxygen, providing a second line of defense [39, 1, 2].

$$2H_2O_2 \xrightarrow{Catalase} 2H_2O + O_2$$

- **Glutathione Peroxidase (GPX):** This enzyme protects against damage, particularly within cell membranes, by reducing hydrogen peroxide and lipid peroxides [39, 1, 2].

$$H_2O_2 + 2GSH \longrightarrow 2H_2O + GSSG$$

$$ROOH + 2GSH \xrightarrow{GP_x} ROH + H_2O + GSSG$$

2.2.2.2 Non-Enzymatic Endogenous Antioxidants

These antioxidant molecules are produced within our bodies and work alongside enzymes to provide additional protection against free radicals. These include:

- **Glutathione (GSH):** This tripeptide is a primary internal antioxidant, capable of directly neutralizing free radicals and regenerating other antioxidants for continued protection [71, 1, 2].
- **Uric Acid:** Although it can have pro-oxidant effects under certain conditions, uric acid primarily acts as an antioxidant scavenger [72].
- **Other Endogenous Antioxidants:** Our bodies also produce bilirubin, melatonin, lipoic acid, and coenzyme Q10, which contribute to antioxidant defenses in various ways [72, 2].

2.2.2.3 Exogenous Non-Enzymatic Antioxidants

Exogenous antioxidants, obtained through dietary sources or supplementation, bolster the body's inherent antioxidant defenses. These compounds provide multifaceted protection through various mechanisms of action. They fall into two primary categories:

Natural Antioxidants Derived primarily from plant-based foods, they offer a rich source of antioxidant compounds including:

- **Vitamins:** Key antioxidant vitamins include:
  - Ascorbic Acid (Vitamin C): This water-soluble vitamin exhibits potent ROS scavenging activity, particularly against hydroxyl, peroxyl, and superoxide radicals. Ascorbic acid also regenerates other antioxidants (like vitamin E) and acts as an enzymatic cofactor in antioxidant defenses [72, 2].
  - Tocopherols and Tocotrienols (Vitamin E): These lipid-soluble compounds effectively protect cellular membranes from lipid peroxidation and play a role in neutralizing singlet oxygen [71, 72, 2].
  - Provitamin A Carotenoids (e.g., Beta-carotene, Lycopene): This class of antioxidants offers strong scavenging capabilities against singlet oxygen and peroxyl radicals, contributing to membrane protection and reducing oxidative damage [71, 2].
- **Phenolic Compounds:** This vast and chemically diverse class encompasses:
  - Flavonoids (e.g., Quercetin, Catechins, Anthocyanins): Flavonoids offer multifactorial antioxidant protection, including direct ROS scavenging, metal ion chelation, and the ability to influence antioxidant gene expression [2, 73].

- Phenolic Acids (e.g., Caffeic Acid, Ferulic Acid): These compounds function as radical scavengers, metal chelators, and upregulators of endogenous antioxidant systems [74, 73].
- Other Phenolics (e.g., Curcumin, Resveratrol): Numerous plant-derived phenolics exhibit unique antioxidant properties alongside potential anti-inflammatory and chemopreventive activities [74].

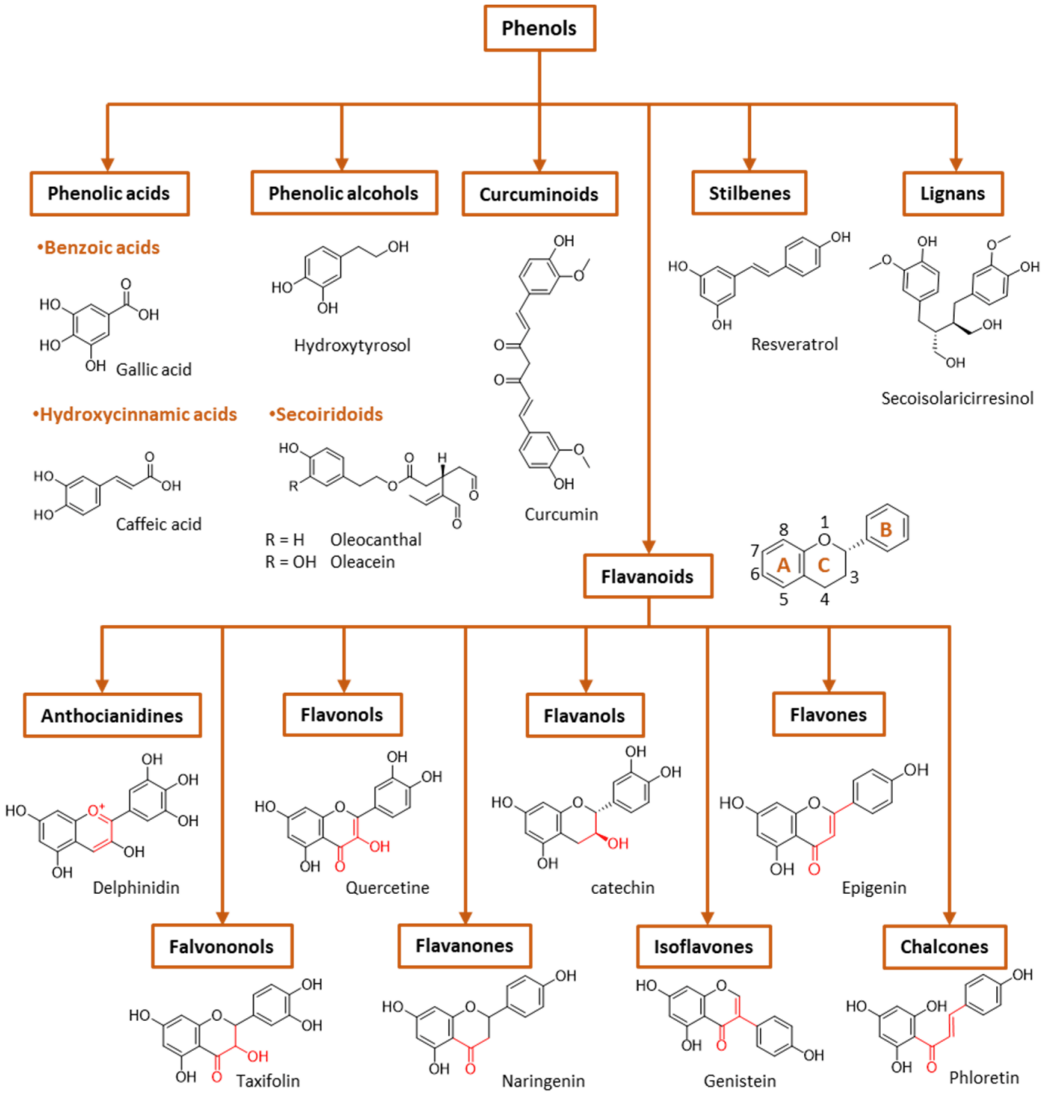

Figure 2.4: General classification of polyphenols.

Synthetic Antioxidants Human-made chemical compounds that prevent or delay the oxidation of other substances. Synthetic antioxidants can mimic naturally occurring antioxidants or have completely novel structures. [62, 56, 75]:
Many synthetic antioxidants are low-molecular-weight molecules. This means they have a relatively small size and simple chemical structure. Because of this, they easily penetrate

materials and interact with other molecules. They have different chemical structures, such as alcohols/diols, phenols, benzene derivatives, isoprenoids, aldehydes, amino acid derivatives, indole-amines, fatty acid derivatives, etc., as depicted in Figure 2.5. [76].

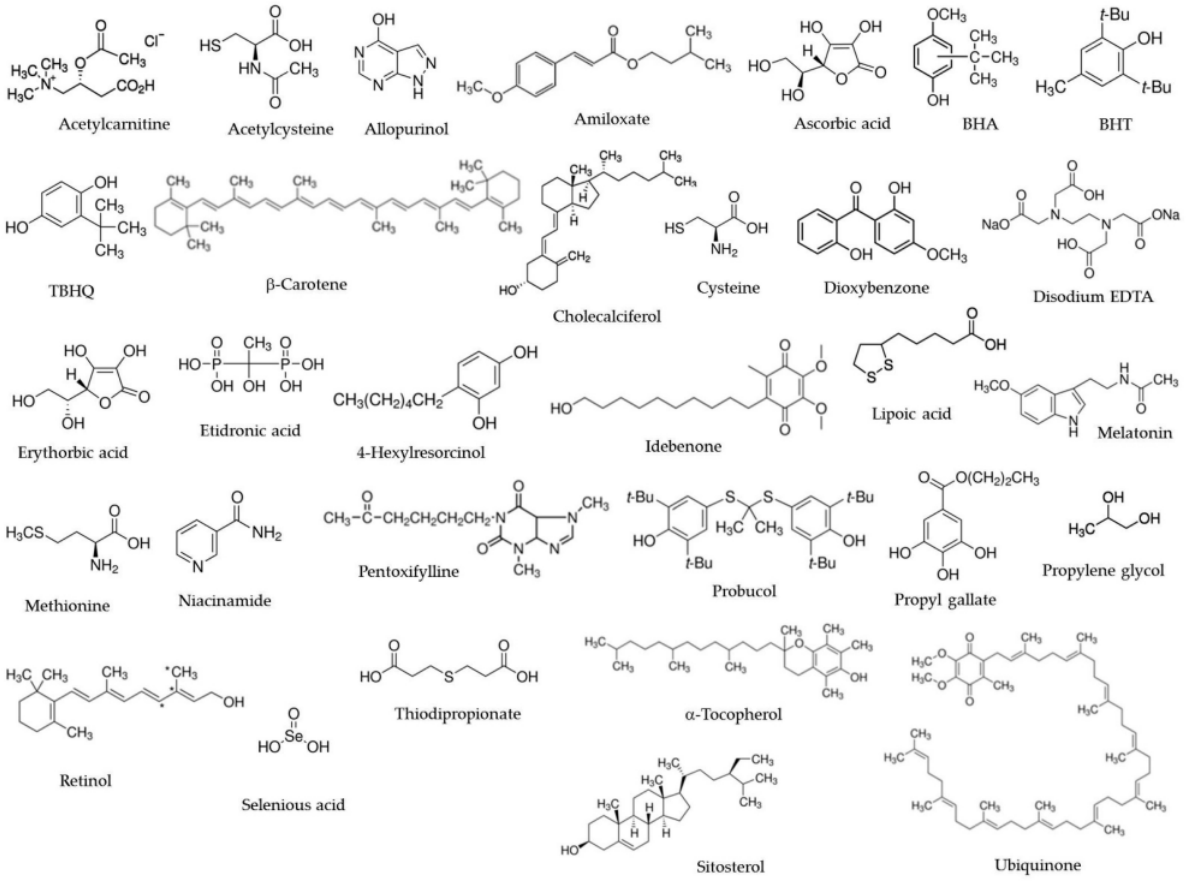

Figure 2.5: Chemical structure of approved principal synthetic low-molecular-weight antioxidants

2.2.3 Mechanisms of Action

2.2.3.1 Free Radical Scavenging

Direct scavenging is a crucial mechanism by which antioxidants protect cells, disrupting the damaging chain reactions initiated by free radicals. The most prominent mechanisms for free radical scavenging are [39]:

Hydrogen Atom Transfer (HAT): Antioxidants with available hydroxyl groups $(-OH)$ or other labile hydrogen atoms donate a hydrogen atom (with its electron) to a free radical. This transforms the radical into a more stable molecule, effectively breaking oxidative chain reactions [66, 70].

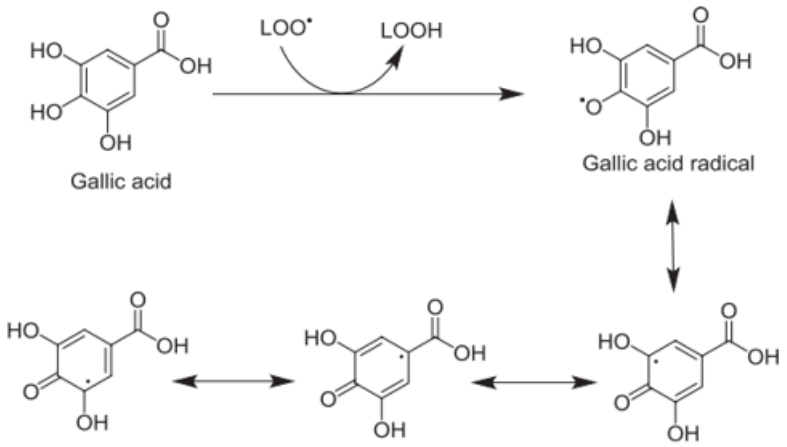

Figure 2.6: The reaction of gallic acid with free radicals and its stabilization of gallic acid-free radical.

Single Electron Transfer (SET): Here, an antioxidant donates a single electron to the free radical, again stabilizing it [66, 70].

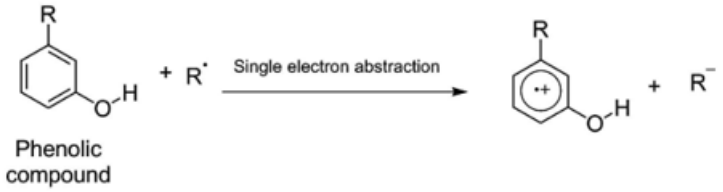

Figure 2.7: Mechanism of single-electron abstraction reaction (SET).

Sequential Proton Loss Electron Transfer (SPLET): In this mechanism, the antioxidant first donates a proton (H+) to a free radical, transforming it into an anion. This anion then readily donates an electron to stabilize itself. SPLET is particularly relevant for antioxidants with acidic functional groups under specific pH conditions [See Figure 2.8][66].

2.2.3.2 Metal Ion Chelation

Metal ions like iron and copper can catalyze free radical generation (eq).

$$Fe^2 + (or\ Cu^+) + H_2O_2 \rightarrow Fe^{3+}(or\ Cu^{2+}) + OH + OH^- \quad (1)$$

Antioxidants capable of metal chelation bind these ions, preventing their participation in harmful reactions. Compounds that contain multiple oxygen, nitrogen, or sulfur atoms often have chelating abilities [66, 77].

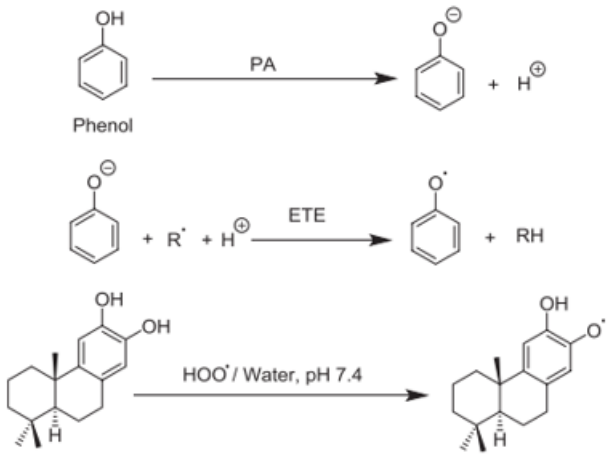

Figure 2.8: Mechanism of sequential proton loss electron transfer (SPLET).

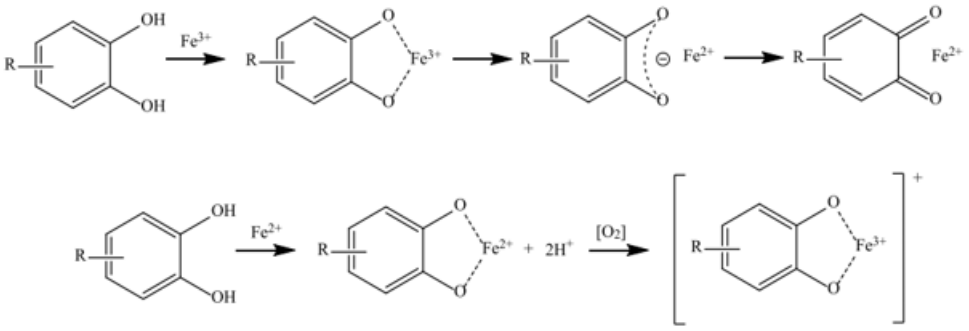

Figure 2.9: Phenolic acid derivated chelating Fe^3 and Fe^2

[73, 78]

2.2.3.3 Enzyme Modulation

Antioxidants can influence enzymes that either promote free radical generation (e.g., NADPH oxidase) or participate in antioxidant defense systems (e.g., superoxide dismutase, catalase) [39, 77, 71].

2.2.4 Methods for Evaluating Antioxidant Activity

Understanding the efficacy of natural and synthetic antioxidants is critical for their selection and application. A diverse array of assays exists, each illuminating specific aspects of antioxidant action. Here's an overview of widely used methods:

2.2.4.1 DPPH Assay (2,2-diphenyl-1-picrylhydrazyl)

The DPPH assay is a classic method that measures the ability of an antioxidant to scavenge and neutralize the stable DPPH radical (deep purple). This involves hydrogen atom transfer (HAT) and/or single electron transfer (SET) mechanisms. The color change from purple to yellow indicates antioxidant capacity. It is commonly used to test compounds like Vitamin C, flavonoids, phenolic acids, and food samples [62, 70, 73, 78].

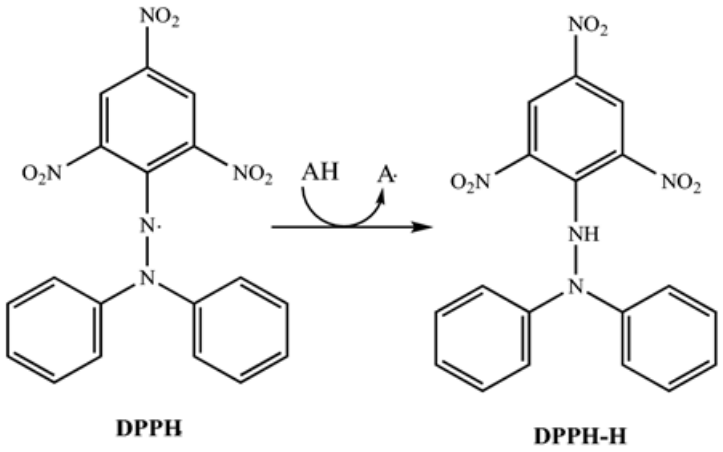

Figure 2.10: Theorical mechanism of DPPH in the presence of an antioxidant.

2.2.4.2 ABTS Assay (2,2'-azinobis (3ethylbenzothiazoline-6-sulfonic acid))

The ABTS assay works on a similar principle as DPPH but utilizes the ABTS radical (blue-green). Like DPPH, ABTS can operate through HAT and/or SET mechanisms. It has the advantage of being suitable for both water and lipid-soluble antioxidants. It is commonly used to analyze Vitamin E, carotenoids, polyphenols, and diverse extracts [62, 70, 73, 78].

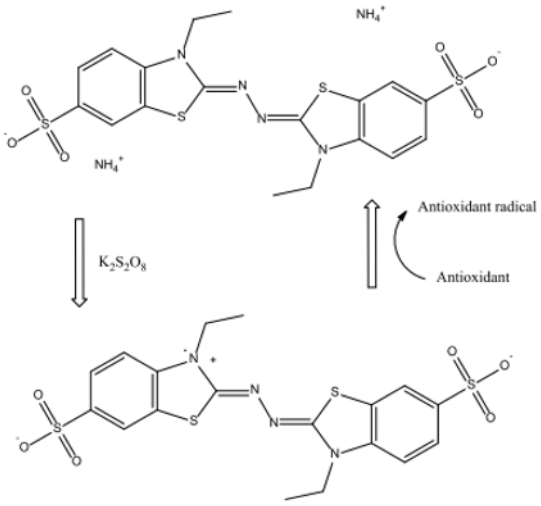

Figure 2.11: Prposed ABTS mechanism.

2.2.4.3 FRAP Assay (Ferric Reducing Antioxidant Power)

The FRAP assay focuses on the SET mechanism, specifically measuring an antioxidant's ability to reduce ferric iron (Fe3+) to ferrous iron (Fe2+). This process also causes a color change, offering an indication of an antioxidant's potential power as a reducing agent [62, 73, 78].

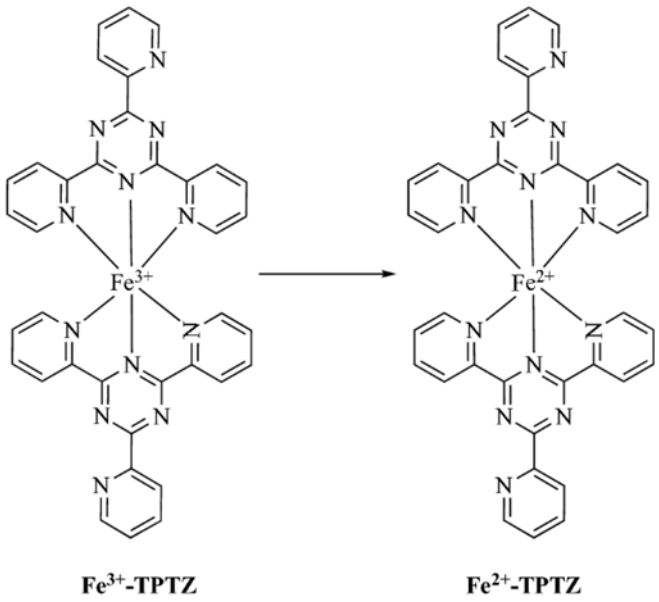

Figure 2.12: FRAP reductive mechanism by antioxidant species.

2.2.4.4 ORAC Assay (Oxygen Radical Absorbance Capacity)

The ORAC assay assesses an antioxidant's ability to protect against damage caused by peroxyl radicals. It can involve HAT and/or SET mechanisms and reflects the antioxidant's ability to protect against lipid peroxidation. Methods Based on Preventing Oxidative Damage [62, 73, 78].

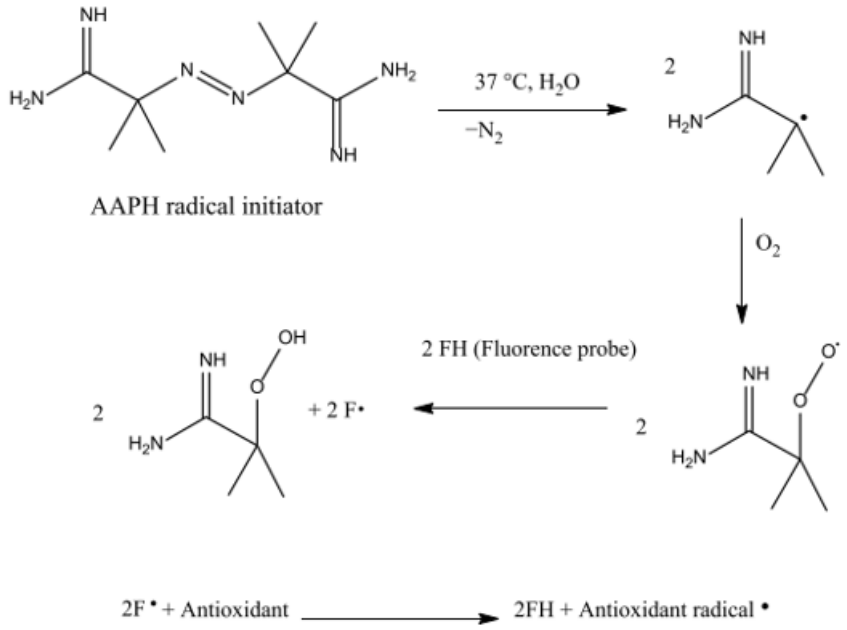

Figure 2.13: AAPH generates free radicals and afterwards.

2.2.4.5 Thiobarbituric Acid Reactive Substances (TBARS) Assay

The TBARS assay measures malondialdehyde (MDA), a product of lipid peroxidation. It is used to gauge an antioxidant's protective effect in food or biological samples [62, 73, 78].

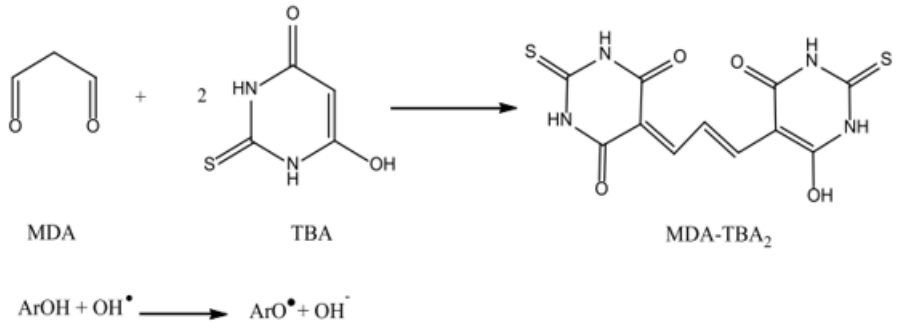

Figure 2.14: Presentation of the formation reaction MA-TRARS.

2.2.4.6 FTC (Ferric Thiocyanate) and FOX (ferrous oxidation xylenol orange) Assays

Both the FTC and FOX assays quantify lipid peroxidation products by monitoring the formation of colored complexes with ferric ions [62, 73, 78].

2.2.5 Applications of synthetic Antioxidants

Synthetic small Antioxidants find diverse applications across research, industry, and health due to their ability to combat the harmful effects of oxidative stress. Their potential in therapeutic interventions, as dietary supplements, within pharmaceuticals and cosmetics, and as food additives underscores their multifaceted benefits.

2.2.5.1 Therapeutic Interventions/ Pharmaceutical Antioxidants

Synthetic Antioxidants demonstrate significant potential as therapeutic agents, both as primary interventions and as adjunctive therapies targeting oxidative stress [67, 72, 79, 80, 81]. Several key mechanisms underpin their pharmacological properties. Direct scavenging of reactive oxygen species (ROS) neutralizes potential cellular damage, a mechanism employed by melatonin, retinol (vitamin A), and lipoic acid. Melatonin displays broad-spectrum antioxidant activity, mitigating DNA, lipid, and protein damage, contributing to its applications in sleep disorders, neurodegenerative conditions, and potential cancer therapy [82, 83]. Retinol similarly protects against DNA damage while stimulating endogenous antioxidant enzymes, finding clinical use in anti-cancer therapy, dermatology, and studies on immune modulation [84, 85]. Lipoic acid's ability to both scavenge ROS and regenerate antioxidants like vitamin C and E expands its therapeutic potential into diabetic neuropathy treatment, heavy metal detoxification, and research into neurodegenerative diseases and viral infections [86, 87].

The activation of antioxidant enzymes is another crucial pharmacological mechanism. Zinc, as a cofactor for enzymes like superoxide dismutase (SOD) and glutathione peroxidase, fosters free radical elimination. This underlies potential applications in inflammation management, wound healing, and possible reduction of viral infection severity [88, 89]. Selenium, integral to glutathione peroxidase activity, protects against lipid peroxidation and DNA damage, leading to research avenues in cancer prevention, atherosclerosis, and immune modulation [76].

Compounds exhibiting multifunctional properties offer broader therapeutic scope. Idebenone, uniquely combines ROS scavenging with enhancement of ATP production, establishing its role in neuroprotection against conditions like Alzheimer's disease and

Leber's Hereditary Optic Neuropathy [90, 91]. Pentoxifylline, recognized for its use in peripheral vascular disorders, exerts free-radical scavenging and anti-inflammatory effects, extending its research focus to conditions like diabetic kidney disease and potential use as a supportive therapy in viral infections [92, 93]. Probucol, primarily an anti-cholesterolemic agent, exhibits antioxidant action against lipid peroxidation, contributing to its applications in atherosclerosis and vascular disease treatment [94].

It's important to note that research on antioxidants within therapeutic contexts is constantly evolving. Clinical trials, particularly for complex pathologies like COVID-19, investigate the role of synthetic antioxidants compounds such as N-acetyl cysteine, ebselen , and high-dose vitamins C and D as adjuncts in treatment protocols [95, 96, 97, 98, 76]. The study of synergistic effects between different antioxidants may yield more effective therapeutic strategies than isolated compounds in some diseases. Individualized approaches optimizing dosage and antioxidant combinations will likely become essential for maximizing therapeutic benefits.

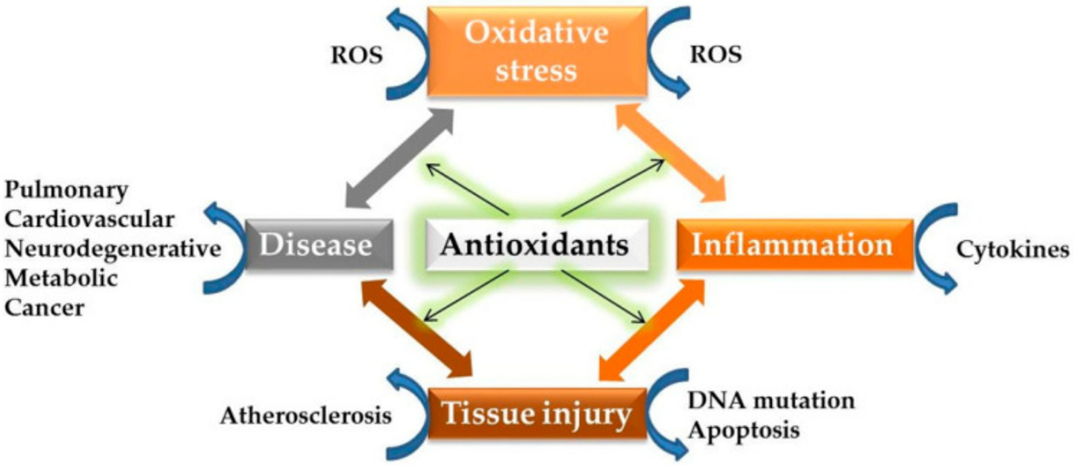

Figure 2.15: Effectiveness of antioxidants in the disease-specific pathways.

2.2.5.2 Dietary Antioxidants and Supplementation

A diet rich in fruits, vegetables, and other plant-based foods provides a natural source of diverse antioxidants. In addition, targeted antioxidant supplementation is being explored for potential benefits in both specific disease management and healthy individuals [76]. For example, vitamins C, E, D3, and zinc are being researched for their potential adjunctive role in various chronic conditions and for supporting specific functions like macular health or preventing cognitive decline [99, 100]. Other supplements like niacinamide, methionine, and lipoic acid play influential roles in metabolism and redox balance

[101, 86] . These compounds contribute to the body's antioxidant defenses by stimulating glutathione synthesis and reducing oxidative stress markers, potentially offering benefits beyond their primary roles in the body.
However, it's important to personalize antioxidant supplementation based on evidence-based recommendations, individual health needs, appropriate dosage and route of administration. Monitoring individual oxidative stress levels could further refine antioxidant intervention strategies.

2.2.5.3 Cosmeceutical Applications

The incorporation of dietary antioxidants into cosmeceuticals has yielded positive results [102]. The combination of vitamins C and E has proven beneficial for anti-aging purposes and enhancing skin luminosity [103]. Topical melatonin has displayed a protective function against UV-induced skin damage and emerges as a potential treatment for androgenic alopecia in new lipid nanocarrier formulations [104].

2.2.5.4 Food Industry and Antioxidant Additives

The food industry relies heavily on both synthetic and natural-identical antioxidants to prevent rancidity, preserve nutritional value, and maintain the sensory qualities of processed foods [66].
Two primary mechanisms are employed by synthetic food-grade antioxidants. Chain-breaking antioxidants, including butylated hydroxyanisole (BHA) [105],butylated hydroxytoluene (BHT) [106], and propyl gallate (PG), halt the propagation of free radical chain reactions by donating hydrogen atoms, ultimately stabilizing lipids and other food components. Another strategy involves metal chelators, such as disodium EDTA [107] and erythorbic acid [108]. These substances bind to metal ions (like iron and copper) that would otherwise catalyze harmful oxidation reactions, offering an additional layer of protection in food preservation.

2.2.6 Safety Considerations of Synthetic Antioxidants

The comprehensive assessment of safety profiles and the identification of potential adverse effects associated with synthetic antioxidants are of paramount importance for their responsible use and further development. Critical considerations include:

- **Dosage and Pro-Oxidant Potential:** While essential for combating oxidative stress, certain synthetic antioxidants can paradoxically become pro-oxidants at elevated concentrations or with prolonged exposure. Understanding dose-dependent effects

and establishing optimal therapeutic ranges are critical for mitigating the risk of unintended oxidative damages [62, 72, 109].

- **Drug-Antioxidant Interactions:** The potential for synthetic antioxidants to interfere with drug metabolism, either through inhibition or induction of cytochrome P450 enzymes, warrants investigation. These interactions could lead to altered drug efficacy or unforeseen toxicities, particularly in polypharmacy scenarios [110].
- **Specific Toxicities and Long-Term Impacts:** While evidence remains contested in some cases, certain synthetic antioxidants, including the widely used food additives BHA and BHT, have been associated with potential carcinogenic effects or other health concerns. Rigorous long-term safety studies are essential to fully elucidate the potential risks associated with particular antioxidants [111].

The translation of novel synthetic antioxidants into clinical therapies presents significant challenges. Key steps include the identification of compounds demonstrating antioxidant activity, the investigation of their precise mechanisms of action across various biological models (in vitro and in vivo), and comprehensive toxicological assessment [71, 112].

Chapter 3

Computational Insights into Antioxidant Behavior

Introduction

Computational chemistry has become a cornerstone of modern scientific inquiry, offering indispensable tools for unraveling the complexities of molecular systems. As experimental techniques advance, computational methods have emerged as powerful allies, facilitating the exploration of chemical phenomena with remarkable precision and efficiency.

This chapter provides an overview of the theoretical methodologies employed in this work, with a particular focus on DFT, molecular docking, and predictive ADMET modeling. Through these techniques, we delve into the molecular intricacies of antioxidants, exploring their structural properties, mechanisms of action, and potential therapeutic applications.

3.1 Density Functional Theory (DFT)

Density Functional Theory (DFT) has emerged as a powerful computational tool in modern chemistry, offering valuable insights into molecular structure, stability, and reactivity. Unlike traditional methods that solve the complex Schrödinger equation for all electrons in a system, DFT utilizes the electron density $(\rho(r))$– the probability of finding an electron at a specific point in space (r)– as the fundamental variable [113].

3.1.1 Key Principles

- **Hohenberg-Kohn Theorems:** These two theorems form the cornerstone of DFT. The first theorem establishes a one-to-one correspondence between the electron density and the ground-state energy of a system. The second theorem guarantees

the existence of a functional (a function of a function, in this case the electron density functional) that yields the system's total energy [114].

- **Kohn-Sham Equations:** These equations translate the many-electron problem into a set of single-electron Schrödinger-like equations. Each electron interacts with an effective potential that incorporates the effects of all other electrons and the nuclei [115].

DFT calculations are inherently approximations due to the unknown form of the exact exchange-correlation functional. Therefore, the choice of functional and basis set becomes paramount:

3.1.2 Functionals

There are three main types of functionals:

3.1.2.1 Local functionals (local density approximation, LDA)

This method is called local because the value of the functional at a point in space depends only on the electron density (ρ at that point. The results obtained are correct if the electron density does not have inhomogeneous regions.

3.1.2.2 Non-local functionals (generalized gradient approximation, GGA)

In the case where the electron density has inhomogeneous regions, corrections to the local methods should be included. This uses the gradient of the electron density at the points considered, which represent a measure of the inhomogeneity at those points. The most widely used methods are BLYP [115] (named after its three authors: Becke, Lee and Parr) and BP86 [116] (named after the authors: Becke and Perdew).

3.1.2.3 Hybrid functionals

This name comes from the fact that a Hartree-Fock (HF) exchange term is introduced in addition to the classical functionals describing the exchange energy. The most well-known is B3LYP [117] (stands for Becke-3 parameter-Lee, Yang Parr).

3.1.3 Atomic Orbital Basis Sets

Basis sets provide a collection of mathematical functions used to approximate the atomic orbitals within a molecule. This approximation simplifies the complex Schrödinger equation, making DFT calculations feasible [118]. The predominant basis function type in DFT is Gaussian-Type Orbitals (GTOs) due to their computational advantages, GTOs resemble

simplified hydrogen atom orbitals.

A careful selection of the appropriate basis set is essential for ensuring suitable accuracy and computational efficiency for the system of interest.

3.1.3.1 Pople Basis Sets

Pople basis sets [119] represent a widely used class of basis sets, offering a balance between accuracy and computational demands. Key notations and their implications include:

- **Minimal Basis Sets (e.g., STO-3G):** These employ a single basis function per atomic orbital. While computationally inexpensive, they provide a less refined molecular representation.
- **Split-Valence Basis Sets (e.g., 3-21G, 6-31G):** These utilize multiple basis functions for valence orbitals, allowing for greater flexibility and improved accuracy in describing chemical bonding.
- **Polarization Functions (e.g., 6-31G(d,p)):** The inclusion of 'd' or '*' signifies the addition of basis functions with higher angular momentum (p, d, etc.). These are crucial for accurately modeling the electronic structure in bonding environments and lone pairs, aspects fundamental to Schiff base chemistry and reactivity.
- **Diffuse Functions (e.g., 6-31+G(d,p)):** The '+' or 'd' indicates the presence of very extended functions, important for describing weakly bound electrons or anionic species. This is relevant for Schiff bases exhibiting charge-transfer behavior or those involved in metal complexation.

3.1.3.2 Dunning's Correlation-Consistent Basis Sets (e.g., cc-pVDZ, cc-pVTZ)

These sets offer a systematic approach to achieving higher accuracy by increasing the basis set size. The notations DZ (double zeta), TZ (triple zeta), etc., indicate the quality of the basis set [120].

3.2 Time-Dependent Density Functional Theory (TD-DFT)

TD-DFT extends the principles of traditional (ground-state) DFT to the dynamic realm of excited states. While DFT primarily focuses on the ground-state electron density, TD-DFT considers a time-dependent density evolving under the influence of an external perturbation (often electromagnetic radiation) [121].

TD-DFT enables the calculation of energies associated with transitions from a molecule's ground state to its various excited states. This information is essential for constructing absorption and emission spectra. Analysis of the TD-DFT output reveals which molecular orbitals contribute to specific transitions, providing insights into the electron redistribution upon excitation.

3.3 Density functional theory studies of the antioxidants

Theoretical methods, such as density functional theory (DFT), have been employed for the primary assessment of natural and synthesized antioxidants instead of using pharmacological methodologies because of economic benefits and high accuracy.

In order to do that, two strategies are being employed. The first strategy, the orbital vertical method (also known as Koopmans' approximation), involves calculating the energy difference between the highest occupied molecular orbital (HOMO) and the lowest unoccupied molecular orbital (LUMO). This approach allows us to derive several descriptors for comparing the antioxidant properties of different molecules. The second strategy focuses on vertical energies, which are determined by the difference in total electronic and thermal enthalpies. This helps to identify the antioxidants' preferred mechanisms of action [122, 123].

3.3.1 Frontier Molecular Orbital (FMO) Analysis

FMO theory provides a powerful lens for exploring the chemical reactivity and antioxidant potential of molecules. Analyzing the properties of the highest occupied molecular orbital (HOMO), the lowest unoccupied molecular orbital (LUMO), and the energy differences between them offers valuable insights into how antioxidants interact with reactive oxygen species (ROS). The Key FMO Descriptors for Antioxidant Activity are:

- **HOMO Energy:** The HOMO represents the highest energy orbital with paired electrons. The lower the HOMO energy, the more readily an antioxidant can donate an electron to neutralize a free radical. This electron-donating ability is a hallmark of antioxidant activity [124, 125, 126].
- **HOMO-LUMO Gap:** This energy difference reflects both the molecule's stability and its responsiveness to excitation. Antioxidants with smaller HOMO-LUMO gaps tend to be more reactive due to easier electron transitions. This often translates to stronger free radical scavenging [127, 128].

- **Ionization Potential (IP) and Electron Affinity (EA):** Rooted in Koopmans' theorem, IP and EA quantify the energy involved in removing (IP) and adding (EA) an electron. Antioxidants with low IP and high EA are more prone to donate and accept electrons, respectively. These processes underpin their capability to interact with ROS [129, 130].
- **Hardness (η) and Softness (S):** Derived from IP and EA, hardness and softness are complementary concepts. Hard antioxidants exhibit resistance to charge transfer, translating to lower reactivity and typically weaker antioxidant potential [124]. Conversely, soft antioxidants readily engage in charge transfer processes, potentially facilitating free radical scavenging.

$$\mu \approx -\chi = -\frac{I+A}{2} \text{ (Electronegativity)} \quad (1)$$

$$\eta \approx \frac{I-A}{2} \text{ (Chemical hardness)} \quad (2)$$

$$\zeta = \frac{1}{2\eta} \text{ (Softness)} \quad (3)$$

$$\omega = \frac{\mu^2}{2\eta} \text{ (Electrophilicity index)} \quad (4)$$

$$I = -E_{HOMO} \text{ (Ionization potential)} \quad (5)$$

$$A = -E_{LUMO} \text{ (Electron affinity)} \quad (6)$$

3.3.2 Antioxidant Mechanisms

Phenolic compounds exhibit diverse mechanisms for neutralizing free radicals. Three primary pathways [122, 131, 132, 133, 134] are :

3.3.2.1 Hydrogen Atom Transfer (HAT)

The phenolic hydroxyl group (ArOH) donates a hydrogen atom $(H^{\bullet})$ to a radical species $X^{\bullet}$, forming a less reactive phenoxyl radical $ArO^{\bullet}$ [Eq. 7]. The ease of HAT is determined by the bond dissociation enthalpy (BDE) of the O-H bond – a lower BDE indicates stronger antioxidant potential.

$$ArOH + X^{\bullet} \rightarrow ArO^{\bullet} + XH \quad (7)$$

$$BDE = H(ArO^{\bullet}) + H(H^{\bullet}) - H(ArOH) \quad (8)$$

3.3.2.2 Single Electron Transfer-Proton Transfer (SET-PT)

Initial electron donation from the antioxidant forms a radical cation $(ArOH^{\bullet+})$ [Eq. 9]. Deprotonation follows [Eq. 10]. This mechanism's favorability is influenced by the ionization potential (IP) and proton dissociation enthalpy (PDE) – lower values promote antioxidant reactivity via SET-PT.

$$ArOH + X^{\bullet} \rightarrow ArOH^{\bullet+} + X^{-} \quad (9)$$

$$ArOH^{\bullet+} \rightarrow ArO^{\bullet} + H^{+} \quad (10)$$

$$IP = H(ArOH^{\bullet+}) + H(e^{-}) - H(ArOH) \quad (11)$$

$$PDE = H(ArO^{\bullet}) + H(H^{+}) - H(ArOH^{\bullet+}) \quad (12)$$

3.3.2.3 Sequential Proton Loss Electron Transfer (SPLET)

The antioxidant first deprotonates (ArO^{-}), forming an anion [Eq 13]. Subsequent electron transfer yields the phenoxyl radical[Eq 14]. This mechanism depends on the proton affinity (PA) and electron transfer enthalpy (ETE) – lower values indicate greater SPLET likelihood.

$$ArOH \rightarrow ArO^{-} + H^{+} \quad (13)$$

$$ArO^{-} + X^{\bullet} + H^{+} \rightarrow ArO^{\bullet} + XH \quad (14)$$

$$PA = H(ArO^{-}) + H(H^{+}) - H(ArOH) \quad (15)$$

$$ETE = H(ArO^{\bullet}) + H(e^{-}) - H(ArO^{-}) \quad (16)$$

These pathways can coexist, with their relative contributions depending on the specific antioxidant, free radical species, and the environment [135].
Solvent polarity critically impacts the preferred mechanism. Polar solvents (e.g., water) stabilize charged intermediates, promoting SET-PT and SPLET [39].

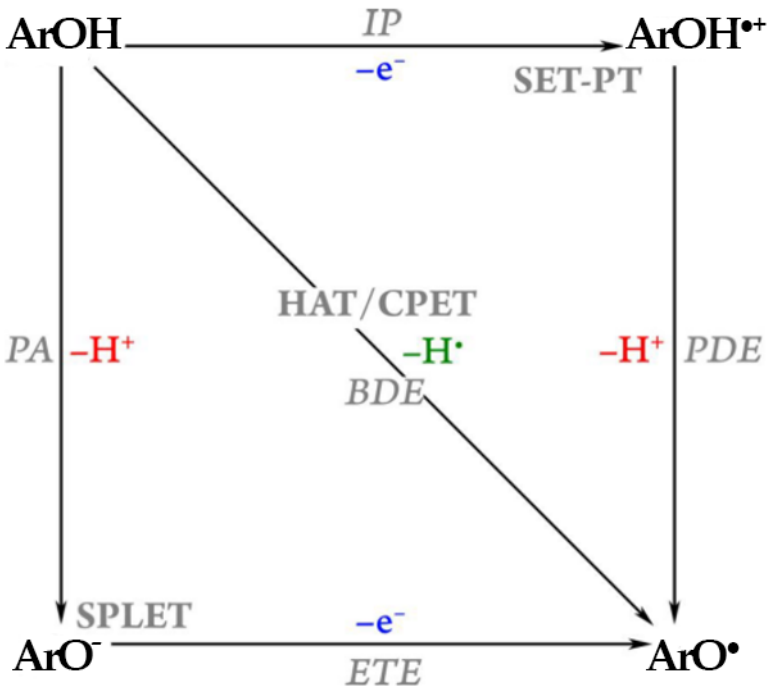

Figure 3.1: O'Farell-Jencks diagram of each single step involved in common reaction mechanisms

3.3.3 Choosing functionals for antioxidant studies

The selection of the B3LYP density functional aligns with its widespread use in antioxidant studies [See Figure 3.2], proven efficacy in the study of phenolic compounds and its favorable balance between computational cost and accuracy, making it well-suited for analyzing the phenolic Schiff bases under investigation. To accurately represent the complex charge distributions, potential radical formation, and ionic species essential for antioxidant mechanisms, the $6-311+G(d,p)$ basis set was employed. Its inclusion of polarization (d) and diffuse (+) functions ensures robust modeling capacity. Furthermore, the IEF-PCM solvation model was chosen to efficiently simulate the diverse solvent environments (water, ethanol, chloroform, benzene) and their anticipated influence on the preferred antioxidant mechanisms exhibited by the phenolic Schiff bases. This approach enables a comprehensive assessment of solvent effects on antioxidant activity.

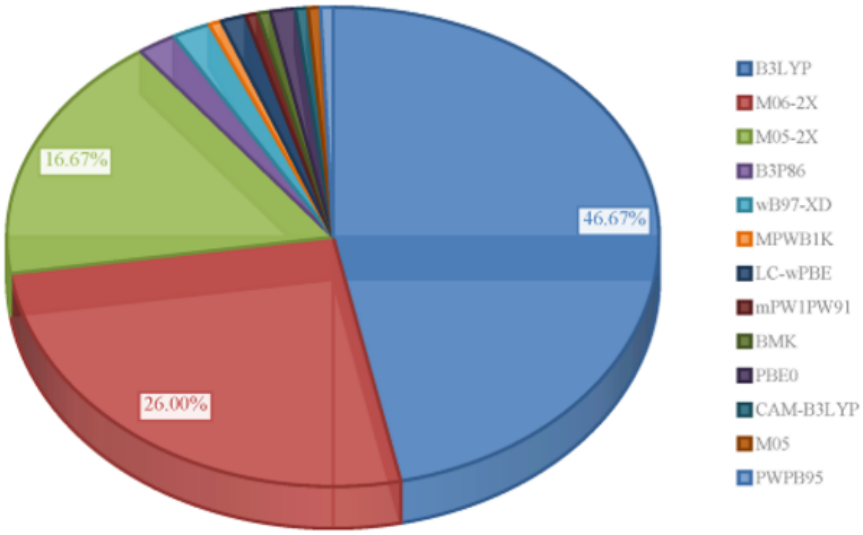

Figure 3.2: Share of functionals in articles published in the years from 2022-2018 [123]

3.4 Molecular docking

Molecular docking has emerged as a cornerstone computational technique within the structure-based drug discovery (SBDD) paradigm. It offers a powerful in-silico approach to predict the binding interactions between small molecules (ligands) and their macromolecular targets, typically proteins, at an atomic level [136]. This predictive capability empowers researchers to gain crucial insights into the behavior of ligands, such as nutraceuticals, within the binding pocket of a target protein. By elucidating the underlying biochemical mechanisms governing these interactions, molecular docking serves as a valuable tool for drug discovery and optimization [137].

Researchers employ a diverse set of molecular docking programs for their studies. Popular options include AutoDock, AutoDock Vina, Discovery Studio, Surflex, AutoDock GOLD, Glide, MCDock, MOE-Dock, FlexX, DOCK, LeDock, rDock, ICM, Cdcker, LigandFit, FRED, and UCSF Dock

3.4.1 Theory of Docking

Molecular docking is a computational technique used to model the interaction between a ligand and a receptor, typically a protein. The process has two key components: sampling algorithms and scoring functions. Sampling algorithms explore how the ligand can fit within the protein's binding site, identifying potential orientations and conformations. Scoring functions then evaluate how favorable these conformations are in terms of binding energy [137, 138, 139].

3.4.1.1 Search Algorithms

Search algorithms face the challenge of efficiently exploring the many ways a flexible ligand can interact within a protein's active site [140]. Here are common classes of search algorithms:

Systematic Methods These involve methodically exploring conformations. Subtypes include:

- **Conformational Search:** Gradually altering the ligand's structure through bond rotations and translations.
- **Fragmentation:** Docking smaller sections of the ligand and building the final configuration piece by piece.
- **Database Search:** Utilizing pre-existing libraries of potential ligand conformations.

Stochastic Methods Introduce randomness to explore conformations. Subtypes include:

- **Monte Carlo:** Randomly positions the ligand, evaluates the configuration, and iterates.
- **Genetic Algorithms:** Model an evolutionary process where new ligand configurations are generated based on the "fitness" (score) of previous generations.
- **Tabu Search:** Prevents revisiting previously explored areas of the search space to ensure wider exploration.

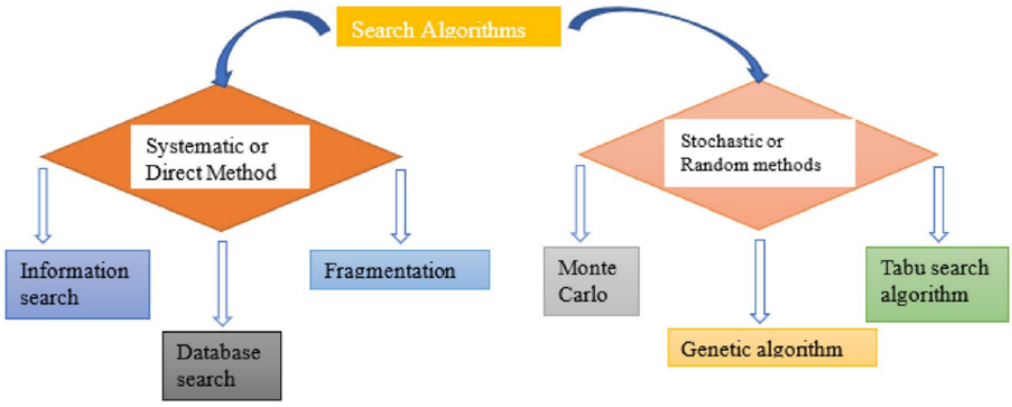

Figure 3.3: Classes of search algorithm mechanisms

3.4.1.2 Scoring Functions

Scoring functions rank potential ligand-protein complexes to indicate how likely they are to form [141, 140]. Common categories include:

- **Force Field-Based:** Calculate binding affinity by modeling non-bonded interactions (van der Waals forces, hydrogen bonds, electrostatic interactions) and internal energy associated with bond angles and torsion [142].
- **Empirical:** Use statistical analysis of known complexes to assess the favorability of specific interactions (i.e., hydrogen bonding between different atom pairs) [143].
- **Knowledge-Based:** Derive statistical potentials from databases of known structures to predict the likelihood of interactions between specific atom types and distances [144].

3.4.2 AutoDock Software

Developed by the Scripps Research Institute, AutoDock [145] is a free and open-source program widely used for molecular docking simulations. It offers capabilities for both rigid and flexible docking simulations, allowing researchers to analyze various ligand-receptor interactions.

AutoDock utilizes a Lamarckian genetic algorithm to strategically position ligand molecules within the binding pocket of a receptor. Additionally, it incorporates various scoring functions to assess the binding affinity between ligands and receptors. The software supports a range of file formats commonly used in molecular modeling, including PDB, MOL2, and SDF [137].

For researchers interested in exploring ligand-receptor interactions, AutoDock provides a valuable tool readily available at url: `http://autodock.scripps.edu.`

3.5 The Prediction of Activity Spectra for Substances (PASS)

The Prediction of Activity Spectra for Substances (PASS) is a freely accessible, web-based platform designed to guide researchers in exploring the potential biological activities of organic compounds. Based solely on a compound's structural formula, PASS can predict with impressive accuracy (approximately 95%) a wide array of activities, including pharmacological actions, mechanisms of action, toxicities, and more [146, 147].

3.5.1 Methodology and Principles

PASS operates on a fundamental principle: compounds with similar structures often exhibit similar biological effects. At its core, PASS houses a vast database of known bioactive compounds. When a query compound is submitted, PASS employs the following steps [148]:

- **Structural Analysis:** The compound's structure is represented by Multilevel Neighborhoods of Atoms (MNA) descriptors, allowing for detailed analysis.
- **Database Comparison:** PASS compares the MNA descriptors against its database of known compounds.
- **Bayesian Predictions:** Using Bayesian statistics, PASS calculates the probability that the query compound will exhibit specific biological activities, expressed as 'Pa' (probability of being active) and 'Pi' (probability of being inactive).

3.5.2 Interpreting PASS Results

PASS offers researchers invaluable insights into a compound's potential effects. Understanding the probability values (Pa and Pi) is key [149]:

- **High Pa, Low Pi:** Indicates a strong likelihood that the compound will exhibit the predicted activity.
- **Balancing Risk and Reward:** Researchers can adjust probability thresholds to prioritize compounds based on their tolerance for false positives and false negatives.
- **Novelty Factor:** Compounds with lower Pa values may be less similar to known drugs, offering potential for discovering entirely new classes of bioactive molecules.

The predictive potential of PASS makes it an invaluable resource across several scientific domains. In the realm of drug discovery, PASS can be employed to repurpose existing drugs by identifying new targets. Conversely, it can guide the discovery of novel drug candidates exhibiting activity against specific biological targets. Moreover, PASS plays a role in toxicological assessments, aiding in the early prediction of potential adverse effects [147].

3.6 ADMET Properties

ADMET stands for Absorption, Distribution, Metabolism, Excretion, and Toxicity. It represents a crucial aspect of drug discovery and development, aiming to predict the pharmacokinetic and drug-likeness properties of chemical compounds prior to their synthesis or experimentation. This predictive modeling approach utilizes computational methods

and databases to evaluate various aspects of a compound's behavior within biological systems [150, 151].

3.6.1 Absorption

The absorption of a drug refers to its ability to enter the bloodstream and reach the target site. Computational models are employed to predict parameters such as the gastrointestinal absorption, blood-brain barrier permeability, and skin permeability. These predictions help assess the bioavailability and efficacy of potential drug candidates.

3.6.2 Distribution

Distribution pertains to the dissemination of a drug throughout the body after absorption. Computational tools assist in estimating the volume of distribution, which indicates the extent of drug distribution in various tissues and organs. Predictive models also consider factors like protein binding and tissue-specific accumulation, providing insights into the compound's distribution profile.

3.6.3 Metabolism

Metabolism involves the biotransformation of drugs by enzymes in the body, primarily in the liver. ADMET models predict the metabolic stability of compounds by identifying potential sites of metabolism and assessing their susceptibility to enzymatic reactions. Understanding a drug's metabolic pathways aids in optimizing its pharmacological properties and minimizing toxicity.

3.6.4 Excretion

Excretion refers to the elimination of drugs and their metabolites from the body, mainly through urine and feces. Computational approaches estimate parameters such as renal clearance, hepatic clearance, and half-life to evaluate the compound's excretory behavior. Predictions of excretion pathways help in determining dosing regimens and potential drug interactions.

3.6.5 Toxicity

Assessing the toxicity profile of a compound is critical for ensuring its safety and minimizing adverse effects. ADMET models predict various types of toxicity, including hepatotoxicity, cardiotoxicity, genotoxicity, and cytotoxicity, using structural alerts, quantitative structure-activity relationship (QSAR) models, and other computational techniques. By

identifying potential toxicities early in the drug development process, researchers can prioritize safer candidates for further evaluation.

3.6.6 SwissADME

Among the array of computational ADMET tools, SwissADME (url: http://www.swissadme.ch) stands out as a freely accessible and user-friendly web-based platform developed by the Molecular Modelling group of the Swiss Institute of Bioinformatics. SwissADME enables researchers to input molecular structures (SMILES format or by drawing) and obtain predictions for a wide range of physicochemical properties, pharmacokinetic parameters, and potential drug-likeness [152]. It employs various computational models, including the "BOILED-Egg" [153] for predicting brain and intestinal absorption, and leverages curated datasets to assess compliance with rules such as Lipinski's Rule of Five [154].

Chapter 4

Materials and Methods: A Detailed Exposition

Introduction

In the preceding chapters, we have explored the fundamental concepts of antioxidant activity, and elaborated a comprehensive study on Schiff bases, their synthesis, biological activities. Chapter Four builds upon this foundation by focusing on the practical aspects of the research, detailing the materials and methods used in the synthesis of Schiff base derivatives, as well as the computational and experimental procedures employed to analyze them. This chapter is essential as it provides the experimental foundation and computational analysis that support the findings and conclusions of the research.

4.1 Materials and instrumentation

This thesis is based on research work conducted within the Physical Chemistry Laboratory at the University of 8 Mai 1945 – Guelma.

- All chemicals and solvents used in this work were of high-purity grade and employed without additional purification procedures.
- UV-Vis Spectroscopy: A Shimadzu UV-visible spectrophotometer equipped with 1.0 cm matched quartz cells was used to measure electronic absorption spectra in the 200-500 nm range within three solvents: benzene, chloroform, and ethanol. This analysis was performed at the Applied Chemistry Laboratory, University of Guelma, Algeria.
- FT-IR Spectroscopy: A Perkin Elmer Spectrum One FT-IR instrument was employed to obtain Fourier-transform infrared (FT-IR) spectra using potassium bromide (KBr) pellets. This analysis was conducted at the Industrial Analysis and Materials Engineering Laboratory, University of Guelma, Algeria.
- NMR Spectroscopy: A Bruker Avance 300 spectrometer operating at 75.5 MHz was

used to record proton nuclear magnetic resonance (^{1}H NMR) spectra at ambient temperature, using deuterated dimethyl sulfoxide (DMSO-d6) as the solvent. This analysis was carried out at the Laboratory for the Synthesis and Physical Chemistry of Molecules of Biological Interest (SPCMIB), University of Toulouse Paul Sabatier, France."

4.2 Synthesis of Schiff Base Derivatives

The Schiff base derivatives N-(2-hydroxybenzylidene)-m-chloroaniline, N-(2-hydroxybenzylidene)-m-nitroaniline, and N-(2-hydroxybenzylidene)-m-methoxyaniline were synthesized following established procedures [155].
Salicylic aldehyde and the corresponding amine (equimolar quantities) were dissolved in a minimal volume of pure ethanol. Then the reaction mixture was refluxed at 60°C for 2 hours with continuous monitoring by thin-layer chromatography (TLC). The resulting precipitate was filtered and washed thoroughly with ethanol to obtain the desired product. The solid product obtained was purified by recrystallization from ethanol, and the synthesis pathway is shown in Figure 4.1.

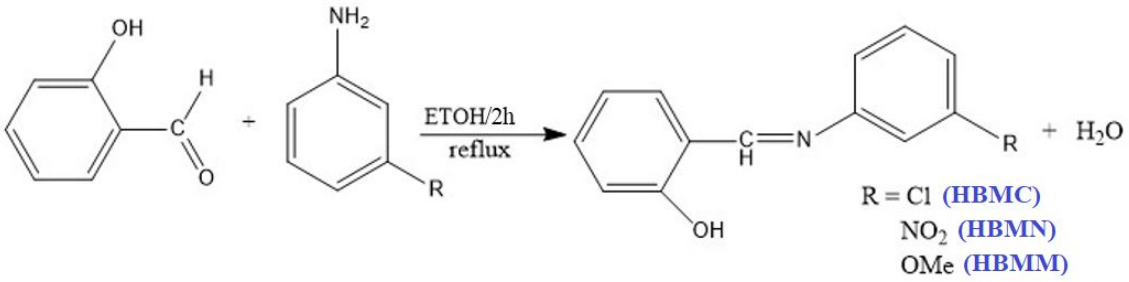

Figure 4.1: Synthesis reaction of the schiff base derivatives

All Schiff bases were obtained with satisfactory yields ranging from 71 to 85%. The melting points of the synthesized Schiff bases are in accordance with those reported in the literature [156]. They exhibit excellent stability at room temperature and can be stored for extended periods. The key physicochemical properties of these Schiff bases are summarized in Table 4.1.

Table 4.1: Physicochemical properties of synthesized Schiff bases

Schiff base	**Molecular formula**	**Molecular weight** (g/mol)	**Yield** %	**Melting point** (K)
HBMC	$C_{13}H_{10}ClNO$	231.68	85.91	371
HBMN	$C_{13}H_{10}N_2O_3$	242.23	80.54	392
HBMM	$C_{14}H_{13}NO_2$	227.26	71.22	335

4.3 DFT calculations

- Density functional theory (DFT) calculations were performed using the Gaussian 09W software package. To optimize molecular structures and calculate vibrational frequencies, the B3LYP hybrid functional was chosen, along with the 6-311G+ (d, p) basis set [157, 158, 159, 117, 160]. This combination of theoretical methods is widely used in computational chemistry for its balance of accuracy and efficiency.
- Calculated molecular structures were confirmed to be stable, indicated by the absence of imaginary frequencies in the vibrational analysis. To ensure accurate comparison with experimental infrared (IR) spectroscopy data, a standard scaling factor of 0.9688 [161] was applied to the computed vibrational frequencies. VEDA 4 software [162] enabled analysis of the potential energy distribution (PED), providing insight into the specific vibrational modes associated with each predicted frequency.
- To simulate the ultraviolet-visible (UV-Vis) absorption spectra of the molecules, calculations were performed using Time-Dependent Density Functional Theory (TD-DFT). The CAM-B3LYP functional and the 6-311+G(d,p) basis set were chosen for this task, considering their effectiveness in modeling electronic excitations [163]. Furthermore, a solvent model (IEFPCM) was incorporated to account for the influence of solvent [164]. To identify the key electronic transitions responsible for the predicted absorption bands, GaussSum 3.0 software was used to analyze the results.
- To calculate the total enthalpy at 298.15 K, High-precision single-point energy calculations were conducted using the B3LYP/6-311+G (d, p) level of theory. These were combined with vibrational analysis results to determine the essential thermal contributions to enthalpy. Established literature values were utilized to obtain the enthalpies of hydrogen $(H^{\bullet})$, electron (e^{-}), and proton (H^{+}) under both gas-phase and solvated conditions [165, 166, 167, 168]. To accurately model the effects of the surrounding environment on the enthalpy, the IEF-PCM solvent model was incorporated into the calculations.

4.4 Computational Docking Protocol

Preparation

- The target protein (UQCRB, PDB ID: 1NTK) [169] was prepared for docking using AutoDockTools 4 (ADT) [145]. This involved removing co-crystallized ligands, water molecules, and cofactors from the protein structure, followed by the addition of polar hydrogens and calculation of Kollman charges.
- Ligands were optimized at the B3LYP/6-311+G(d,p) level of theory and assigned flexibility (rotatable bonds) within ADT. Protein structure was maintained as rigid.

Docking Simulation

- AutoDock 4.0 was employed to perform molecular docking with the prepared ligands and target protein. The Lamarckian Genetic Algorithm (LGA) guided the search for potential binding conformations and calculated binding energies.

Analysis and Visualization

- Discovery Studio 4.0 [170] and ADT were utilized to analyze docked poses. This included identifying potential binding pockets and visualizing detailed ligand-protein interactions.

Validation of Docking Method

To assess the accuracy of the docking protocol, the co-crystallized ligand from the UQCRB protein structure ($PDBID : 1NTK$) was re-docked using the same protocol described above:

- The co-crystallized ligand was retrieved from the PDB structure of UQCRB (1NTK).
- The extracted ligand was prepared following the same steps used for the studied compounds ($B3LYP/6-311+G(d,p)$ optimization and assigning flexibility within ADT).
- The docked pose of the known ligand was then compared with its original position in the crystal structure using the Root Mean Square Deviation (RMSD) value. The low RMSD (below 2.0 Å) indicates that the docking protocol can reliably reproduce the binding mode of known ligands.

4.5 In Silico ADMET Assessment

- The pkCSM web server [171] was employed to computationally predict crucial ADMET (absorption, distribution, metabolism, excretion, toxicity) properties of the investigated compounds. This platform provides rapid and reliable estimations, streamlining the drug discovery process.
- To evaluate the drug-likeness of our compounds, the SwissADME platform [152] was utilized. This tool assesses adherence to established guidelines for favorable pharmacological properties (Lipinski, Ghose, Veber, Egan, Muegge).

Chapter 5

Analysis and Findings

5.1 ^{1}H NMR Analysis

Analysis of the ^{1}H NMR spectra (see Figures 5.1 , 5.2 , 5.3) revealed key structural features of the investigated compounds. A characteristic singlet signal within the range of δ 13.25-12.51 ppm was consistently observed, indicating the presence of phenolic -OH protons [172, 173, 174]. Furthermore, the formation of salicylideneanilines was supported by a distinct singlet signal at δ 8.7 ppm, corresponding to the azomethine (-HC=N) protons [172, 173, 174, 175, 176]. Multiplet signals in the range of δ 8.19-6.8 ppm were attributed to aromatic protons [172, 177]. Notably, HBMM displayed a unique singlet signal at approximately 3.8 ppm, consistent with the presence of its methoxy group [175].

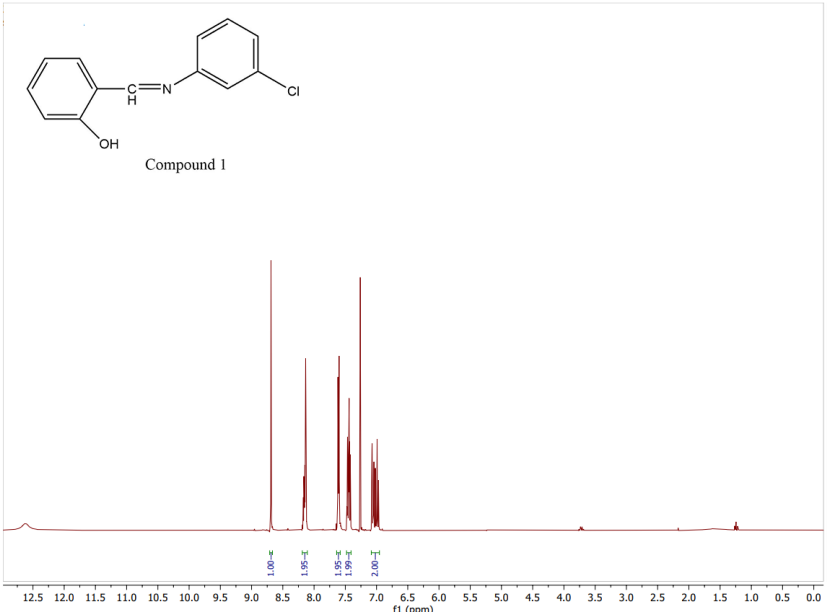

Figure 5.1: The 1H-NMR spectra of HBMC

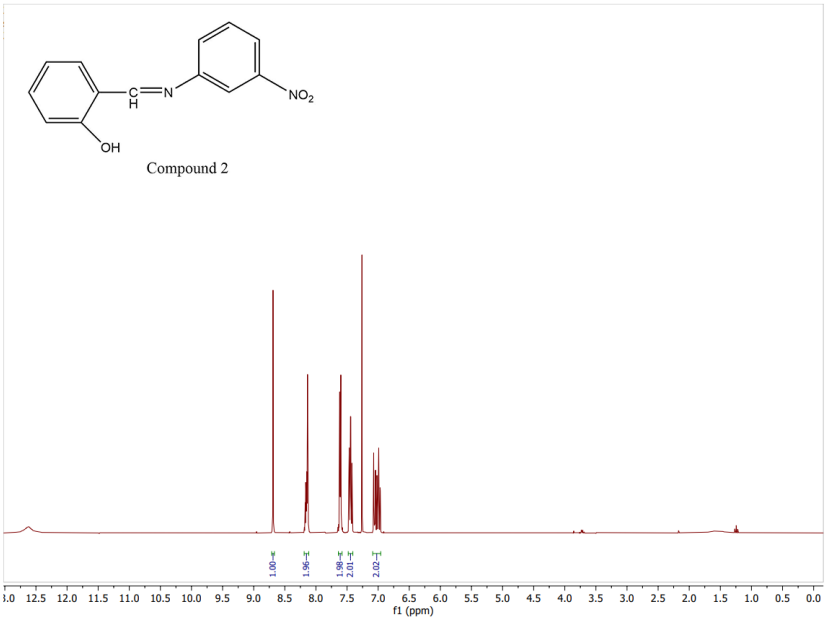

Figure 5.2: The 1H-NMR spectra of HBMN

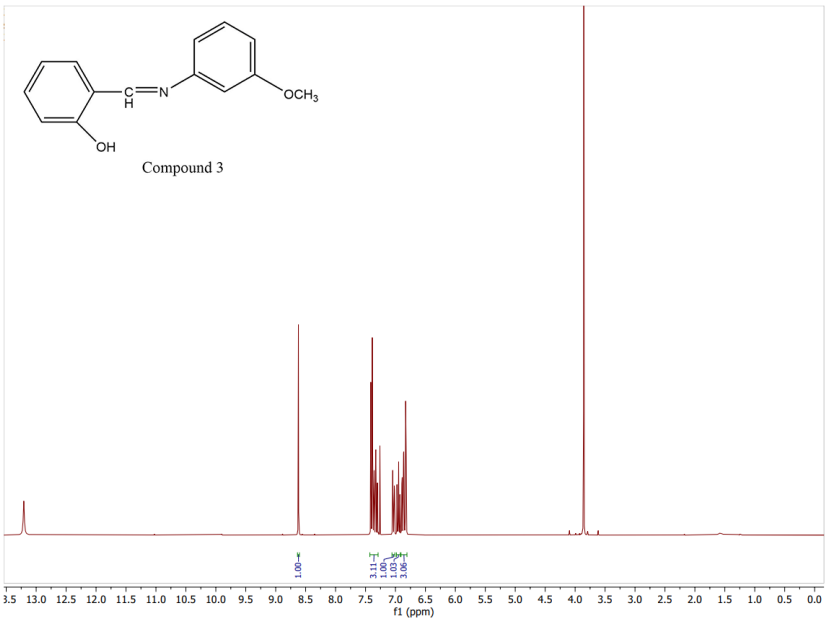

Figure 5.3: The 1H-NMR spectra of HBMM

5.2 Vibrational spectra analysis

Detailed vibrational assignments for the investigated compounds are provided in Tables S1-S2, S3, combining experimental IR data with theoretical calculations. Figures 5.4, 5.5, 5.6 offer a visual comparison of the experimental and simulated IR spectra, facilitating the analysis of vibrational modes.

Phenolic O-H stretching vibrations characteristically appear within the 3550-3200 cm^{-1} region [178]. Our experimental IR spectra confirmed this, with HBMC, HBMN, and HBMM exhibiting O-H stretches at 3440, 3450, and 3446 cm^{-1}, respectively. These experimental values were closely mirrored by theoretical calculations, which predicted corresponding vibrations at 3726, 3728, and 3694 cm^{-1}

The presence of a strong absorption band within the 1645-1605 cm^{-1} region is a hallmark of the azomethine (Ar-CH=N-Ar) functional group [179]. This characteristic C=N stretching vibration confirms the formation of our Schiff base compounds. The specific position of this peak can be influenced by substituents on the aromatic rings. Experimentally, we observed C=N stretches at 1620 cm^{-1} (HBMC), 1623 cm^{-1} (HBMN), and 1619 cm^{-1} (HBMM). These values align closely with the computationally predicted vibrations at 1624, 1625, and 1634 cm^{-1}, respectively.

Aromatic C=C stretching vibrations characteristically appear within the 1650-1200 cm^{-1} spectral region [180, 181]. Computational analysis predicted these modes in our compounds within the ranges 1599-1252 cm^{-1}, 1586-1290 cm^{-1}, and 1593-1288 cm^{-1}, aligning well with the experimental observations (1590-1279 cm^{-1}, 1573-1278 cm^{-1}, and 1597-1284 cm^{-1}, respectively).

Phenolic C-O stretches are typically found between 1300-1200 cm^{-1} [179]. Experimentally, we observed C-O vibrations at 1187 cm^{-1} (HBMC), 1191 cm^{-1} (HBMN), and 1257 cm^{-1} (HBMM). These values correspond closely to the theoretically predicted peaks at 1207 cm^{-1} (HBMC and HBMN) and 1253 cm^{-1} (HBMM).

The C-Cl stretch in HBMC was identified experimentally at 678 cm^{-1}, aligning closely with the computationally predicted value of 682 cm^{-1}. This falls within the expected 790-505 cm^{-1} range for C-Cl stretching vibrations [179].

As anticipated, the nitro group in HBMN exhibited two characteristic absorptions in the IR spectrum. The asymmetric NO_2 stretch was observed at 1523 cm^{-1} and the symmetric NO_2 stretch at 1352 cm^{-1}. These experimental frequencies correspond well with the theoretical calculations (1534 cm^{-1} and 1329 cm^{-1}, respectively), and fall within the typical ranges for nitro group vibrations [182, 183].

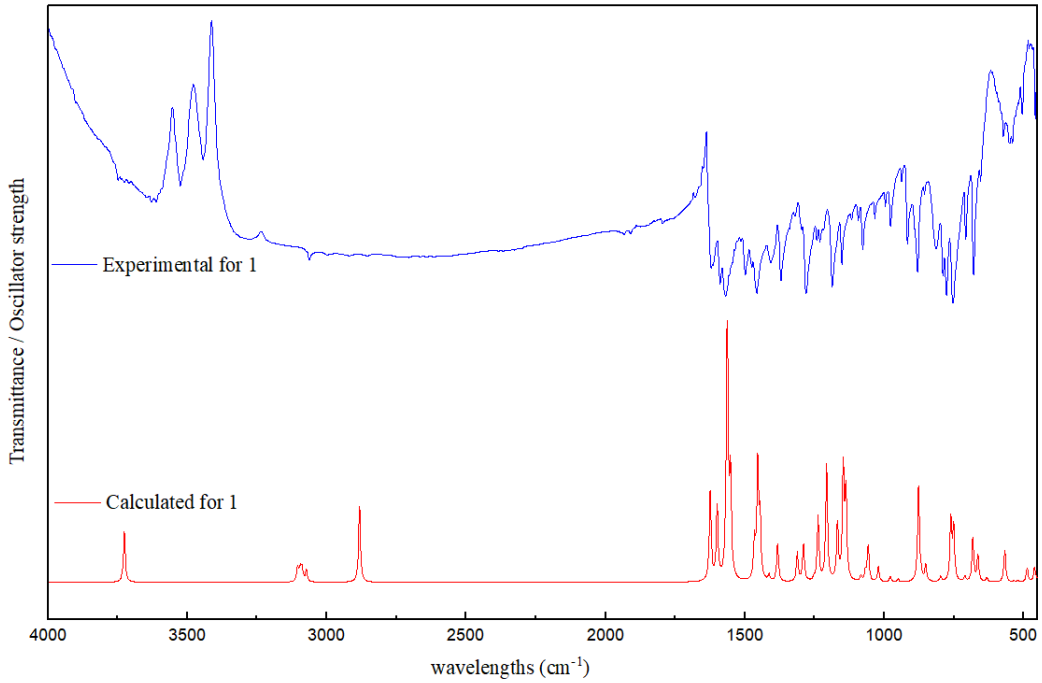

Figure 5.4: Experimental (top) and calculated (bottom) IR spectra of HBMC (1)

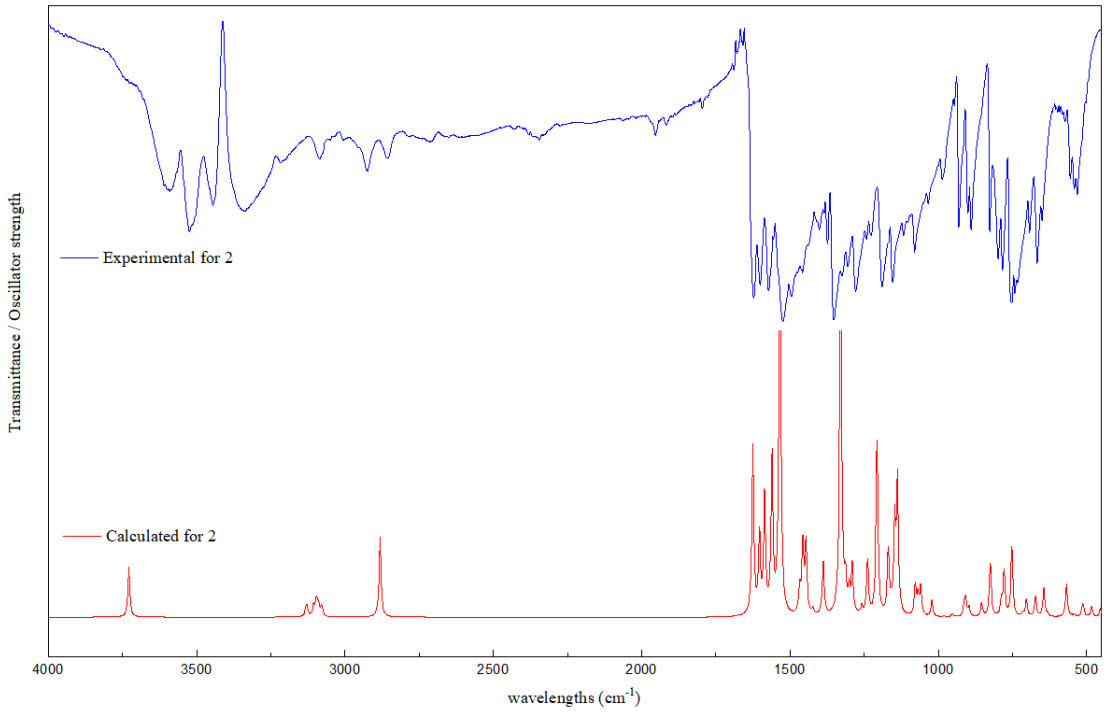

Figure 5.5: Experimental (top) and calculated (bottom) IR spectra of HBMN (2)

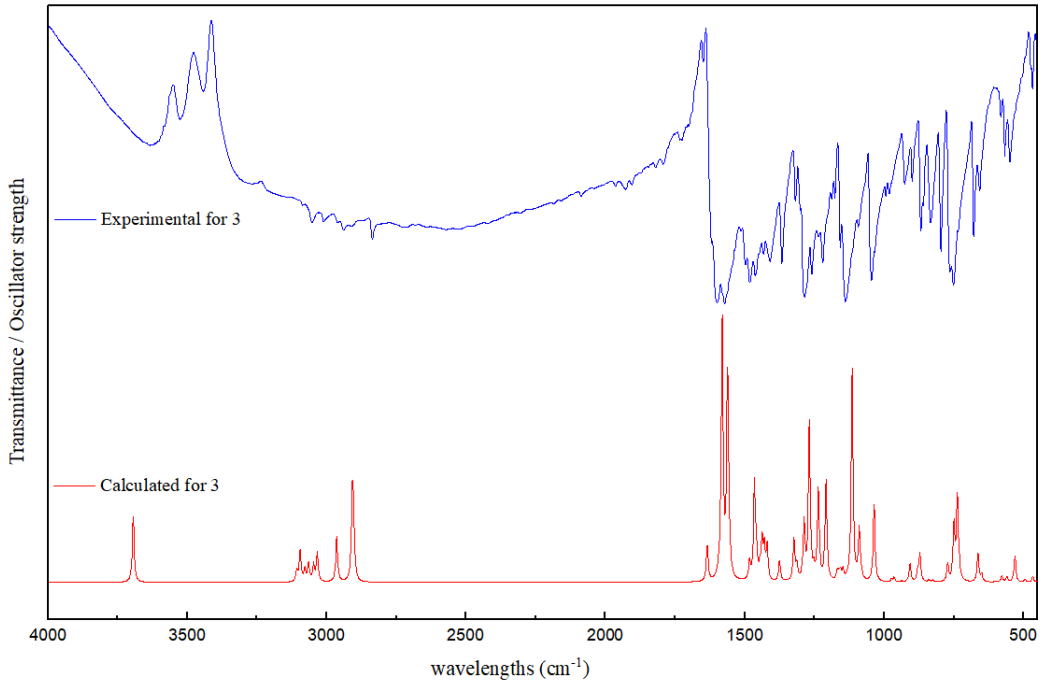

Figure 5.6: Experimental (top) and calculated (bottom) IR spectra of HBMN (3)

5.3 UV-Vis analysis

The UV-Vis spectra of ortho-hydroxy Schiff bases are significantly influenced by proton tautomerism. The phenol-imine form is characterized by absorption bands in the 300-400 nm range, while the keto-amine form exhibits a distinctive absorption above 400 nm [184]. Solvent polarity plays a crucial role in tautomeric equilibrium: polar solvents can stabilize both tautomers, whereas nonpolar solvents favor the phenol-imine form [185].

The influence of solvent polarity on the electronic properties of the investigated compounds was explored using UV-Vis spectroscopy. Spectra were recorded in three solvents with varying polarities: ethanol (polar protic), chloroform (polar aprotic), and benzene (apolar) (Figure 5.7). Gratifyingly, all compounds displayed two distinct absorption bands regardless of the solvent. The first band, positioned within the 262-269 nm range, is characteristic of a $\pi \rightarrow \pi^*$ electronic transition. The second band, observed between 331-340 nm, is attributed to an $n \rightarrow \pi^*$ transition. These transitions are consistent with the presence of azomethine and aromatic ring functionalities within the molecules [175, 46].

The UV-Vis spectra provide strong evidence for the predominance of the enol tautomer in all investigated solvents, as indicated by the consistent absorption bands below 400 nm

[184, 186]. This finding is supported by theoretical calculations, which predict two distinct spectral bands in the ranges 268-285 nm and 338-344 nm. Table 5.1 further elucidates the specific molecular orbital transitions underlying these predicted spectral features.

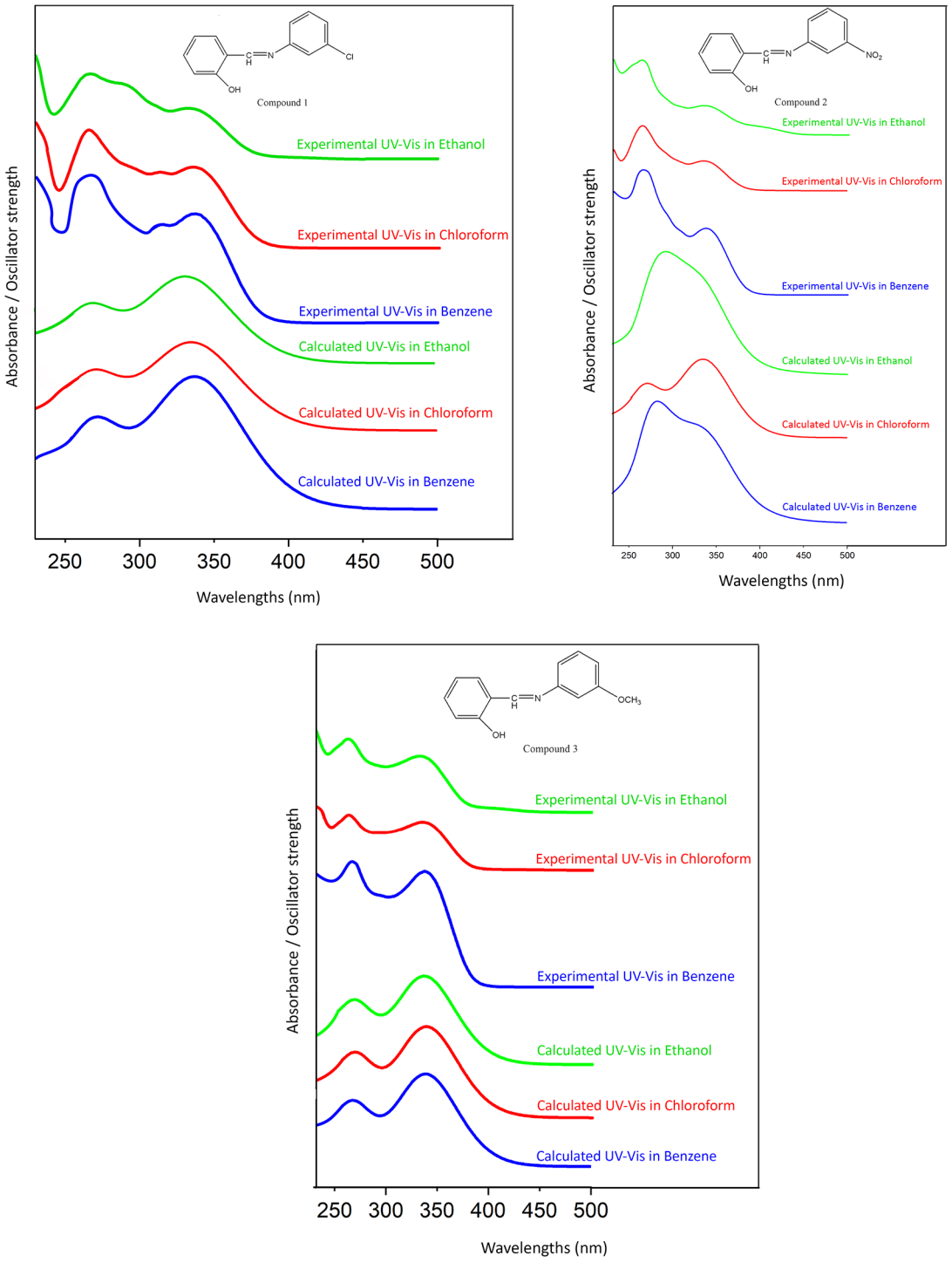

Figure 5.7: The experimental and computed UV parameters in different solvents of HBMC, HBMN and HBMM.

Table 5.1: Wavelength, oscillator strength, major contributions of calculated transitions for HBMC, HBMN and HBMM.

	Solvant	Exp. λ (nm)	Cal. λ (nm)	Oscillator strength	Major contributions
HBMC	Ethanol	265	269	0.3199	H-4->LUMO (11%), H-3->LUMO (69%)
		335	339	0.4477	HOMO->LUMO (97%)
	Chloroform	265	270	0.3212	H-4->LUMO (11%), H-3->LUMO (70%)
		335	342	0.4553	HOMO->LUMO (97%)
	Benzene	265	270	0.3215	H-4->LUMO (11%), H-3->LUMO (71%)
		335	344	0.4553	HOMO->LUMO (97%)
HBMN	Ethanol	264	285	0.2952	H-3->LUMO (92%), H-2->L+1 (2%)
		340	338	0.3823	HOMO->L+1 (96%)
	Chloroform	265	281	0.2631	H-6->LUMO (22%), H-3->LUMO (67%)
		340	341	0.3836	HOMO->L+1 (95%)
	Benzene	264	277	0.4015	H-3->LUMO (81%), H-2->L+1 (11%)
		340	342	0.3411	H-1->LUMO (24%), HOMO->L+1 (72%)
HBMM	Ethanol	262	268	0.3351	H-4->LUMO (14%), H-3->LUMO (70%)
		331	340	0.4912	HOMO->LUMO (97%)
	Chloroform	262	268	0.3385	H-4->LUMO (14%), H-3->LUMO (71%)
		334	342	0.4637	HOMO->LUMO (97%)
	Benzene	267	269	0.3401	H-4->LUMO (14%), H-3->LUMO (71%)
		335	344	0.4797	HOMO->LUMO (97%)

5.4 Global reactivity descriptors

Global reactivity descriptors (Table 5.2) were calculated in the gas phase to probe the stability and potential antioxidant properties of the studied Schiff bases. Of particular interest are the energies of the highest occupied molecular orbital (HOMO) and lowest unoccupied molecular orbital (LUMO), as these frontier orbitals influence free radical scavenging mechanisms. In phenolic antioxidants, the HOMO composition reveals sites prone to hydrogen atom abstraction, a key step in radical scavenging. Generally, a higher

HOMO energy suggests enhanced electron-donating ability, while a lower LUMO energy implies stronger electron-accepting capability, both of which are beneficial for antioxidant activity [126, 135].

The energy gap between the HOMO and LUMO orbitals provides crucial insights into a molecule's kinetic stability and reactivity. Smaller energy gaps generally indicate greater reactivity and reduced stability [187, 128].

Table 5.2: Calculated quantum chemical molecular properties for HBMC, HBMN and HBMM.

Parameters	HBMC	HBMN	HBMM
HOMO (eV)	-6,412	-6,665	-5,97
LUMO (eV)	-2,433	-3,012	-1,829
Energy gap ΔE (eV)	3,979	3,653	4,141
Electronic chemica potential μ (eV)	-4,422	-4,838	-3,899
Electronegativity χ (eV)	4,422	4,838	3,899
Hardness η (eV)	1,989	1,826	2,07
Softness ζ (eV)	0,251	0,274	0,241
Electrophilicity index ω (eV)	4,915	6,409	3,672
$\|\|\mu\rightarrow\|\|$(D)	2,2444	5,5247	0,9026
α (u, a)	-99,413	-109,235	-87,489

Among the investigated Schiff bases, HBMM possesses the highest HOMO energy (Table 3), signifying its superior electron-donating ability. Calculated energy gaps for HBMC, HBMN, and HBMM (3.98, 3.65, and 4.14 eV, respectively) suggest that HBMN likely exhibits the highest reactivity. Consequently, the molecules' chemical stability can be ordered as follows: HBMM > HBMN > HBMC.

The electrophilicity index (ω) quantifies a molecule's propensity to accept electrons. Our analysis revealed that HBMM has the strongest electron-donating character, while HBMN is the most potent electron acceptor.

Global hardness (η) and softness (S) offer complementary insights into molecular stability and reactivity. A lower hardness value implies decreased stability, while a higher softness value suggests greater chemical reactivity. HBMN exhibits the lowest calculated hardness in the gas phase, indicating lower stability compared to the other molecules. Its corresponding high softness value suggests that it readily participates in charge-transfer mechanisms. To gain a comprehensive understanding of these charge-transfer processes, considering electronegativity (χ) alongside these descriptors is important.

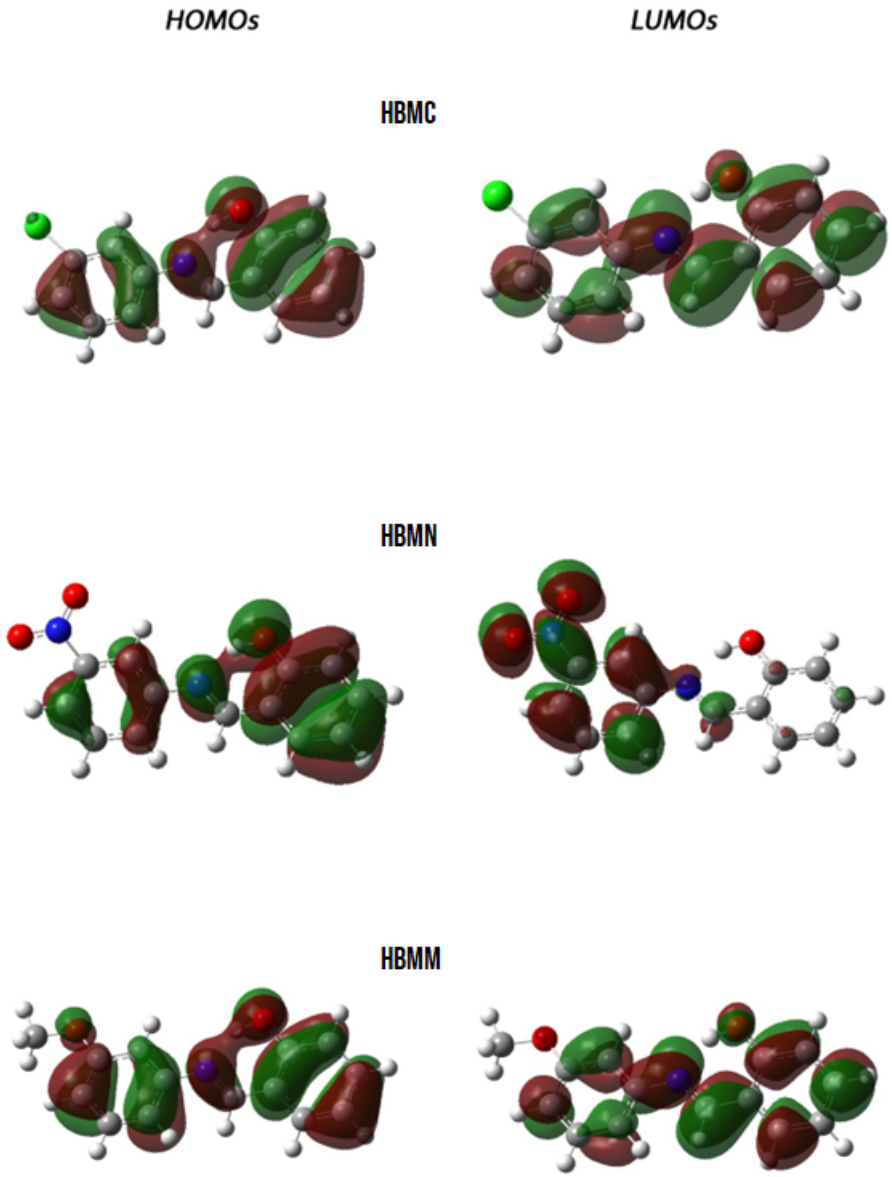

Figure 5.8: plots of the frontier molecular orbitals for HBMC, HBMN and HBMM.

The electronic chemical potential (μ), with its negative sign convention, indicates a molecule's tendency to attract electrons. Our calculations reveal that HBMM possesses a lower electronegativity than the other compounds, signifying a greater propensity to donate electrons rather than capture them. This characteristic is desirable for antioxidant activity. Furthermore, a lower chemical potential suggests that an electron is more likely to escape from the molecule. The significantly lower μ value of HBMM implies enhanced electron-donating ability. Taken together, these reactivity descriptors suggest that HBMM has promising potential as an antioxidant by participating in electron-scavenging mechanisms.

Molecular electrostatic potential (MEP) maps were generated at the 6-311+G (d,p) level of theory to visualize electron density distribution and predict reactive sites within compounds 1-3. MEP analysis is valuable for understanding electrophilic and nucleophilic reactivity [188, 189]. In these maps, regions of high electron density (prone to electrophilic attack) are colored red, while areas of low electron density (susceptible to nucleophilic attack) are shown in blue [190].

Our MEP maps (Figure 5.9) reveal concentrated negative potential around the oxygen atoms, with minima between -29.95 and -24 kcal/mol. Conversely, the most positive potential regions (maxima between 24 and 29.95 kcal/mol) surround the phenolic hydroxyl hydrogen atoms. These findings suggest that electron and hydrogen atom donation to oxidizing species is most likely to occur at these positively charged sites.

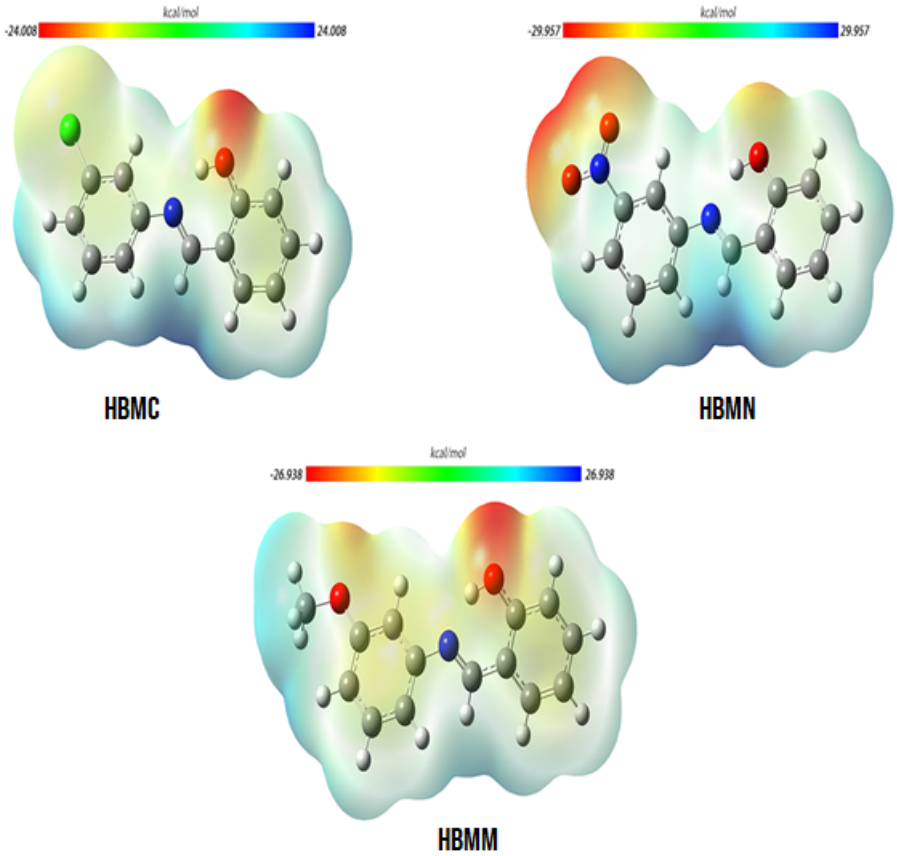

Figure 5.9: Molecular electrostatic potential maps of HBMC, HBMN and HBMM

5.5 Antioxidant Mechanism

The antioxidant activity of phenolic compounds is primarily attributed to their phenolic hydroxyl groups, which can neutralize free radicals through several potential mechanisms. Importantly, these mechanisms (such as HAT, SET-PT, and SPLET) can operate simultaneously, with their relative importance influenced by the specific solvent and radical species [135].

To gain deeper insights into these antioxidant mechanisms, we employed density functional theory (DFT) calculations. This approach allows the quantification of key thermodynamic parameters (BDE, IP, PDE, PA, and ETE) associated with different radical scavenging pathways [122]. Calculated enthalpies at 298.15 K, along with the established antioxidant Trolox as a reference, provide the basis for our analysis.

5.5.1 HAT mechanism

In the HAT mechanism, the bond dissociation enthalpy (BDE) of the phenolic O-H bond is a key indicator of antioxidant potential [191, 192]. Lower BDE values signify easier hydrogen atom donation. Our calculations (Table 5.3) reveal that HBMC consistently exhibits the lowest BDE among the investigated compounds, both in the gas phase and across different solvents. This suggests HBMC possesses the greatest hydrogen-donating ability, followed by HBMN and HBMM Intriguingly, the calculated BDE values for all three compounds are comparable to the reference antioxidant Trolox, implying promising antioxidant activity.

Solvent effects on BDE were observed, with values generally increasing from the gas phase to solvated environments. However, BDEs remained relatively similar for each compound across the studied solvents. Notably, water consistently yielded the lowest BDE values.

5.5.2 SET-PT mechanism

The SET-PT mechanism is another important pathway for antioxidant activity [134]. Ionization potentials (IP) and proton dissociation enthalpies (PDE) provide valuable insights into this mechanism. As seen in Table 5.3, HBMM exhibits the lowest IPs across all environments, indicating the strongest electron-donating ability among the investigated compounds. IP trends differed from those of BDE, likely because IP reflects the entire molecular structure, while BDE is more sensitive to local substituent effects [134]. While

IPs for our compounds were higher than the Trolox reference, they suggest potential antioxidant activity.

Solvent choice significantly influenced IP values. A consistent decrease in IP was observed from the gas phase to solvated environments, following the trend: gas > benzene > ethanol > water > chloroform. This supports the influence of solvent polarity on cation radical stability, a key intermediate in the SET-PT mechanism [134, 193]. Polar solvents stabilize charged species and promote π-electron delocalization, enhancing electron transfer efficiency.

PDEs, also crucial in SET-PT, were significantly reduced in solvents compared to the gas phase. This aligns with the stabilizing effect of polar solvents on protons and radical cations, promoting easier proton dissociation.

5.5.3 SPLET mechanism

The SPLET mechanism plays a crucial role in antioxidant behavior [126, 122, 192, 194]. Our analysis reveals that HBMN consistently exhibits the lowest proton affinity (PA) values across all environments (Table 5.3), signifying its strongest potential for deprotonation. PDE values show similar trends, decreasing significantly from the gas phase to solvents. This decrease aligns with the enhanced solvation of protons in solvent environments. Substantial differences in PA between the gas phase and solvents (detailed values provided) further highlight how solvents promote deprotonation.

Electron transfer enthalpies (ETE) follow the order: HBMM < HBMC < HBMN. Importantly, ETE values are consistently lower than the ionization potentials (IP) of the corresponding neutral molecules. This reduced energy barrier for electron transfer supports the potential of our compounds to act as electron donors in antioxidant reactions.

Our calculations reveal a distinct shift in the dominant antioxidant mechanism depending on the environment. In the gas phase, the HAT mechanism appears most thermodynamically favorable, as supported by the relatively lower BDE values compared to IP and PA. However, in polar solvents, the SPLET mechanism gains prominence due to decreased PA values, reflecting easier deprotonation.

Analysis of calculated enthalpies in polar solvents (e.g., ethanol, benzene) highlights the thermodynamic preference for the SPLET mechanism. HBMC exhibits the lowest overall enthalpy associated with the SPLET pathway (PA+ETE), suggesting its superior

potential for radical scavenging activity [135]. Furthermore, the consistently lower ETE values (compared to BDE and IP) across all compounds underscore the thermodynamic advantage of the SPLET mechanism over HAT and SET-PT.

Table 5.3: The calculated thermodynamic parameters of tested compounds in gas and solvents at the B3LYP/6-311+G(d,p)

		BDE	IP	PDE	IP+PDE	PA	ÉTÉ	PA+ETE
Gas	HBMC	80,309	178,835	215,770	394,604	325,970	68,634	394,604
	HBMN	80,366	185,784	208,878	394,662	321,206	73,456	394,662
	HBMM	83,607	163,837	234,066	397,903	334,567	63,336	397,903
	Trolox	73,614	157,767	230,143	387,909	346,908	41,002	387,909
Water	HBMC	391,358	116,497	6,051	122,548	38,741	83,807	122,548
	HBMN	392,221	119,518	3,893	123,411	38,156	85,256	123,411
	HBMM	393,951	107,374	17,767	125,141	41,814	83,327	125,141
	Trolox	383,796	98,197	16,790	114,986	52,104	62,882	114,986
Ethanol	HBMC	393,109	124,338	0,160	124,497	34,778	89,719	124,497
	HBMN	393,334	126,901	-2,178	124,723	33,843	90,879	124,723
	HBMM	395,837	114,899	12,327	127,225	38,666	88,559	127,225
	Trolox	380,701	100,903	11,186	112,090	44,100	67,990	112,090
$CHCl_3$	HBMC	393,115	69,969	33,618	103,587	82,669	20,918	103,587
	HBMN	394,090	74,340	30,221	104,561	81,672	22,890	104,561
	HBMM	396,382	58,823	48,031	106,854	88,295	18,559	106,854
	Trolox	386,081	50,456	46,097	96,552	99,245	-2,693	96,552
Benzene	HBMC	393,286	155,364	21,225	176,589	88,130	88,459	176,589
	HBMN	394,359	161,290	16,371	177,661	86,225	91,436	177,661
	HBMM	396,870	143,026	37,147	180,173	95,238	84,935	180,173
	Trolox	386,652	135,581	34,374	169,955	106,785	63,170	169,955

All values are in kcal/mol

5.6 PASS and Molecular docking computations

PASS analysis revealed that HBMC, HBMN, and HBMM have a high probability (Pa values ≥ 0.7) of interacting with several potential therapeutic targets (Table 4). Of particular interest is their predicted inhibition of Ubiquinol-Cytochrome C Reductase Binding Protein (UQCRB), with Pa values of 0.84, 0.903, and 0.805 respectively. UQCRB is a vital component of the mitochondrial electron transport chain, critical for cellular energy production. However, complex III, of which UQCRB is part, is also a significant source of reactive oxygen species (ROS). Overproduction of ROS leads to oxidative stress, a hallmark of many diseases including cancer, neurodegeneration, and cardiovascular disorders [6] . Studies

show that UQCRB dysregulation can worsen oxidative stress, while its downregulation can reduce angiogenesis and potentially hinder tumor growth [7, 195]. Therefore, the predicted inhibition of UQCRB by our Schiff base derivatives offers a multi-pronged therapeutic strategy: reducing ROS production (antioxidant effect) and potentially combating diseases where UQCRB is overactive.

Table 5.4: PASS prediction for the bioactivity of the HBMC, HBMN and HBMM

HBMC			**HBMN**			**HBMM**		
Pa	Pi	Name of the inhibitor	Pa	Pi	Name of the inhibitor	Pa	Pi	Name of the inhibitor
0,84	**0,02**	**Ubiquinol-cytochrome-c reductase inhibitor**	0,904	0,003	Glucan endo-1,6-beta-glucosidase inhibitor	0,906	0,007	Aspulvinone dimethylallyltransferase inhibitor
0,802	0,02	Chlordecone reductase inhibitor	**0,903**	**0,005**	**Ubiquinol-cytochrome-c reductase inhibitor**	**0,805**	**0,031**	**Ubiquinol-cytochrome-c reductase inhibitor**
0,783	0,005	HMGCS2 expression enhancer	0,854	0,005	Monodehydroascorbate reductase (NADH) inhibitor	0,766	0,004	Insulysin inhibitor
0,792	0,014	Taurine dehydrogenase inhibitor	0,852	0,003	3-Phytase inhibitor	0,778	0,024	Chlordecone reductase inhibitor
0,786	0,022	Antiseborrheic	0,848	0,002	Hydroxylamine reductase (NADH) inhibitor	0,761	0,02	Taurine dehydrogenase inhibitor
0,764	0,004	Insulysin inhibitor	0,841	0,003	Laccase inhibitor	0,756	0,03	Gluconate 2-dehydrogenase (acceptor) inhibitor
0,77	0,019	Glycosylphosphatidylinos phospholipase D inhibitor	0,831	0,004	HMGCS2 expression enhancer	0,73	0,008	HMGCS2 expression enhancer
0,753	0,015	Dehydro-L-gulonate decarboxylase inhibitor	0,826	0,003	Phosphatidylserine decarboxylase inhibitor	0,72	0,02	Dehydro-L-gulonate decarboxylase inhibitor
0,733	0,001	Falcipain 3 inhibitor	0,828	0,008	Arylacetonitrilase inhibitor	0,706	0,021	Feruloyl esterase inhibitor
0,744	0,02	NADPH peroxidase inhibitor	0,822	0,005	Bisphosphoglycerate phosphatase inhibitor			
0,759	0,045	Aspulvinone dimethylallyltransferase inhibitor	0,803	0,003	Hyponitrite reductase inhibitor			
0,751	0,046	Membrane integrity agonist	0,813	0,018	Saccharopepsin inhibitor			
0,704	0,014	2-Hydroxyquinoline 8-monooxygenase inhibitor	0,813	0,018	Acrocylindropepsin inhibitor			
0,705	0,018	Glutathione thiolesterase inhibitor	0,813	0,018	Chymosin inhibitor			

**Pa: Probability to be active. **Pi: Probability to be inactive.*

Molecular docking is a valuable computational tool in drug design, allowing researchers to predict how potential drug molecules interact with their target proteins. To assess the inhibitory potential of HBMC, HBMN, and HBMM against the UQCRB protein, we conducted a molecular docking study. Among the three inhibitors, HBMM displayed the most favorable binding energy (-7.68 kcal/mol), followed by HBMN (-7.25 kcal/mol) and HBMC (-6.44 kcal/mol). These affinities are comparable to similar molecular systems reported in previous studies [177, 196] . Calculated inhibition constants (Ki) provide additional support: 2.34, 4.80, and 19.13 μM for HBMC, HBMN, and HBMM,

respectively. The Ki value indicates the drug concentration required for effective enzyme inhibition [197].

Table 5.5: Docking results of the binding affinity (ΔGbind) and inhibition constant (Ki) values for different poses of inhibitors HBMC, HBMN and HBMM in UQCRB active site.

	HBMC		**HBMN**		**HBMM**	
Conformatios of Ligand	ΔG_{bind} (kcal/mol	K_i (μM)	ΔG_{bind} (kcal/mol	K_i (μM)	ΔG_{bind} (kcal/mol	K_i (μM)
1	-6,44	19,13	-7,25	4,81	-7,68	2,34
2	-6,33	23,06	-7,08	6,5	-7,68	2,36
3	-6,32	23,12	-6,94	8,12	-7,67	2,39
4	-6,24	26,61	-6,51	16,96	-7,65	2,46
5	-6,24	26,76	-6,5	17,09	-7,63	2,54
6	-6,25	27,48	-6,49	17,4	-7,63	2,56
7	-6,2	28,67	-6,18	29,56	-7,63	2,57
8	-6,12	32,83	-6,49	17,56	-7,62	2,61
9	-5,69	67,67	-6,48	17,87	-7,55	2,9
10	-5,68	68,98	-6,38	21,07	-7,54	2,96

Our molecular docking results (Figures 5.10, 5.11 , 5.12 , Table 5.6) reveal a rich network of interactions governing the binding of HBMC, HBMN, and HBMM within the UQCRB active site. Let's examine the key highlights:

- Conventional hydrogen bonds play a crucial role in anchoring all three compounds. The phenolic hydroxyl groups consistently form strong hydrogen bonds with ASP228 and SER35, indicating their importance in UQCRB binding. Notably, HBMN's nitro group also establishes essential hydrogen bonds with LYS227. The short bond distances (< 3 Å) reinforce the strength of these interactions.
- Aromatic rings in the studied compounds engage in various hydrophobic interactions, contributing to overall stability. Pi-pi stacking (e.g., with TYR224) and pi-alkyl interactions (e.g., with HIS201 and LEU residues) are particularly prevalent. The methoxy group in HBMM also participates in hydrophobic interactions.
- The chlorine atom in HBMC engages in alkyl interactions with LEU200 and LEU21, potentially adding to binding specificity. The nitro group of HBMN establishes key hydrogen bonds and likely plays a vital role in its strong interaction with UQCRB.
- Weaker but still significant interactions are observed. Carbon hydrogen bonds (e.g., with ALA17) and pi-sigma interactions contribute to the overall binding landscape.

This intricate pattern of interactions underscores the potential of your Schiff base derivatives to bind favorably within the UQCRB active site. The presence of strong hydrogen

bonds, in particular, suggests their capacity for potent and specific inhibition. This, coupled with their antioxidant properties, makes them promising leads for further drug development targeting UQCRB-linked diseases.

Table 5.6: Binding interactions of HBMC, HBMN and HBMM with the active site of UQCRB protein

Residue	Compound	Interacting groups of compounds	Category	Type	Distance (Å)
ASP228	HBMC	OH	H-Bond	Conventional Hydrogen Bond	2,010402
ASN32		O atom	H-Bond	Carbon Hydrogen Bond	3,728983
SER35		OH	H-Bond	Conventional Hydrogen Bond	2,060828
TYR224		Phenolic ring	Hydrophobic	Pi-Pi Stacked	4,813270
ILE27		Phenolic ring	Hydrophobic	Pi-Alkyl	5,258602
LEU21		Chlorophenyl ring	Hydrophobic	Pi-Sigma	3,854900
LEU21		Cl atom	Hydrophobic	Alkyl	4,422685
HIS201		Cl atom	Hydrophobic	Pi-Alkyl	4,383668
LEU200		Cl atom	Hydrophobic	Alkyl	4,057369
LYS227	HBMN	O (Nitro group)	H- Bond	Conventional Hydrogen Bond	2,756822
LYS227		O (Nitro group)	H- Bond	Conventional Hydrogen Bond	2,836927
TYR224		nitrophenyl ring	Hydrophobic	Pi-Pi Stacked	5,799949
ALA17		OH	H- Bond	Conventional Hydrogen Bond	2,371877
LEU21		Phenolic ring	Hydrophobic	Pi-Sigma	3,623571
LEU200		Phenolic ring	Hydrophobic	Pi-Sigma	3,448381
PHE220		Nitrophenyl ring	Hydrophobic	Pi-Pi T-shaped	5,684992
ASP228	HBMM	OH	H-Bond	Conventional Hydrogen Bond	3,00271
ASP228		OH	H-Bond	Conventional Hydrogen Bond	2,85004
SER35		OH	H-Bond	Conventional Hydrogen Bond	1,97392
HIS201		C (methoxy group)	Hydrophobic	Pi-Alkyl	4,82415
LEU197		C (methoxy group)	Hydrophobic	Alkyl	4,56579
ALA17		C (methoxy group)	H- Bond	Carbon Hydrogen Bond	3,19353
LEU21		Metoxyphenyl ring	Hydrophobic	Pi-Sigma	3,48294
LEU200		Metoxyphenyl ring	Hydrophobic	Pi-Sigma	3,83196

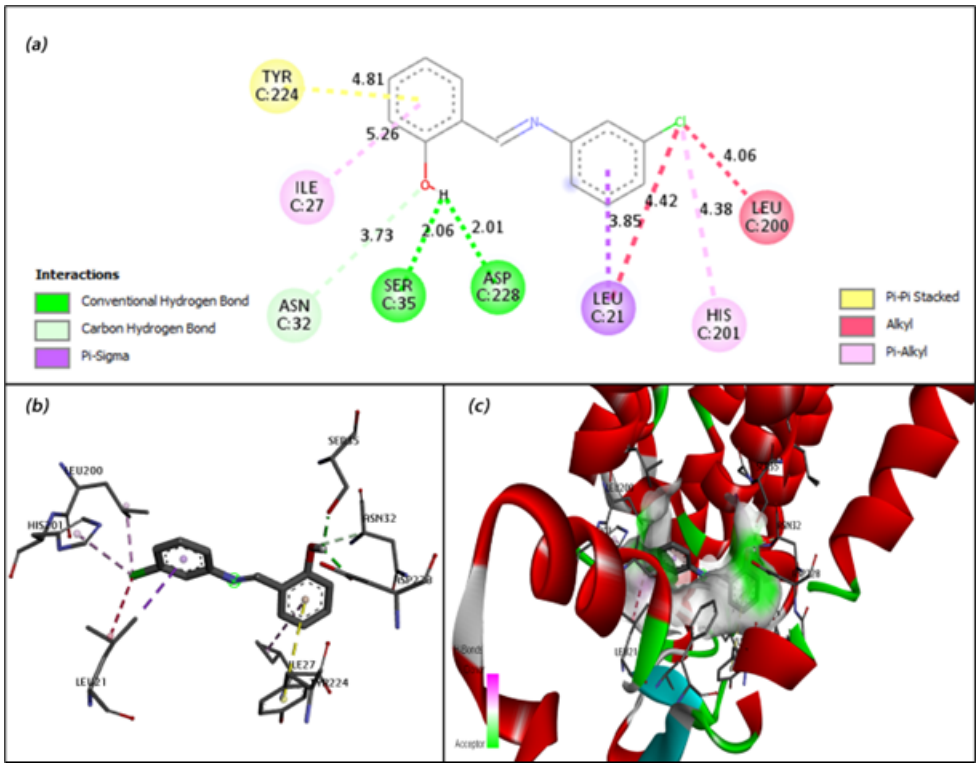

Figure 5.10: (a) HBMC and UQCRB interactions (2D). (b) HBMC and UQCRB interactions (3D). (c) HBMC binds at the active site of UQCRB).

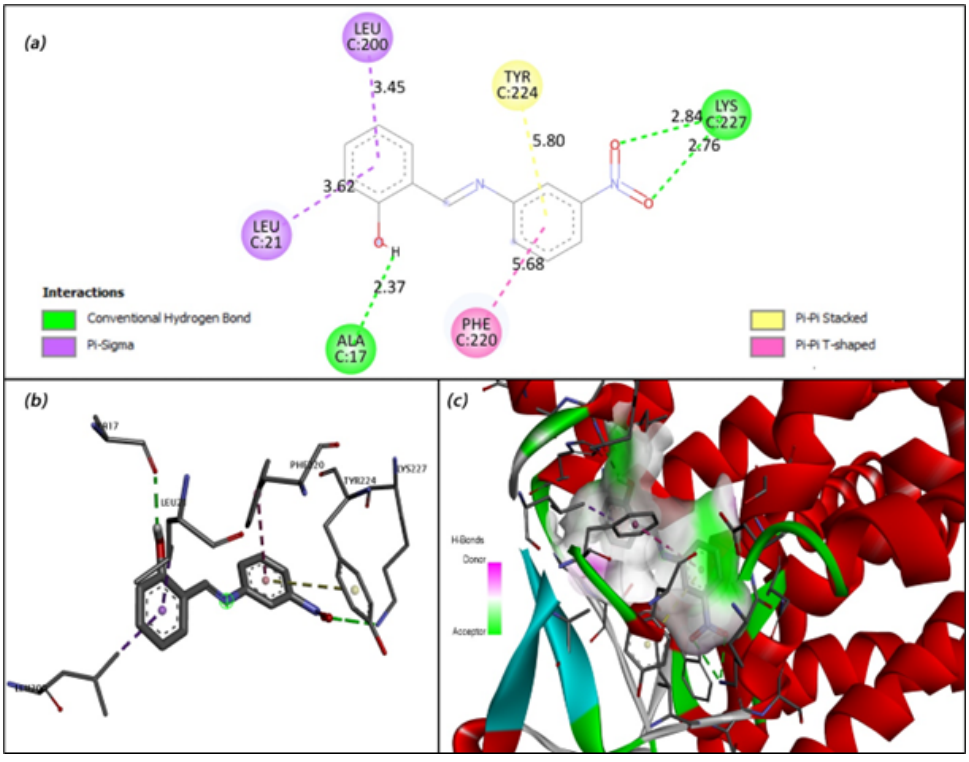

Figure 5.11: (a) Compound HBMN and UQCRB interactions (2D). (b) HBMN and UQCRB interactions (3D). (c) HBMN binds at the active site of UQCRB.

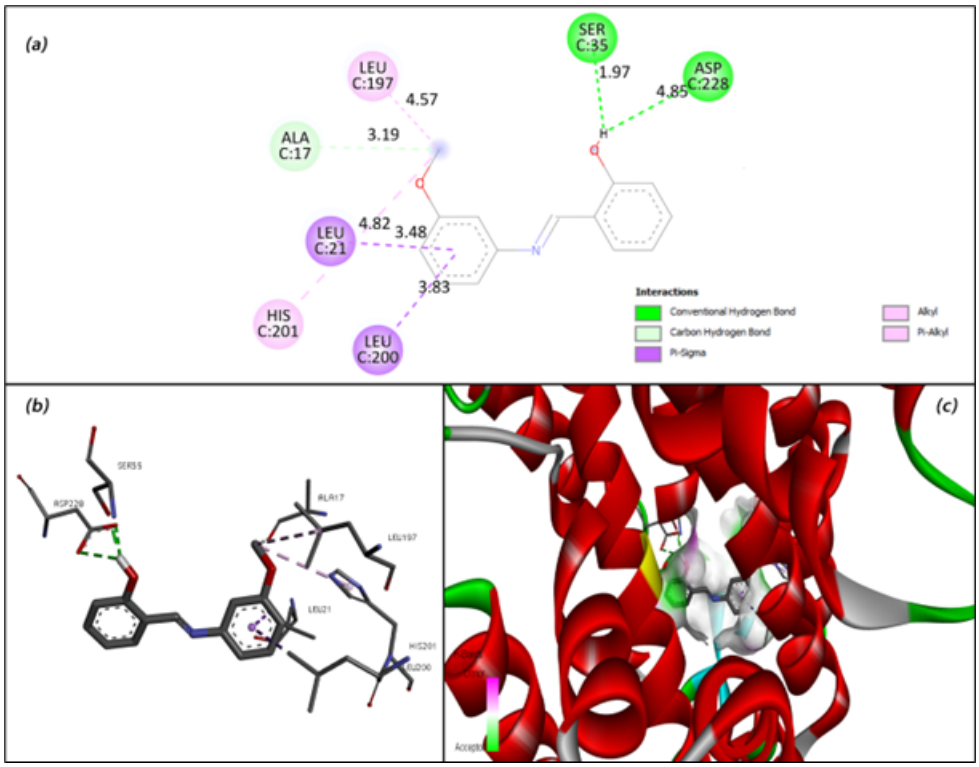

Figure 5.12: (a) HBMM and UQCRB interactions (2D). (b) HBMM and UQCRB interactions (3D). (c) HBMM binds at the active site of UQCRB

5.7 Prediction of pharmacokinetics and drug-likeness properties

5.7.1 ADME properties analysis

Schiff bases, due to their chemical versatility and diverse biological activities, hold significant promise as therapeutic agents. However, to realize their full potential as pharmaceuticals, understanding their absorption, distribution, metabolism, excretion (ADME), and toxicity properties is crucial. Thorough ADME profiling guides drug development and helps anticipate potential challenges like drug-drug interactions or side effects.

5.7.1.1 Absorption

Our computational analysis reveals encouraging absorption characteristics for the investigated Schiff base derivatives. All compounds demonstrate high Caco-2 permeability values (0.933 to 1.677), surpassing the threshold (>0.90) for good absorption. Moreover, their predicted intestinal absorption rates lie within the favorable 90-93% range. Collectively, these findings strongly suggest that our compounds have the potential to be well-absorbed following oral administration, which represents a significant advantage for

drug development.

5.7.1.2 Distribution

- **BBB Permeability:** Our compounds exhibit low predicted blood-brain barrier (BBB) permeability (LogBB values). This suggests limited distribution into the brain, which could be advantageous in avoiding CNS side effects, especially if the therapeutic target is outside the CNS. HBMC shows slightly higher BBB permeability, which warrants consideration if CNS effects are a concern.
- **CNS Access:** All compounds exhibit low CNS permeability (LogPS values). This aligns with the BBB findings and further reinforces the likelihood of limited CNS activity.

5.7.1.3 Metabolism

- **CYP Interactions:** Our Schiff bases likely interact with the CYP450 enzyme system, particularly CYP3A4, where they are predicted to be both substrates and inhibitors. This highlights the need to consider potential drug-drug interactions during development. Interestingly, only HBMC shows potential to inhibit CYP2D6.

5.7.1.4 Excretion and Toxicity

- **Clearance:** The predicted clearance rates for the compounds fall within an acceptable range. This suggests they may have a suitable duration of action in the body.
- **Toxicity:** Our analysis indicates a favorable initial toxicity profile for all three compounds. This is promising, but further safety studies are essential.

These findings provide valuable insights into the ADME characteristics of our Schiff base derivatives. The potential for CYP interactions, particularly with CYP3A4, warrants careful attention during further development. The limited CNS penetration could be beneficial depending on the specific therapeutic goals. The favorable initial toxicity profile is encouraging.

Table 5.7: In-silico ADME-Tox properties of the newly synthesized compounds

Properties	Unit	HBMC	HBMN	HBMM
Absorption				
Caco2 permeability	Numeric (log Papp in 10-6 cm/s)	1.677	0.933	1.654
Intestinal absorption (human)	Numeric (% Absorbed)	91.111	90.426	92.959
Distribution				
BBB permeability	Numeric (log BB)	0.357	-0.28	-0.229
CNS permeability	Numeric (log PS)	-1.576	-2.008	-1.686
Metabolism				
CYP2D6 substrate	Categorical (Yes/No)	No	No	No
CYP2D6 inhibitior	Categorical (Yes/No)	Yes	No	No
CYP3A4 substrate	Categorical (Yes/No)	Yes	Yes	Yes
CYP3A4 inhibitior	Categorical (Yes/No)	Yes	Yes	Yes
Excretion				
Total Clearance	Numeric (log ml/min/kg)	0.142	0.180	0.235
Toxicity				
AMES toxicity	Categorical (Yes/No)	No	No	No
Hepatotoxicity	Categorical (Yes/No)	No	No	No
Skin Sensitisation	Categorical (Yes/No)	No	No	No

5.7.2 Physicochemical Properties Analysis

5.7.2.1 Lipinski's Rule

All three compounds (HBMC, HBMN, HBMM) fully adhere to Lipinski's Rule of Five:

- Molecular weight under 500 g/mol ensures reasonable size.
- LogP values below 5 indicate suitable lipophilicity for potential cell permeability.
- Hydrogen bond acceptor counts ($\leq$10) are within acceptable limits.
- Hydrogen bond donor counts ($\leq$5) are within acceptable limits.
- Molar refractivity values fall within the ideal range (40-130), supporting their drug-like characteristics.

5.7.2.2 Beyond Lipinski

- Rotatable Bonds (RB): Counts of 2-3 suggest good flexibility, which could aid in binding to target sites.

- TPSA (Topological Polar Surface Area): TPSA values indicate moderate polarity. However, HBMN has a slightly higher TPSA (78.41), suggesting potentially lower cell permeability compared to the other two compounds.
- LogS (Solubility): Values in the -3.5 to -4 range indicate moderate water solubility.

Table 5.8: Physicochemical properties and drug-likeness prediction of the synthesized compounds

Physicochemical Properties	**HBMC**	**HBMN**	**HBMM**
Molecular Weight (MW <500 g/mol)	231.682	242.234	227.263
Lipophility (Log P ≤5)	3.7962	3.051	3.1514
hydrogen bond Acceptors (HBA ≤10)	2	4	3
hydrogen bond Donors (HBD <5)	1	1	1
Molar refractivity (≥ 40 MR 130 ≤)	67.17	70.98	68.65
RB	2	3	3
TPSA	32.59	78.41	41.82
Log S	-4.04	-3.48	-3.50
Drug-likeness			
lipinski	Yes	Yes	Yes
Ghose	Yes	Yes	Yes
Veber	Yes	Yes	Yes
Egan	Yes	Yes	Yes
Muegge	Yes	Yes	Yes
Violation	No	No	No

The studied compounds consistently comply with the Ghose, Veber, Egan, and Muegge drug-likeness filters. This strongly supports their potential to exhibit favorable pharmacokinetic properties.

General Conclusion

This comprehensive study involved the successful synthesis and extensive characterization of three novel Schiff base derivatives, namely HBMC, HBMN, and HBMM. A combination of experimental spectroscopic techniques (FT-IR, 1H NMR, and UV-Vis) and quantum chemical computations (DFT at the B3LYP/6-311G+ (d,p) level) provided strong structural elucidation. Detailed vibrational assignments with potential energy distribution analysis corroborated well with established literature ranges, further confirming the structures.

To explore their potential antioxidant activity, we investigated key mechanisms through meticulously calculated thermodynamic parameters. These included bond dissociation energies (BDEs), ionization potentials (IPs), proton dissociation enthalpies (PDEs), proton affinities (PAs), and electron transfer enthalpies (ETEs) under diverse solvent conditions (water, ethanol, chloroform, and benzene). Our findings suggest a solvent-dependent shift in the dominant antioxidant mechanism. Specifically, the SPLET mechanism appears most favorable in polar media, while the HAT mechanism likely prevails in the gas phase. Among the investigated compounds, HBMC consistently exhibited the lowest BDE, IP, and ETE values, signaling its superior potential capacity for radical scavenging. Theoretical ADME-Tox profiling underscored the promising drug-like characteristics of our compounds. Importantly, they adhered to Lipinski's Rule of Five, along with the Ghose, Veber, Egan, and Muegge filters. Key physicochemical properties, including LogP, TPSA, rotatable bond count, and solubility, suggest favorable absorption, bioavailability, and the potential to interact effectively with target binding sites.

Molecular docking studies shed light on the potential therapeutic application of these derivatives as Ubiquinol-Cytochrome C reductase binding protein (UQCRB) inhibitors. UQCRB, a vital component of mitochondrial complex III, plays a role in oxidative stress and has been implicated in various diseases. All three compounds demonstrated fa-

vorable binding interactions within the UQCRB active site, with HBMM displaying the strongest binding affinity (-7.68 kcal/mol). The specific residues involved in hydrogen bonding, π-stacking, and hydrophobic interactions enhance our understanding of the binding mechanism.

This multifaceted research offers valuable insights into the antioxidant properties and therapeutic potential of novel Schiff bases. From this perspective, several exciting avenues for further investigation emerge. Firstly, in vitro and in vivo assays are crucial to validate the predicted antioxidant activity and UQCRB inhibition. These experimental validations will provide a strong foundation for subsequent pre-clinical studies. Secondly, targeted experiments to elucidate the dominant radical scavenging mechanisms in different environments would complement the theoretical predictions and offer a more comprehensive understanding of the antioxidant potential. Furthermore, in-depth toxicity assessments of the most promising leads are paramount for their development as pharmaceuticals or safe food additives. In conclusion, this study lays the groundwork for further development of Schiff base derivatives with multifaceted applications, potentially combating oxidative stress and addressing unmet medical needs.

Bibliography

[1] Tugba Raika Kıran, Onder Otlu, and Aysun Bay Karabulut. Oxidative stress and antioxidants in health and disease. *Journal of Laboratory Medicine*, 47(1):1–11, 2023.

[2] Klaudia Jomova, Renata Raptova, Suliman Y Alomar, Saleh H Alwasel, Eugenie Nepovimova, Kamil Kuca, and Marian Valko. Reactive oxygen species, toxicity, oxidative stress, and antioxidants: Chronic diseases and aging. *Archives of toxicology*, 97(10):2499–2574, 2023.

[3] Narendra Kumar Chaudhary, Biswash Guragain, Siyanand Kumar Chaudhary, and Parashuram Mishra. Schiff base metal complex as a potential therapeutic drug in medical science: A critical review. *Bibechana*, 18(1):214–230, 2021.

[4] Pallavi Jain and Prashant Singh. *Structural and Biological Applications of Schiff Base Metal Complexes*. CRC Press, 2023.

[5] Senthil Kumar Raju, Archana Settu, Archana Thiyagarajan, Divya Rama, Praveen Sekar, and Shridharshini Kumar. Biological applications of schiff bases: An overview. *GSC Biological and Pharmaceutical Sciences*, 21(3):203–215, 2022.

[6] Hyun-Chul Kim, Junghwa Chang, Hannah S Lee, and Ho Jeong Kwon. Mitochondrial uqcrb as a new molecular prognostic biomarker of human colorectal cancer. *Experimental & molecular medicine*, 49(11):e391–e391, 2017.

[7] Hye Jin Jung, Ki Hyun Kim, Nam Doo Kim, Gyoonhee Han, and Ho Jeong Kwon. Identification of a novel small molecule targeting uqcrb of mitochondrial complex iii and its anti-angiogenic activity. *Bioorganic & medicinal chemistry letters*, 21(3): 1052–1056, 2011.

[8] Hugo Schiff. Mittheilungen aus dem universitätslaboratorium in pisa: Eine neue reihe organischer basen. *European Journal of Organic Chemistry*, 131:118–119, 2023.

[9] A Xavier and N Srividhya. Synthesis and study of schiff base ligands. *IOSR Journal of Applied Chemistry*, 7(11):06–15, 2014.

[10] JM Sayer, B Pinsky, A Schonbrunn, and W Washtien. Mechanism of carbinolamine formation. *Journal of the American Chemical Society*, 96(26):7998–8009, 1974.

[11] Nuriye Tuna Subasi. Overview of schiff bases. In *Schiff Base in Organic, Inorganic and Physical Chemistry*. IntechOpen, 2022.

[12] Abdullahi Owolabi Sobola, Gareth Mostyn Watkins, and Bernadus Van Brecht. Synthesis, characterization and antimicrobial activity of copper (ii) complexes of some ortho-substituted aniline schiff bases; crystal structure of bis (2-methoxy-6-imino) methylphenol copper (ii) complex. *South African Journal of Chemistry*, 67: 45–51, 2014.

[13] Jonathan Clayden, Nick Greeves, and Stuart Warren. *Organic chemistry*. Oxford University Press, USA, 2012.

[14] Manoj Kumar. Recent advances in 3d-block metal complexes with bi, tri, and tetradentate schiff base ligands derived from salicylaldehyde and its derivatives: Synthesis, characterization and applications. *Coordination Chemistry Reviews*, 488: 215176, 2023. ISSN 0010-8545.

[15] Sayed Suliman Shah, Dawood Shah, Ibrahim Khan, Sajjad Ahmad, Umar Ali, and A Rahman. Synthesis and antioxidant activities of schiff bases and their complexes: An updated review. *Biointerface Res. Appl. Chem*, 10:6936–6963, 2020.

[16] Irfankhan R Pathan and Milind K Patel. A comprehensive review on the synthesis and applications of schiff base ligand and metal complexes: A comparative study of conventional heating, microwave heating, and sonochemical methods. *Inorganic Chemistry Communications*, page 111464, 2023.

[17] Ankit Sharma and S. Arora. A review study on green synthesis of schiff bases. *INDIAN JOURNAL OF APPLIED RESEARCH*, pages 69–72, 04 2023. doi: 10.36106/ijar/9529205.

[18] Anahed A Yaseen, Emaad TB Al-Tikrity, Mohammed H Al-Mashhadani, Nadia Salih, and Emad Yousif. An overview: Using different approaches to synthesis new schiff bases materials. *Journal of university of Anbar for Pure science*, 15(2):53–59, 2021.

[19] Yosef Bayeh, Fekiya Mohammed, Mamo Gebrezgiabher, Fikre Elemo, Mesfin Getachew, and Madhu Thomas. Synthesis, characterization and antibacterial ac-

tivities of polydentate schiff bases, based on salicylaldehyde. *Advances in Biological Chemistry*, 10(05):127–139, 2020.

[20] Chérifa Boulechfar, Hana Ferkous, Amel Delimi, Amel Djedouani, Abdesalem Kahlouche, Abir Boublia, Ahmad S Darwish, Tarek Lemaoui, Rajesh Verma, and Yacine Benguerba. Schiff bases and their metal complexes: a review on the history, synthesis, and applications. *Inorganic Chemistry Communications*, page 110451, 2023.

[21] Shridharshini Kumar, Praveen Sekar, and Senthil Kumar Raju. A review on microwave-assisted synthesis and biomedical applications of schiff bases. *Advance Pharmaceutical Journal*, 8:1–16, 2023.

[22] Hulya Celik and Müslüm Kuzu. Microvawe assisted synthesis of n-(methyl and methoxy) benzylidene-4-fluoroaniline derivatives and their carbonic anhydrase i and ii inhibition properties. *analytical chemistry*, 3:4, 2019.

[23] Seema Nagar, Smriti Raizada, and Neha Tripathee. A review on various green methods for synthesis of schiff base ligands and their metal complexes. *Results in Chemistry*, page 101153, 2023.

[24] Bedi Pooja, Malkania Lalit, Gupta Richa, and T Pramanik. Microwave assisted green synthesis of schiff bases in lemon juice medium. *Res. J. Chem. Environ*, 22:19–23, 2018.

[25] Hadi Kargar, Mehdi Fallah-Mehrjardi, Reza Behjatmanesh-Ardakani, Vajiheh Torabi, Khurram Shahzad Munawar, Muhammad Ashfaq, and Muhammad Nawaz Tahir. Sonication-assisted synthesis of new schiff bases derived from 3-ethoxysalicylaldehyde: Crystal structure determination, hirshfeld surface analysis, theoretical calculations and spectroscopic studies. *Journal of Molecular Structure*, 1243:130782, 2021.

[26] Tunde L Yusuf, Segun D Oladipo, Sulaimon A Olagboye, Sizwe J Zamisa, and Gideon F Tolufashe. Solvent-free synthesis of nitrobenzyl schiff bases: Characterization, antibacterial studies, density functional theory and molecular docking studies. *Journal of Molecular Structure*, 1222:128857, 2020.

[27] F Nworie, F Nwabue, N Elom, and S Eluu. Schiff bases and schiff base metal complexes: from syntheses to applications. *Journal of Basic and Applied Research in Biomedicine*, 2(3):295–305, 2016.

[28] D Chaturvedi and M Kamboj. Role of schiff base in drug discovery research. *Chem Sci J*, 7(2):e114, 2016.

[29] Mohammad Nasir Uddin, Sayeda Samina Ahmed, and SM Rahatul Alam. Biomedical applications of schiff base metal complexes. *Journal of Coordination Chemistry*, 73 (23):3109–3149, 2020.

[30] Ursula Theuretzbacher, Karen Bush, Stephan Harbarth, Mical Paul, John H Rex, Evelina Tacconelli, and Guy E Thwaites. Critical analysis of antibacterial agents in clinical development. *Nature Reviews Microbiology*, 18(5):286–298, 2020.

[31] Jessica Ceramella, Domenico Iacopetta, Alessia Catalano, Francesca Cirillo, Rosamaria Lappano, and Maria Stefania Sinicropi. A review on the antimicrobial activity of schiff bases: Data collection and recent studies. *Antibiotics*, 11(2):191, 2022.

[32] Cleiton M Da Silva, Daniel L da Silva, Luzia V Modolo, Rosemeire B Alves, Maria A de Resende, Cleide VB Martins, and Ângelo de Fátima. Schiff bases: A short review of their antimicrobial activities. *Journal of Advanced research*, 2(1):1–8, 2011.

[33] Raji Sankar and TM Sharmila. Schiff bases-based metallo complexes and their crucial role in the realm of pharmacology. a review. *Results in Chemistry*, page 101179, 2023.

[34] Ana O de Souza, Fabio Galetti, Célio L Silva, Beatriz Bicalho, Márcia M Parma, Sebastião F Fonseca, Anita J Marsaioli, Angela CLB Trindade, Rossimíriam P Freitas Gil, Franciglauber S Bezerra, et al. Antimycobacterial and cytotoxicity activity of synthetic and natural compounds. *Química Nova*, 30:1563–1566, 2007.

[35] BC Ejelonu, OE Oyeneyin, OE Akele, and SA Olagboye. Synthesis, characterization and antimicrobial properties of pd (ii), cr (iii), ni (ii) and co (ii) metal complexes of aniline and sulphadiazine schiff bases as mixed ligands. *American Journal of Chemical Research*, 2:1–9, 2018.

[36] Mirsada Salihović, Mirha Pazalja, Selma Špirtović Halilović, Elma Veljović, Irma Mahmutović-Dizdarević, Sunčica Roca, Irena Novaković, and Snežana Trifunović. Synthesis, characterization, antimicrobial activity and dft study of some novel schiff bases. *Journal of Molecular Structure*, 1241:130670, 2021.

[37] Lei Shi, Hui-Ming Ge, Shu-Hua Tan, Huan-Qiu Li, Yong-Chun Song, Hai-Liang Zhu, and Ren-Xiang Tan. Synthesis and antimicrobial activities of schiff bases derived from 5-chloro-salicylaldehyde. *European journal of medicinal chemistry*, 42(4):558–564, 2007.

[38] Hafiz Muhammad Adeel Sharif, Dildar Ahmed, and Hira Mir. Antimicrobial salicylaldehyde schiff bases: Synthesis, characterization and evaluation. *Pak. J. Pharm. Sci*, 28(2):449–455, 2015.

[39] Sonia Losada-Barreiro, Zerrin Sezgin-Bayindir, Fátima Paiva-Martins, and Carlos Bravo-Díaz. Biochemistry of antioxidants: Mechanisms and pharmaceutical applications. *Biomedicines*, 10(12):3051, 2022.

[40] Khurram Shahzad Munawar, Shah Muhammad Haroon, Syed Ammar Hussain, and Hamid Raza. Schiff bases: multipurpose pharmacophores with extensive biological applications. *J Basic Appl Sci*, 14:217–229, 2018.

[41] Irena Kostova and Luciano Saso. Advances in research of schiff-base metal complexes as potent antioxidants. *Current medicinal chemistry*, 20(36):4609–4632, 2013.

[42] Wail Al Zoubi, Abbas Ali Salih Al-Hamdani, and Mosab Kaseem. Synthesis and antioxidant activities of schiff bases and their complexes: a review. *Applied Organometallic Chemistry*, 30(10):810–817, 2016.

[43] Manoj Kumar Rajshree Khare, , and Sunil Vats. Schiff bases and their transition metal complexes: A review. 12:1–10, 2022.

[44] Muhammad Aslam, Itrat Anis, Rashad Mehmood, Lubna Iqbal, Samina Iqbal, InamUllah Khan, Muhammad Salman Chishti, and Shagufta Perveen. Synthesis and biological activities of 2-aminophenol-based schiff bases and their structure–activity relationship. *Medicinal Chemistry Research*, 25:109 – 115, 2015.

[45] Arif Mermer, Neslihan Demirbas, Harun Uslu, Ahmet Demirbas, Sule Ceylan, and Yakup Sirin. Synthesis of novel schiff bases using green chemistry techniques; antimicrobial, antioxidant, antiurease activity screening and molecular docking studies. *Journal of Molecular Structure*, 1181:412–422, 2019. ISSN 0022-2860.

[46] Can Alaşalvar, Aytaç Güder, Halil Gökçe, Çiğdem Albayrak Kaştaş, and Raziye Çatak Çelik. Theoretical, spectroscopic and antioxidant activity studies on (e)-2-[(2-fluorophenylimino)methyl]-4-hydroxyphenol and
(e)-2- [(3-fluorophenylimino)methyl] -4-hydroxyphenol compounds. *Journal of Molecular Structure*, 1133:37–48, 2017. ISSN 0022-2860.

[47] Ayşegül ŞENOCAK and Hüseyin AKBAŞ. Palladium complexes of no type schiff bases: synthesis, characterization and antioxidant activities. *Cumhuriyet Science Journal*, 42:68–74, 03 2021. doi: 10.17776/csj.824566.

[48] Garima Matela. Schiff bases and complexes: a review on anti-cancer activity. *Anti-Cancer Agents in Medicinal Chemistry (Formerly Current Medicinal Chemistry-Anti-Cancer Agents)*, 20(16):1908–1917, 2020.

[49] Martin Kratky, Magdalena Dzurkova, Jiri Janousek, Klara Konecna, Frantisek Trejtnar, Jirina Stolarikova, and Jarmila Vinsova. Sulfadiazine salicylaldehyde-based schiff bases: Synthesis, antimicrobial activity and cytotoxicity. *Molecules*, 22(9):1573, 2017.

[50] Harmeet Kaur, Siong Meng Lim, Kalavathy Ramasamy, Mani Vasudevan, Syed Adnan Ali Shah, and Balasubramanian Narasimhan. Diazenyl schiff bases: Synthesis, spectral analysis, antimicrobial studies and cytotoxic activity on human colorectal carcinoma cell line (hct-116). *Arabian Journal of Chemistry*, 13(1):377–392, 2020.

[51] C Karthik, L Mallesha, S Nagashree, P Mallu, V Patil, and S Kumar. Schiff bases of 4-(methylthio) benzaldehydes: Synthesis, characterization, antibacterial, antioxidant and cytotoxicity studies. *Current Chemistry Letters*, 5(2):71–82, 2016.

[52] Heng Luo, Yu-fen Xia, Bao-fei Sun, Li-rong Huang, Xing-hui Wang, Hua-yong Lou, Xu-hui Zhu, Wei-dong Pan, Xiao-dong Zhang, et al. Synthesis and evaluation of in vitro antibacterial and antitumor activities of novel n, n-disubstituted schiff bases. *Biochemistry Research International*, 2017, 2017.

[53] Nilay Akkuş Taş, Ayşegül Şenocak, and Ali Aydın. Preparation and cytotoxicity evaluation of some amino acid methyl ester schiff bases. *J. Turkish Chem. Soc., Sect. Chem*, 5(2):585–606, 2018.

[54] D Saipriya, Arun Prakash, Suvarna G Kini, K Pai, Subhankar Biswas, et al. Design, synthesis, antioxidant and anticancer activity of novel schiff's bases of 2-amino benzothiazole. *Indian Journal of Pharmaceutical Education & Research*, 52, 2018.

[55] Fereshteh Ahmadinejad, Simon Geir Møller, Morteza Hashemzadeh-Chaleshtori, Gholamreza Bidkhori, and Mohammad-Saeid Jami. Molecular mechanisms behind free radical scavengers function against oxidative stress. *Antioxidants*, 6(3):51, 2017.

[56] Neeti Mehla, Aditi Kothari Chhajer, Kanishka Kumar, Shefali Dahiya, and Vanshika Mohindroo. Applications of antioxidants: A review. *Plant Antioxidants and Health*, pages 1–29, 2021.

[57] Bryan C Dickinson and Christopher J Chang. Chemistry and biology of reactive oxygen species in signaling or stress responses. *Nature chemical biology*, 7(8):504–511, 2011.

[58] Helmut Sies, Carsten Berndt, and Dean P Jones. Oxidative stress. *Annual review of biochemistry*, 86:715–748, 2017.

[59] Carlo M Bergamini, Stefania Gambetti, Alessia Dondi, and Carlo Cervellati. Oxygen, reactive oxygen species and tissue damage. *Current pharmaceutical design*, 10(14): 1611–1626, 2004.

[60] Jennifer N Moloney and Thomas G Cotter. Ros signalling in the biology of cancer. In *Seminars in cell & developmental biology*, volume 80, pages 50–64. Elsevier, 2018.

[61] Zahraa Kamil Kadhim Lawi, Feryal Ameen Merza, Shiama Rabeea Banoon, Mohammed Abd Ali Jabber Al-Saady, and Aswan Al-Abboodi. Mechanisms of antioxidant actions and their role in many human diseases: A review. *Journal of Chemical Health Risks*, 11(Special Issue: Bioactive Compounds: Their Role in the Prevention and Treatment of Diseases):45–57, 2021.

[62] Márcio Carocho and Isabel CFR Ferreira. A review on antioxidants, prooxidants and related controversy: Natural and synthetic compounds, screening and analysis methodologies and future perspectives. *Food and chemical toxicology*, 51:15–25, 2013.

[63] Sergio Di Meo, Tanea T Reed, Paola Venditti, Victor Manuel Victor, et al. Role of ros and rns sources in physiological and pathological conditions. *Oxidative medicine and cellular longevity*, 2016, 2016.

[64] Helmut Sies and Dean P Jones. Reactive oxygen species (ros) as pleiotropic physiological signalling agents. *Nature reviews Molecular cell biology*, 21(7):363–383, 2020.

[65] Celia Andrés Juan, José Manuel Pérez de la Lastra, Francisco J Plou, and Eduardo Pérez-Lebeña. The chemistry of reactive oxygen species (ros) revisited: outlining their role in biological macromolecules (dna, lipids and proteins) and induced pathologies. *International Journal of Molecular Sciences*, 22(9):4642, 2021.

[66] Alam Zeb. Concept, mechanism, and applications of phenolic antioxidants in foods. *Journal of Food Biochemistry*, 44(9):e13394, 2020.

[67] Monika Barteková, Adriana Adameová, Anikó Görbe, Kristína Ferenczyová, Ol'ga Pecháňová, Antigone Lazou, Naranjan S Dhalla, Péter Ferdinandy, and Zoltán Giricz. Natural and synthetic antioxidants targeting cardiac oxidative stress and redox signaling in cardiometabolic diseases. *Free Radical Biology and Medicine*, 169:446–477, 2021.

[68] Gabriele Pizzino, Natasha Irrera, Mariapaola Cucinotta, Giovanni Pallio, Federica Mannino, Vincenzo Arcoraci, Francesco Squadrito, Domenica Altavilla, Alessandra

Bitto, et al. Oxidative stress: harms and benefits for human health. *Oxidative medicine and cellular longevity*, 2017, 2017.

[69] Shampa Chatterjee. Oxidative stress, inflammation, and disease. In *Oxidative stress and biomaterials*, pages 35–58. Elsevier, 2016.

[70] N Francenia Santos-Sanchez, Raul Salas-Coronado, Claudia Villanueva-Canongo, and Beatriz Hernandez-Carlos. Antioxidant compounds and their antioxidant mechanism. *Antioxidants*, 10:1–29, 2019.

[71] Barry Halliwell. Understanding mechanisms of antioxidant action in health and disease. *Nature Reviews Molecular Cell Biology*, 25(1):13–33, 2024.

[72] Saikat Sen and Raja Chakraborty. The role of antioxidants in human health. In *Oxidative stress: diagnostics, prevention, and therapy*, pages 1–37. ACS Publications, 2011.

[73] İlhami Gulcin. Antioxidants and antioxidant methods: An updated overview. *Archives of toxicology*, 94(3):651–715, 2020.

[74] Attila Hunyadi. The mechanism (s) of action of antioxidants: From scavenging reactive oxygen/nitrogen species to redox signaling and the generation of bioactive secondary metabolites. *Medicinal research reviews*, 39(6):2505–2533, 2019.

[75] DR Berdahl, RI Nahas, and JP Barren. Synthetic and natural antioxidant additives in food stabilization: current applications and future research. *Oxidation in foods and beverages and antioxidant applications*, pages 272–320, 2010.

[76] Mihaela Stoia and Simona Oancea. Low-molecular-weight synthetic antioxidants: classification, pharmacological profile, effectiveness and trends. *Antioxidants*, 11(4): 638, 2022.

[77] Jian-Ming Lü, Peter H Lin, Qizhi Yao, and Changyi Chen. Chemical and molecular mechanisms of antioxidants: experimental approaches and model systems. *Journal of cellular and molecular medicine*, 14(4):840–860, 2010.

[78] Marios C Christodoulou, Jose C Orellana Palacios, Golnaz Hesami, Shima Jafarzadeh, José M Lorenzo, Rubén Domínguez, Andres Moreno, and Milad Hadidi. Spectrophotometric methods for measurement of antioxidant activity in food and pharmaceuticals. *Antioxidants*, 11(11):2213, 2022.

[79] Henry Jay Forman and Hongqiao Zhang. Targeting oxidative stress in disease: Promise and limitations of antioxidant therapy. *Nature Reviews Drug Discovery*, 20 (9):689–709, 2021.

[80] Kumari Neha, Md Rafi Haider, Ankita Pathak, and M Shahar Yar. Medicinal prospects of antioxidants: A review. *European journal of medicinal chemistry*, 178: 687–704, 2019.

[81] Thecla Okeahunwa Ayoka, Benjamin O Ezema, Chijioke Nwoye Eze, and Charles Okeke Nnadi. Antioxidants for the prevention and treatment of non-communicable diseases. *Journal of Exploratory Research in Pharmacology*, 7(3):178–188, 2022.

[82] Russel J Reiter, Dun-xian Tan, Juan C Mayo, Rosa M Sainz, Josefa Leon, and Zbigniew Czarnocki. Melatonin as an antioxidant: biochemical mechanisms and pathophysiological implications in humans. *Acta Biochimica Polonica*, 50(4):1129–1146, 2003.

[83] Sibel Suzen. Melatonin and synthetic analogs as antioxidants. *Current drug delivery*, 10(1):71–75, 2013.

[84] Ziad Moussa, ZM Judeh, and Saleh A Ahmed. Nonenzymatic exogenous and endogenous antioxidants. *Free radical medicine and biology*, 1:11–22, 2019.

[85] Ana Amelia de Carvalho Melo-Cavalcante, Leonardo da Rocha Sousa, Marcus Vinícius Oliveira Barros Alencar, Jose Victor de Oliveira Santos, Ana Maria Oliveira da Mata, Márcia Fernanda Correia Jardim Paz, Ricardo Melo de Carvalho, Nárcia Mariana Fonseca Nunes, Muhammad Torequl Islam, Anderson Nogueira Mendes, et al. Retinol palmitate and ascorbic acid: Role in oncological prevention and therapy. *Biomedicine & Pharmacotherapy*, 109:1394–1405, 2019.

[86] Stela Dragomanova, Simona Miteva, Ferdinando Nicoletti, Katia Mangano, Paolo Fagone, Salvatore Pricoco, Hristian Staykov, and Lyubka Tancheva. Therapeutic potential of alpha-lipoic acid in viral infections, including covid-19. *Antioxidants*, 10 (8):1294, 2021.

[87] Gerreke Ph Biewenga, Guido RMM Haenen, and Aalt Bast. The pharmacology of the antioxidant lipoic acid. *General Pharmacology: The Vascular System*, 29(3):315–331, 1997.

[88] Ananda S Prasad. Zinc is an antioxidant and anti-inflammatory agent: its role in human health. *Frontiers in nutrition*, 1:14, 2014.

[89] Sung Ryul Lee et al. Critical role of zinc as either an antioxidant or a prooxidant in cellular systems. *Oxidative medicine and cellular longevity*, 2018, 2018.

[90] Nuri Gueven, Pranathi Ravishankar, Rajaraman Eri, and Emma Rybalka. Idebenone: When an antioxidant is not an antioxidant. *Redox biology*, 38:101812, 2021.

[91] Imre Zs Nagy. Chemistry, toxicology, pharmacology and pharmacokinetics of idebenone: a review. *Archives of gerontology and geriatrics*, 11(3):177–186, 1990.

[92] Simone Kreth, Carola Ledderose, Benjamin Luchting, Florian Weis, and Manfred Thiel. Immunomodulatory properties of pentoxifylline are mediated via adenosine-dependent pathways. *Shock*, 34(1):10–16, 2010.

[93] Claudia O Zein, Rocio Lopez, Xiaoming Fu, John P Kirwan, Lisa M Yerian, Arthur J McCullough, Stanley L Hazen, and Ariel E Feldstein. Pentoxifylline decreases oxidized lipid products in nonalcoholic steatohepatitis: new evidence on the potential therapeutic mechanism. *Hepatology*, 56(4):1291–1299, 2012.

[94] AK Tikhaze, BZ Lankin, GG Konovalova, KB Shumaev, AI Kaminnyi, AI Kozachenko, SM Gurevich, LG Nagler, TM Zaitseva, and VV Kukharchuk. Antioxidant probucol as an effective scavenger of lipid radicals in low density lipoproteins in vivo and in vitro. *Bulletin of Experimental Biology and Medicine*, 128:818–821, 1999.

[95] Helmut Sies and Michael J Parnham. Potential therapeutic use of ebselen for covid-19 and other respiratory viral infections. *Free Radical Biology and Medicine*, 156: 107–112, 2020.

[96] Claudio Santi, Cecilia Scimmi, and Luca Sancineto. Ebselen and analogues: Pharmacological properties and synthetic strategies for their preparation. *Molecules*, 26 (14):4230, 2021.

[97] Zhongcheng Shi and Carlos A Puyo. N-acetylcysteine to combat covid-19: an evidence review. *Therapeutics and Clinical Risk Management*, pages 1047–1055, 2020.

[98] Gregorio Paolo Milani, Marina Macchi, and Anat Guz-Mark. Vitamin c in the treatment of covid-19. *Nutrients*, 13(4):1172, 2021.

[99] Jennifer R Evans and John G Lawrenson. Antioxidant vitamin and mineral supplements for slowing the progression of age-related macular degeneration. *Cochrane Database of Systematic Reviews*, (7), 2017.

[100] Anne WS Rutjes, David A Denton, Marcello Di Nisio, Lee-Yee Chong, Rajesh P Abraham, Aalya S Al-Assaf, John L Anderson, Muzaffar A Malik, Robin WM Vernooij, Gabriel Martínez, et al. Vitamin and mineral supplementation for maintaining cognitive function in cognitively healthy people in mid and late life. *Cochrane Database of Systematic Reviews*, (12), 2018.

[101] Mariano Catanesi, Laura Brandolini, Michele d'Angelo, Elisabetta Benedetti, Maria Grazia Tupone, Margherita Alfonsetti, Enrico Cabri, Daniela Iaconis, Maddalena Fratelli, Annamaria Cimini, et al. L-methionine protects against oxidative stress and mitochondrial dysfunction in an in vitro model of parkinson's disease. *Antioxidants*, 10(9):1467, 2021.

[102] Ramsha Usman and Navneeta Bharadvaja. Nutricosmetics: Role in health, nutrition, and cosmetics. *Proceedings of the Indian National Science Academy*, 89(3):584–599, 2023.

[103] Hien Thi Hoang, Ju-Young Moon, and Young-Chul Lee. Natural antioxidants from plant extracts in skincare cosmetics: Recent applications, challenges and perspectives. *Cosmetics*, 8(4):106, 2021.

[104] Tobias W Fischer, Ralph M Trüeb, Gabriella Hänggi, Marcello Innocenti, and Peter Elsner. Topical melatonin for treatment of androgenetic alopecia. *International journal of trichology*, 4(4):236, 2012.

[105] Nele Festjens, Michaël Kalai, Joél Smet, Ann Meeus, Rudy Van Coster, Xavier Saelens, and Peter Vandenabeele. Butylated hydroxyanisole is more than a reactive oxygen species scavenger. *Cell Death & Differentiation*, 13(1):166–169, 2006.

[106] Wallace Snipes, Stanley Person, Alec Keith, and James Cupp. Butylated hydroxytoluene inactivated lipid-containing viruses. *Science*, 188(4183):64–66, 1975.

[107] Anne Marie Roussel, Isabelle Hininger-Favier, Robert S Waters, Mireille Osman, Karen Fernholz, and Richard A Anderson. Edta chelation therapy, without added vitamin c, decreases oxidative dna damage and lipid peroxidation. *Alternative Medicine Review*, 14(1):56, 2009.

[108] JA Ribeiro, M Seifert, J Vinholes, CV Rombaldi, L Nora, and RFF Cantillano. Erythorbic acid and sodium erythorbate effectively prevent pulp browning of minimally processed 'royal gala'apples. *Italian Journal of Food Science*, 31(3), 2019.

[109] Zai-Qun Liu. Antioxidants may not always be beneficial to health. *Nutrition*, 30(2): 131–133, 2014.

[110] Brian D Lawenda, Kara M Kelly, Elena J Ladas, Stephen M Sagar, Andrew Vickers, and Jeffrey B Blumberg. Should supplemental antioxidant administration be avoided during chemotherapy and radiation therapy? *Journal of the national cancer institute*, 100(11):773–783, 2008.

[111] Xiaoqing Xu, Aimei Liu, Siyi Hu, Irma Ares, María-Rosa Martínez-Larrañaga, Xu Wang, Marta Martínez, Arturo Anadón, and María-Aránzazu Martínez. Synthetic phenolic antioxidants: Metabolism, hazards and mechanism of action. *Food Chemistry*, 353:129488, 2021.

[112] Muhammad Kamran Khan, Larysa Paniwnyk, and Sadia Hassan. Polyphenols as natural antioxidants: sources, extraction and applications in food, cosmetics and drugs. *Plant Based "Green Chemistry 2.0" Moving from Evolutionary to Revolutionary*, pages 197–235, 2019.

[113] David A. Dixon. *Density Functional Theory*, pages 1–7. Springer International Publishing, Cham, 2016. ISBN 978-3-319-39193-9. doi: 10.1007/978-3-319-39193-9_17-1.

[114] Pierre Hohenberg and Walter Kohn. Inhomogeneous electron gas. *Physical review*, 136(3B):B864, 1964.

[115] Walter Kohn and Lu Jeu Sham. Self-consistent equations including exchange and correlation effects. *Physical review*, 140(4A):A1133, 1965.

[116] John P Perdew. Density-functional approximation for the correlation energy of the inhomogeneous electron gas. *Physical Review B*, 33(12):8822, 1986.

[117] Chengteh Lee, Weitao Yang, and Robert G Parr. Development of the colle-salvetti correlation-energy formula into a functional of the electron density. *Physical review B*, 37(2):785, 1988.

[118] *Basis Sets*, pages 115–138. Springer Berlin Heidelberg, Berlin, Heidelberg, 2008. ISBN 978-3-540-77304-7. doi: 10.1007/978-3-540-77304-7_6.

[119] W. J. Hehre, W. A. Lathan, R. Ditchfield, M. D. Newton, and J. A. Pople. Gaussian 70. Quantum Chemistry Program Exchange, Program No. 237, 1970.

[120] Hong-Zhou Ye and Timothy C Berkelbach. Correlation-consistent gaussian basis sets for solids made simple. *Journal of Chemical Theory and Computation*, 18(3):1595–1606, 2022.

[121] Adele D Laurent and Denis Jacquemin. Td-dft benchmarks: a review. *International Journal of Quantum Chemistry*, 113(17):2019–2039, 2013.

[122] Samira Mahmoudi, Mehrdad Mohammadpour Dehkordi, and Mohammad Hossein Asgarshamsi. Density functional theory studies of the antioxidants—a review. *Journal of Molecular Modeling*, 27(9):271, 2021.

[123] Maciej Spiegel. Current trends in computational quantum chemistry studies on antioxidant radical scavenging activity. *Journal of Chemical Information and Modeling*, 62(11):2639–2658, 2022.

[124] S Mohamad Reza Nazifi, Mohammad H Asgharshamsi, Mehrdad M Dehkordi, and Krzysztof K Zborowski. Antioxidant properties of aloe vera components: a dft theoretical evaluation. *Free radical research*, 53(8):922–931, 2019.

[125] Keivan Akhtari, Keyumars Hassanzadeh, Bahareh Fakhraei, Nahid Fakhraei, Halaleh Hassanzadeh, and Seyed Amir Zarei. A density functional theory study of the reactivity descriptors and antioxidant behavior of crocin. *Computational and Theoretical Chemistry*, 1013:123–129, 2013.

[126] Zorica D Petrović, Jelena Đorović, Dušica Simijonović, Vladimir P Petrović, and Zoran Marković. Experimental and theoretical study of antioxidative properties of some salicylaldehyde and vanillic schiff bases. *RSC Advances*, 5(31):24094–24100, 2015.

[127] Dian Alwani Zainuri, Ibrahim Abdul Razak, and Suhana Arshad. Crystal structure, spectroscopic characterization and dft study of two new linear fused-ring chalcones. *Acta Crystallographica Section E: Crystallographic Communications*, 74(10):1427–1432, 2018.

[128] Ersin Temel, Can Alaşalvar, Halil Gökçe, Aytaç Güder, Çiğdem Albayrak, Yelda Bingöl Alpaslan, Gökhan Alpaslan, and Nefise Dilek. Dft calculations, spectroscopy and antioxidant activity studies on (e)-2-nitro-4-[(phenylimino) methyl] phenol. *Spectrochimica Acta Part A: Molecular and Biomolecular Spectroscopy*, 136: 534–546, 2015.

[129] Talapunur Vikramaditya, Jeng-Da Chai, and Shiang-Tai Lin. Impact of non-empirically tuning the range-separation parameter of long-range corrected hybrid functionals on ionization potentials, electron affinities, and fundamental gaps. *Journal of Computational Chemistry*, 39(28):2378–2384, 2018.

[130] Felipe A Bulat, Jane S Murray, and Peter Politzer. Identifying the most energetic electrons in a molecule: The highest occupied molecular orbital and the average local ionization energy. *Computational and Theoretical Chemistry*, 1199:113192, 2021.

[131] Monica Leopoldini, Nino Russo, and Marirosa Toscano. The molecular basis of working mechanism of natural polyphenolic antioxidants. *Food chemistry*, 125(2): 288–306, 2011.

[132] Lingling Wang, Fengjian Yang, Xiuhua Zhao, and Yuanzuo Li. Effects of nitro-and amino-group on the antioxidant activity of genistein: A theoretical study. *Food chemistry*, 275:339–345, 2019.

[133] Aiping Xing, Dai Zeng, and Zhihong Chen. Synthesis, crystal structure and antioxidant activity of butylphenol schiff bases: Experimental and dft study. *Journal of Molecular Structure*, 1253:132209, 2022.

[134] Ning Zhang, Yilong Wu, Miao Qiao, Wenjuan Yuan, Xingyu Li, Xuanjun Wang, Jun Sheng, and Chengting Zi. Structure–antioxidant activity relationships of dendrocandin analogues determined using density functional theory. *Structural Chemistry*, 33(3):795–805, 2022.

[135] Anna Sykula, Agnieszka Kowalska-Baron, Aliaksandr Dzeikala, Agnieszka Bodzioch, and Elzbieta Lodyga-Chruscinska. An experimental and dft study on free radical scavenging activity of hesperetin schiff bases. *Chemical Physics*, 517: 91–103, 2019.

[136] RN Sahoo, S Pattanaik, G Pattnaik, S Mallick, and R Mohapatra. Review on the use of molecular docking as the first line tool in drug discovery and development. *Indian Journal of Pharmaceutical Sciences*, 84(5), 2022.

[137] PC Agu, CA Afiukwa, OU Orji, EM Ezeh, IH Ofoke, CO Ogbu, EI Ugwuja, and PM Aja. Molecular docking as a tool for the discovery of molecular targets of nutraceuticals in diseases management. *Scientific Reports*, 13(1):13398, 2023.

[138] D. Astalakshmi et al. Over view on molecular docking: A powerful approach for structure based drug discovery. *International Journal of Pharmaceutical Sciences Review and Research*, 77:146–157, 2022.

[139] Francesca Stanzione, Ilenia Giangreco, and Jason C Cole. Use of molecular docking computational tools in drug discovery. *Progress in Medicinal Chemistry*, 60:273–343, 2021.

[140] Dibya Ranjan Das, Dhanesh Kumar, Pravind Kumar, and Bisnu Prasad Dash. Molecular docking and its application in search of antisickling agent from carica papaya. *Journal of Applied Biology and Biotechnology*, 8(1):105–116, 2020.

[141] Natasja Brooijmans and Irwin D Kuntz. Molecular recognition and docking algorithms. *Annual review of biophysics and biomolecular structure*, 32(1):335–373, 2003.

[142] Jeffrey S Taylor and Roger M Burnett. Darwin: a program for docking flexible molecules. *Proteins: Structure, Function, and Bioinformatics*, 41(2):173–191, 2000.

[143] Ye Li, Xianren Zhang, and Dapeng Cao. The role of shape complementarity in the protein-protein interactions. *Scientific reports*, 3(1):3271, 2013.

[144] Hari K Voruganti and Bhaskar Dasgupta. A novel volumetric criterion for optimal shape matching of surfaces for protein-protein docking. *Journal of Computational Design and Engineering*, 5(2):180–190, 2018.

[145] Garrett M Morris, Ruth Huey, William Lindstrom, Michel F Sanner, Richard K Belew, David S Goodsell, and Arthur J Olson. Autodock4 and autodocktools4: Automated docking with selective receptor flexibility. *Journal of computational chemistry*, 30(16): 2785–2791, 2009.

[146] S Parasuraman. Prediction of activity spectra for substances. *Journal of pharmacology & pharmacotherapeutics*, 2(1):52, 2011.

[147] DA Filimonov, AA Lagunin, TA Gloriozova, AV Rudik, DS Druzhilovskii, PV Pogodin, and VV Poroikov. Prediction of the biological activity spectra of organic compounds using the pass online web resource. *Chemistry of Heterocyclic Compounds*, 50:444–457, 2014.

[148] AV Stepanchikova, AA Lagunin, DA Filimonov, and VV Poroikov. Prediction of biological activity spectra for substances: Evaluation on the diverse sets of drug-like structures. *Current medicinal chemistry*, 10(3):225–233, 2003.

[149] Alexey Lagunin, Alla Stepanchikova, Dmitrii Filimonov, and Vladimir Poroikov. Pass: prediction of activity spectra for biologically active substances. *Bioinformatics*, 16(8):747–748, 2000.

[150] Balakumar Chandrasekaran, Sara Nidal Abed, Omar Al-Attraqchi, Kaushik Kuche, and Rakesh K Tekade. Computer-aided prediction of pharmacokinetic (admet) properties. In *Dosage form design parameters*, pages 731–755. Elsevier, 2018.

[151] Haizhen A Zhong. Admet properties: overview and current topics. *Drug design: principles and applications*, pages 113–133, 2017.

[152] Antoine Daina, Olivier Michielin, and Vincent Zoete. Swissadme: a free web tool to evaluate pharmacokinetics, drug-likeness and medicinal chemistry friendliness of small molecules. *Scientific reports*, 7(1):42717, 2017.

[153] Antoine Daina and Vincent Zoete. A boiled-egg to predict gastrointestinal absorption and brain penetration of small molecules. *ChemMedChem*, 11(11):1117–1121, 2016.

[154] Christopher A Lipinski, Franco Lombardo, Beryl W Dominy, and Paul J Feeney. Experimental and computational approaches to estimate solubility and permeability in drug discovery and development settings. *Advanced drug delivery reviews*, 64:4–17, 2012.

[155] MN Patel, CB Patel, and RP Patel. Chelates of cu (ii) with some bidentate schiff bases. *Journal of Inorganic and Nuclear Chemistry*, 36(12):3868–3870, 1974.

[156] BELGHIT MOHAMED YAZID. *Synthèse, structurale et Etude du Comportement des Ortho–hydroxy bases de Schiff en phase liquide-liquide*. PhD thesis, L'université Mohamed Khider de Biskra, 2016.

[157] Axel D Becke. Density-functional exchange-energy approximation with correct asymptotic behavior. *Physical review A*, 38(6):3098, 1988.

[158] Axel D Becke. Density-functional thermochemistry. i. the effect of the exchange-only gradient correction. *The Journal of chemical physics*, 96(3):2155–2160, 1992.

[159] Warren J Hehre, Robert Ditchfield, and John A Pople. Self—consistent molecular orbital methods. xii. further extensions of gaussian—type basis sets for use in molecular orbital studies of organic molecules. *The Journal of Chemical Physics*, 56(5): 2257–2261, 1972.

[160] M Muthukkumar, C Kamal, G Venkatesh, C Kaya, SAVAŞ Kaya, Israel VMV Enoch, P Vennila, and R Rajavel. Structural, spectral, dft and biological studies on macrocyclic mononuclear ruthenium (ii) complexes. *Journal of Molecular Structure*, 1147: 502–514, 2017.

[161] Jeffrey P Merrick, Damian Moran, and Leo Radom. An evaluation of harmonic vibrational frequency scale factors. *The Journal of Physical Chemistry A*, 111(45): 11683–11700, 2007.

[162] MH Jamroz. Vibrational energy distribution analysis veda 4. *Warsaw Poland*, 2004.

[163] Stevan Armaković and Sanja J Armaković. Atomistica. online–web application for generating input files for orca molecular modelling package made with the anvil platform. *Molecular Simulation*, 49(1):117–123, 2023.

[164] Jacopo Tomasi, Benedetta Mennucci, and Roberto Cammi. Quantum mechanical continuum solvation models. *Chemical reviews*, 105(8):2999–3094, 2005.

[165] Ján Rimarčík, Vladimír Lukeš, Erik Klein, and Michal Ilčin. Study of the solvent effect on the enthalpies of homolytic and heterolytic n–h bond cleavage in p-phenylenediamine and tetracyano-p-phenylenediamine. *Journal of Molecular Structure: THEOCHEM*, 952(1-3):25–30, 2010.

[166] Jelena Tošović, Svetlana Markovic, Dejan Milenkovic, and Zoran Marković. Solvation enthalpies and gibbs energies of the proton and electron-influence of solvation models. *Journal of the Serbian Society for Computational Mechanics*, 10(2):66–76, 2016.

[167] Zoran Marković, Jelena Tošović, Dejan Milenković, and Svetlana Marković. Revisiting the solvation enthalpies and free energies of the proton and electron in various solvents. *Computational and Theoretical Chemistry*, 1077:11–17, 2016.

[168] JJ Fifen, M Nsangou, Z Dhaouadi, O Motapon, and N Jaidane. Solvent effects on the antioxidant activity of 3, 4-dihydroxyphenylpyruvic acid: Dft and td-dft studies. *Computational and Theoretical Chemistry*, 966(1-3):232–243, 2011.

[169] Xiugong Gao, Xiaoling Wen, Lothar Esser, Byron Quinn, Linda Yu, Chang-An Yu, and Di Xia. Structural basis for the quinone reduction in the bc 1 complex: a comparative analysis of crystal structures of mitochondrial cytochrome bc 1 with bound substrate and inhibitors at the qi site. *Biochemistry*, 42(30):9067–9080, 2003.

[170] D.S. Biovia. Discovery studio modeling environment. Release 4, 2015.

[171] Douglas EV Pires, Tom L Blundell, and David B Ascher. pkcsm: predicting small-molecule pharmacokinetic and toxicity properties using graph-based signatures. *Journal of medicinal chemistry*, 58(9):4066–4072, 2015.

[172] Demehin Iyewumi et al. Dft calculations and total antioxidant capacity studies of some substituted monodentate salicylaldimines. *Journal of Scientific Research and Reports*, 27(8):44–54, 2021.

[173] AZ El-Sonbati, WH Mahmoud, Gehad G Mohamed, MA Diab, Sh M Morgan, and SY Abbas. Synthesis, characterization of schiff base metal complexes and their biological investigation. *Applied Organometallic Chemistry*, 33(9):e5048, 2019.

[174] Zainab Moosavi-Tekyeh and Najmeh Dastani. Intramolecular hydrogen bonding in n-salicylideneaniline: Ft-ir spectrum and quantum chemical calculations. *Journal of Molecular Structure*, 1102:314–322, 2015.

[175] Fatih Şen, Kürşat Efil, Yunus Bekdemir, and Muharrem Dinçer. Structural, spectroscopic characterization of (e)-4-chloro-2-((4-methoxybenzylidene) amino) phenol as potential antioxidant compound. *Journal of Molecular Structure*, 1127:645–652, 2017.

[176] Simon Olonkwoh Salihu. Synthesis, spectroscopic and inhibitory study of some substituted schiff bases. *International Journal of Innovative Research and Advanced Studies*, 2017.

[177] Halil Gökce, Yelda Bingöl Alpaslan, Celal Tuğrul Zeyrek, Erbil Ağar, Aytaç Güder, Namık Özdemir, and Gökhan Alpaslan. Structural, spectroscopic, radical scavenging activity, molecular docking and dft studies of a synthesized schiff base compound. *Journal of Molecular Structure*, 1179:205–215, 2019.

[178] Manfred Reichenbächer and Jürgen Popp. *Challenges in molecular structure determination*. Springer Science & Business Media, 2012.

[179] George Socrates. *Infrared and Raman characteristic group frequencies: tables and charts*. John Wiley & Sons, 2004.

[180] Dixit N Sathyanarayana. *Vibrational spectroscopy: theory and applications*. New Age International, 2015.

[181] Arzu Özek Yıldırım, Muhammet Hakkı Yıldırım, and Çiğdem Albayrak Kaştaş. Synthesis, spectroscopic, conceptual dft characterization and molecular docking studies of two versatile di-bromobenzaldehyde derived compounds. *Polycyclic Aromatic Compounds*, 42(8):5599–5615, 2022.

[182] Arzu Özek Yıldırım, M Hakkı Yıldırım, and Çiğdem Albayrak Kaştaş. Keto-enol tautomerism of (e)-2-[(3, 4-dimethylphenylimino) methyl]-4-nitrophenol: Synthesis, x-ray, ft-ir, uv–vis, nmr and quantum chemical characterizations. *Journal of Molecular Structure*, 1127:275–282, 2017.

[183] LJFC Bellamy. *The infra-red spectra of complex molecules*. Springer Science & Business Media, 2013.

[184] Gökhan Kaştaş, Çiğdem Albayrak Kaştaş, and Ahmet Tabak. Investigation of molecular structure and solvent/temperature effect on tautomerism in (e)-4, 6-dibromo-3-methoxy-2-[(p-tolylimino) methyl] phenol, a new thermochromic schiff base, by using xrd, ft-ir, uv–vis, nmr and dft methods. *Spectrochimica Acta Part A: Molecular and Biomolecular Spectroscopy*, 222:117198, 2019.

[185] M Hakkı Yıldırım. Synthesis, spectroscopic characterization and in-silico bioactivity studies of (e)-4, 6-dibromo-2-[(2-bromo-4-methylphenylimino) methyl]-3-methoxyphenol. *Journal of Molecular Structure*, 1245:131141, 2021.

[186] Mohamed Yazid Belghit, Abdelhamid Moussi, and Djamel Barkat. In vitro antifungal activity of some schiffbases derived from ortho-hydroxybenzaldehyde against fusarium. *Journal of Engineering Science and Technology*, 12(6):1709–1722, 2017.

[187] Zakia Messasma, Djouhra Aggoun, Selma Houchi, Ali Ourari, Yasmina Ouennoughi, Fatah Keffous, and Rachid Mahdadi. Biological activities, dft calculations and docking of imines tetradentates ligands, derived from salicylaldehydic compounds as metallo-beta-lactamase inhibitors. *Journal of Molecular Structure*, 1228: 129463, 2021.

[188] Stevan Armaković, Sanja J Armaković, and Jovan P Šetrajčić. Hydrogen storage properties of sumanene. *International Journal of Hydrogen Energy*, 38(27):12190–12198, 2013.

[189] Nora Okulik and Alicia H Jubert. Theoretical study on the structure and reactive sites of non-steroidal anti-inflammatory drugs. *Journal of Molecular Structure: THEOCHEM*, 682(1-3):55–62, 2004.

[190] JS Murray and K Sen. Molecular electrostatic potential concepts and applications elsevier science bv. *Amsterdam, The Netherlands*, 1996.

[191] VV Aswathy, Y Sheena Mary, PJ Jojo, C Yohannan Panicker, Anna Bielenica, Stevan Armaković, Sanja J Armaković, Paulina Brzózka, Sylwester Krukowski, and C Van Alsenoy. Investigation of spectroscopic, reactive, transport and docking properties of 1-(3, 4-dichlorophenyl)-3-[3-(trifluoromethyl) phenyl] thiourea (anf-6): Combined experimental and computational study. *Journal of Molecular Structure*, 1134:668–680, 2017.

[192] Maryam Farrokhnia. Density functional theory studies on the antioxidant mechanism and electronic properties of some bioactive marine meroterpenoids: Sargahydroquionic acid and sargachromanol. *ACS omega*, 5(32):20382–20390, 2020.

[193] Yan-Zhen Zheng, Geng Deng, Qin Liang, Da-Fu Chen, Rui Guo, and Rong-Cai Lai. Antioxidant activity of quercetin and its glucosides from propolis: A theoretical study. *Scientific reports*, 7(1):7543, 2017.

[194] Romesh Borgohain, Jyotirekha G Handique, Ankur Kanti Guha, and Sanjay Pratihar. A theoretical study of antioxidant activity of some schiff bases derived from biologically important phenolic aldehydes and phenylenediamines. *Journal of Physical Organic Chemistry*, 31(2):e3757, 2018.

[195] Hye Jin Jung, Misun Cho, Yonghyo Kim, Gyoonhee Han, and Ho Jeong Kwon. Development of a novel class of mitochondrial ubiquinol–cytochrome c reductase binding protein (uqcrb) modulators as promising antiangiogenic leads. *Journal of medicinal chemistry*, 57(19):7990–7998, 2014.

[196] Ahlam Roufieda Guerroudj, Nourdine Boukabcha, Abdelmadjid Benmohammed, Necmi Dege, Nour El Houda Belkafouf, Nawel Khelloul, Ayada Djafri, and Abdelkader Chouaih. Synthesis, crystal structure, vibrational spectral investigation, intermolecular interactions, chemical reactivity, nlo properties and molecular docking analysis on (e)-n-(4-nitrobenzylidene)-3-chlorobenzenamine: A combined experimental and theoretical study. *Journal of Molecular Structure*, 1240:130589, 2021.

[197] KV Aarthi, Hemamalini Rajagopal, S Muthu, V Jayanthi, and R Girija. Quantum chemical calculations, spectroscopic investigation and molecular docking analysis of 4-chloro-n-methylpyridine-2-carboxamide. *Journal of Molecular Structure*, 1210: 128053, 2020.

Appendix

Table S1. The selected experimental and computed vibrational wavenumbers and their assignments of HBMC.

Assignments	Exp. IR	Scaled	I_{IR}
ν (OH) (100)	3440	3 726	43,48
ν (CH) (99) R2		3 112	0,08
ν (CH) (89) R2		3 106	2,25
ν (CH) (78) R1 +ν ($C_{methine}H$) (13)		3 105	9,17
ν (CH) (93) R1		3 097	7,6
ν (CH) R2 (14) +ν (CH) R2 (80)		3 093	8,07
ν (CH) R1 (13) +ν (CH) R1 (13) +ν CH R1 (70)		3 088	9,48
ν (CH) R1 (79) +ν (CH) R1 (14)		3 073	1,55
ν (CH) R2 (78) +ν (CH) (18) R2		3 073	8,44
ν ($C_{methine}H$) (99)	3062	2 882	65,63
ν (N=C) (61)	1620	1 624	76,56
ν (CC) R1 (47)	1590	1 599	62,34
ν (CC) R2 (36) +ν (CC) R1 (12)	1571	1 564	169,4
ν (CC) R1 (10) +ν (CC) R2 (34)		1 561	68,62
ν (CC) R2 (49) +δ (CCC) R2 (11) +δ (CCC) R2 (11)		1 551	85,11
δ (HCC) R1 (35) +δ (CCC) R1 (17)		1 465	31,82
δ (HCC) R2 (10) +δ (HCC) R2 (42)	1457	1 454	98,6
ν (CC) R1 (29) +δ (HCC) R1 (41)	1441	1 445	50,03
ν (CC) R2 (10) +δ (HC=N) (22)		1 413	5,25
δ (HC=N) (41)	1372	1 382	31,99
ν (CC) R1 (44) +δ (HOC) (18)		1 312	24,79
ν (CC) R2 (51) +δ (HCC) R2 (15) +δ (HCC) R2 (22)		1 293	3,5
ν (CC) R1 (19) +δ (HCC) R1 (27) +δ (HCC) R1 (12)	1279	1 289	29,44
ν (CC) R2 (13) +δ(HCC) R2 (47)		1 252	2,31
ν ($CC_{methine}$) (40) +δ (HOC) (10)	1233	1 237	55,44
ν (OC) (49) +δ (HCC) R1 (10)	1187	1 207	100,61
ν (NC) R2 (18) +δ (HCC) R2 (11)	1152	1 168	48,14
δ (HCC) R2 (54)		1 154	1,04
δ (HOC) (25) +δ (HCC) R1 (44)	1152	1 147	94,33
δ (HCC) R1 (64)		1 138	72,27
ν (CC) R2 (24) +δ (HCC) R2 (29)		1 084	4,85
ν (CC) R1 (11) +δ (CCC) R1 (24) +δ (HOC) (11) +δ (HCC) R1 (10)		1 068	7,86
ν (CC) R2 (25) +δ (HCC) R2 (26)	1077	1 058	30,4
ν (CC) R1 (50) +δ (HCC) R1 (23)		1 021	12,77
ν (CC) R2 (33) +δ (CCC) R2 (47)	978	978	4,75
τ (HCCC) R1 (73)		969	0,12
τ (HCCC) R2 (52)		953	0,52
τ (HCCC) R1 (58) +τ (HCCC) R2 (10)		950	2,2
τ ($HC_{methine}NC$) (76)		930	0,49
δ (CNC) (12) +δ (CCC) R2 (19)	882	877	66,24
τ (HCCC) R2 (70)		877	15,91
τ (HCCC) R2 (11) +τ (HCCC) R2 (74)		868	4,35
ν (OC) (12) +ν (CC) R1 (11) +δ (CCC) R1 (30)		852	12,54
τ (HCCC) R1 (66) +τ (CCCC) R1 (12)		849	2,05
ν (CC) R1 (12) +δ (CCC) R1 (20)		798	4,56
τ (HCCC) R2 (70) + τ(CCCC) R2 (14)	770	761	51,79
τ (HCCC) R1 (76)	753	751	45,15
τ (CCCC) R1 (60)		711	4,23
ν (ClC) (14) +δ (CCC) R2 (15) +δ (CCC) R2 (35)	678	682	36,91
τ (HCCC) R2 (12) +τ (HCCC) R2 (18) +τ (CCCC) R2 (10) +τ (CCCC) R2 (36)		664	22,59
δ (CCC) R2 (20) +δ (CCC) R1 (40)		632	3,64

γ (ClCCC) R2 (72)		577	0,11
δ (CCC) R1 (48)	572	568	27,16
δ (CNC) (63)		535	1,09
τ (HCCC) R1 (10) +τ (CCCC) R1(60)		520	1,46
δ (CCC) R1 (61)		487	12,07
τ (HCCC) R1 (10) +τ (CCCC) R1 (47)		461	12,58
δ (CCO) (48)		444	10,1
τ (HCCC) R2 (14) +τ (CCCC) R2 (48) +τ (CCCC) R2 (10)		435	0,3
ν (ClC) (52) +δ (CCC) R2 (11)		395	1,27

ν, stretching; δ, in-plane bending; τ, torsion; γ, out-of-plane bending. Abbreviations: R1, C1-C6; R2, C10-C15 ring. I_{IR}, IR intensity (km/mol).

Table S2 . The selected experimental and computed vibrational wavenumbers and their assignments of HBMN.

Assignments	Exp. IR	Scaled	IIR
ν (OH) (100)	3450	3 728	40,7
ν (CH) R2 (99)		3 132	6,02
ν (CH) R2 (97)		3 127	6,75
ν (CH) R1 (86)		3 106	8,17
ν (CH) R1 (88)		3 098	6,72
ν (CH) R2 (96)	3090	3 095	9,06
ν (CH) R1 (90)		3 089	8,22
ν (CH) R2 (97)		3 079	7,42
ν (CH) R1 (81)		3 075	1,5
ν ($C_{methine}H$) (99)	2859	2 882	64,98
ν (N=C) (63)	1623	1 625	138,49
ν ($CC_{methine}$) (16) + ν (CC) R1 (38)	1601	1 603	62,49
ν (CC) R2 (39)	1573	1 586	94,78
ν (CC) R1 (45)		1 561	38,53
ν (CC) R2 (46)		1 560	88,35
ν (ON) (76)	1523	1 534	336,84
δ (HCC) R1 (46)		1 467	19,49
δ (HCC) R2 (55)	1457	1 457	56,61
ν (CC) R1 (33) + δ (HCC) R1 (33)		1 446	57,05
ν (CC) R2 (14) +ν (CC) R2 (11) + δ (HCC) R2 (13) + δ (HC)=N (11)		1 423	4,48
ν (N=C) (11) +δ(HC)=N (52)	1372	1 388	43,1
ν (ON) (78) +δ (ONO) (13)	1352	1 329	344,87
ν (CC) R1 (47) + δ (HOC) (16)	1306	1 313	23,05
ν (CC) R2(52) +δ (HCC) R2 (11)		1 301	17,46
ν (CC) R1 (10) +ν (CC) R1 (10) +δ (HCC) R1 (40)	1278	1 290	39,36
δ (HCC) R2 (51)		1 258	6,57
ν ($CC_{methine}$) (40) +δ (HCC) R1(10)	1243	1 239	44,08
ν (OC) (47) + δ (HCC) R1 (15)	1191	1 207	142,66
ν (CC) R2 (11) + ν (NC) R2 (25)	1151	1 169	51,13
δ (HCC) R2 (59)		1 159	5,32
δ (HOC) (25) +δ (HCC) R1 (49)	1149	1 147	72,81
ν (CC) R1) (10) +δ (HCC) R1 (57)		1 138	107,81
ν (CC R2) (30) + δ (HCC) R2 (30)	1076	1 078	24,41
δ (HOC) (12)	803.01	1 068	15,05
ν (CC) R2 (11) + ν (NC) (12) + δ (HCC) R2 (13) +δ (HCC) R2 (22)		1 059	22,88
ν (CC) R1 (57) +δ (HCC) R1 (18)		1 022	13,19
ν (CC) R2 (41) +δ (CCC) R2 (41)		981	0,57

τ (HCCC) R1 (65) +τ (CCCC) R1(15)		971	0,08
τ (HCCC) R2 (64) + τ (CCCC) R2 (14) + τ (CCCC) R2 (11)		968	0,02
τ (HCCC) R1 (80)		952	2,45
τ ($HC_{methine}NC$) (75)		933	0,02
ν (NC) R2 (10) + ν (NC) R2 (15) +δ (ONO) (10) δ+ (CCC) R2 (21)		912	9,59
τ (HCCN) R2 (79)	889	907	12,75
τ (HCCN) R2 (80)		896	6,97
ν ($CC_{methine}$) (10) +ν (OC) R1 (10) + δ (CCC) R1 (10) + δ (CCN) R1(22)		854	9,86
τ (HCCC) R1 (80)		850	1,38
δ (ONO) (29) +δ (CCC) R1 (11)	826	825	43,44
ν (CC R1) (10) +δ (ONO) (20) +δ (CCC) R2 (20)	799	787	11,67
τ (HCCC) R2 (77)	784	778	35,78
τ (HCCC) R1 (77)	754	752	56,04
γ (OCON) (68)		715	2,66
γ (OCON) (66)		703	13,78
δ (ONO) (11) +δ (CCC) R1 (14) +δ (CCC) R2 (31)		672	16,04
τ (HCCC) R2 (10) + τ (HCCC) R2 (12) +τ (CCCC) R2 (50)	668	644	23,39
δ (CCC) R1 (27) +δ (CCC) R2(25)		631	2
ν (CC) R1(11) +δ (CCC) R1(41)		568	26,22
δ (CNC) R2(47)		552	0,91
τ (CCCC) R2 (67)		542	1,71
τ (HCCC) R1(14) +τ (HCCC) R1(10) + τ (CCCC) R1(47)		514	5,38
δ (CNO) (54)		511	6,56
δ (CCO) R1(62)		483	8,48
τ (CCCC) R1 (66)		454	6,62
δ (CCO) R1(47)		427	11,02
τ (HCCC) R2 (15) + τ (CCCC) R2(69)		418	0,04

ν, stretching; δ, in-plane bending; τ, torsion; γ, out-of-plane bending. Abbreviations: R1, C1-C6; R2, C10-C15 ring. I_{IR}, IR intensity (km/mol).

Table S3. The selected experimental and computed vibrational wavenumbers and their assignments of HBMM.

Assignments	Exp. IR	Scaled	IIR
ν (OH) (100)	3446	3 694	56.82
ν (CH) R2 (10) + ν (CH) R2 (84)		3 108	6,86
ν (CH) R2 (90)		3 107	2,68
ν (CH) R1 (87)	3050	3 096	19,44
ν (CH) R2 (89)		3 094	7,97
ν (CH) R1 (81)		3 078	10,79
ν (CH) R2 (88)		3 066	12,3
ν (CH) R1 (87)		3 064	3,84
ν (CH) R1 (93)		3 047	14,31
ν ($C_{methyl}H$) (92)	3008	3 034	25,25
ν ($C_{methyl}H$) (100)	3946	2 964	39,75
ν ($C_{methyl}H$) (92)	2838	2 908	67,06
ν ($C_{methine}H$) (99)		2 904	46,42
ν (N=C) (62) + δ (HC=N) (10)	1619	1 635	30,27
ν (CC) R2 (11) + ν ($C_{methine}C$) (10) + ν (CC R1 (21)		1 593	2,91
ν (CC) R2 (46)	1597	1 581	221,97
ν (CC) R1 (33)	1571	1 563	149,61
ν (CC) R1 (13) + ν (CC) R2 (28) +δ (HCC) R2 (10) +δ (CCC) R2 (11)		1 559	50,48
δ (HCC) R1 (48) + δ (CCC) R1(18)	1498	1 483	15,16
δ (HCC) R2 (11) + δ (HCC) R2 (10) + δ (HCC) R2(27)	1479	1 466	81,76
δ ($HC_{methyl}H$) (71) + τ ($HC_{methyl}OC$) (23)	1463	1 459	23,76

δ ($HC_{methyl}H$) (74) + τ ($HC_{methyl}OC$) (26)		1 446	9,08
ν (CC) R2 (19) + δ (HCC) R2 (29)		1 438	32,72
δ ($HC_{methyl}H$) (55)		1 430	25,92
ν (CC) R2 (21) +δ (HCC) R2 (35)		1 420	28,68
δ (HC=N) (62)	1365	1 375	17,61
ν (CC) R1(28) +ν (CC) R1 (15) + δ (HOC) R1 (26) + δ (HCC) R1 (10)	1317	1 324	35,94
ν (CC) R2 (53) + δ (HCC) R2 (12)		1 314	12,35
ν (CC) R1 (20) +δ (HCC) R1 (31)		1 288	49,3
ν (OC) R2 (12) + δ (HCC) R2 (17)+ δ (HCC) R2 (20)	1284	1 269	136,65
ν (OC) R1 (46)	1257	1 253	8,65
ν (OC) R2 (18) + ν (NC R2) (19)	1220	1 237	77,82
ν ($CC_{methine}$) (42)		1 209	86,15
δ (HCC) R2 (11) + δ ($HC_{methyl}H$) (12) + τ ($HC_{methyl}OC$) (36)		1 169	7,16
δ (HCC) R2 (20) + τ ($HC_{methyl}OC$) (23)		1 163	4,9
ν (CC) R1 (10) + δ (HOC) R1 (16) + δ (HCC) R1 (12) + δ (HCC) R2 (10)		1 157	7,17
ν (CC) R1 (12) +δ (HCC) R1 (71)		1 148	8,88
δ ($HC_{methyl}H$) (25) + τ ($HC_{methyl}OC$) (74)		1 133	0,74
ν (OC_{methyl})) (11) + ν (NC) R2 (22) + ν(OC) R2 (12) + δ (HCC) R2 (22)	1137	1 115	181,73
ν (CC) R1 (14) + ν (CC) R1 (10) + δ (HOC) R1 (13) +δ ($HC_{methyl}H$) (11)	1093	1 090	43,93
ν (CC) R2 (34) + δ (HCC) R2 (36)		1 082	4,22
ν (OC_{methyl}) (48) + δ (HCC) R2 (17)	1044	1 036	65
ν (CC) R1 (46) + δ (HCC) R1 (17)		1 036	1,91
ν (CC) R2 (18) + ν (CC) R2 (19) + δ (CCC) R2 (48)		974	2,23
τ ($HC_{methine}NC$) (70)		965	3,85
τ (HCCC) R1 (73)		951	0,17
τ (HCCC) R2(62) + τ (CCCC) R2 (17)		937	0,99
τ (HCCC) R1 (74)		918	0,82
ν (OC) R2 (10) + ν (NC) R2 (15) + ν (OC_{methyl}) (15) + δ (CCC) R2 (11)	900	908	15,67
ν (OC) R1 (12) + δ (CCC) R1 (53) + δ (CCC) R1 (12)		880	8,74
τ (HCCC) R2(66) + γ (NCCC) R2 (25)	865	872	24,27
τ (HCCC) R2 (84) + γ (OCCC) R2 (10)		840	1,59
τ (HCCC) R1(74) + γ (OCCC) R1 (15)		827	1,6
ν (CC) R1 (10) + δ (CCC) R1 (20)	796	772	14,53
τ (HCCC) R2 (65) + γ (NCCC) R2 (12)		750	47,92
τ (HCCC) R1 (77)	753	738	70,72
ν (CC) R2 (12) + ν (OC) R2 (10) + δ (CCC) R1 (11) + δ (CCC) R2 (19)		731	8,93
τ (HCCC) R1 (17) + γ (OCCC) R1 (51)		717	0,18
τ (HCCC) R2 (15) + τ (HCCC) R2 (10) + τ (HCCC) R2 (28) + τ(CCCC) R2 (26)	657	664	24,45
δ (CCC) R1 (54)		650	6,45
γ (OCCC) R2 (70)		605	0,27
δ (CCC) R1 (22) + δ (CCC) R1 (33)		578	5,51
δ ($C_{methy}OC$) (54)		560	4,65
τ (HCCC) R1 (12) + τ (CCCC) R1 (63)		539	0,91
δ (CCC) R2 (42)	549	531	21,86
δ (CCC) R2 (67)		494	2,49
τ (CCCC) R1 (13) + τ (CCCC) R2 (11) + γ (NCCC) R2 (10) + τ (CCCC) R2 (18)	469	467	5,06
τ (CCCC) R2 (17) + γ(NCCC) R2 (13) + τ(CCCC) R2 (11) + τ (CCCC) R2 (17)		443	0,36
δ (CCO) R1 (62)		431	2,92

ν, stretching; δ, in-plane bending; τ, torsion; γ, out-of-plane bending. Abbreviations: R1, C1-C6; R2, C10-C15 ring. I_{IR}, IR intensity (km/mol).